Near-limit propagation of detonations in annular channels

by

Anne Jesuthasan

Department of Mechanical Engineering

McGill University

Montreal, Quebec, Canada

June 2011

A thesis submitted to McGill University
in partial fulfillment of the requirements of the degree of
Master of Engineering

© Anne Jesuthasan 2011

ABSTRACT

In this study, the near-limit propagation of detonations in annular channels is investigated. Stoichiometric mixtures of methane-oxygen, acetylene-nitrous oxide diluted with 50% argon and acetylene-oxygen diluted with 70% argon are used in the experiments. Detonation velocity as well as smoked foil records of near-limit detonations are obtained. It is found that by normalizing the channel length scale by the ZND reaction length, (i.e. L/Δ_{ZND} , where L is the channel gap) the velocity variations for different channels coalesces to a single curve. Thus the detonation velocity in annular channels depends on the relative role between the geometry and the chemical sensitivity of the mixture. Detonation velocities of the order of half Chapman-Jouguet (CJ) values were observed near the limit which tend to suggest instabilities provide the mechanism to maintain the propagation at such low velocities. The results obtained were compared to Fay's velocity deficit model. Qualitative agreement was obtained for acetyleneoxygen diluted with 70% argon mixtures, but fails to predict in methane-oxygen mixtures. Smoked foil records indicate the detonation structure is irreproducible near the limit. Particularly in thin channels, the detonation structure is significantly affected by the boundary layer.

RÉSUMÉ

Dans cette recherche, la propagation des détonations près de la limite de détonation est étudiée dans des tubes annulaires. Les mélanges stoechiométriques de méthane et d'oxygène, d'acétylène et d'oxide nitreux dilués avec 50% d'argon, ainsi que d'acétylène et d'oxygène dilués avec 70% d'argon sont utilisés dans les expériences. Des mesures de célérité de la détonation ainsi que des tracés des ondes de pression transverses sur feuille de suie ont été obtenus près de la limite de détonation. En normalisant l'espace annulaire par rapport à la longueur de la zone de réaction ZND (i.e. L/Δ_{ZND} , où L est l'espace annulaire), les variations de célérité des détonations pour les différents espaces annulaires se combinent pour former une seule courbe. Des célérités de détonation d'environ la moitié de la valeur Chapman-Jouguet (CJ) ont été observées près de la limite ce qui suggère que les instabilités fournissent le mécanisme nécessaire pour entretenir la propagation malgré le déficit de célérité. Les résultats sont comparés au modèle de perte de célérité de Fay. Un accord qualitatif est obtenu pour le mélange d'acétylène et d'oxygène dilué avec 70% d'argon, mais le modèle ne parvient pas à prédire le déficit de célérité pour le mélange de méthane et d'oxygène. Les tracés sur feuille de suie indiquent que la structure de la détonation n'est pas reproductible près de la limite. Particulièrement pour les espaces annulaires minces, la structure de la détonation est fortement affectée par la couche limite.

ACKNOWLEDGEMENTS

I would like to first thank my outstanding supervisor, Professor John H.S. Lee, for his constant encouragements to better oneself and his unmatched insight and expertise in the field of detonations. I truly appreciate his constant availability and his talent in explaining things clearly and simply. The time I spent in his presence will always be cherished.

I would like to sincerely thank my past and present colleagues from the Optics Laboratory who created the most enjoyable work environment. In particular, many thanks to Yannick Fortin, Jean-Sébastien Grondin, Vsevolods Kamenskihs, Hui Qin and Bo Zhang whose friendship I treasure. I would like to also thank Aloïs Joassard for his help in carrying out experiments. Special thanks to Jimmy Verreault and Zuya Zarei for their constant encouragement throughout my graduate studies. I would like to thank Professor Hoi Dick Ng for his contribution towards this research and express my most sincere gratitude for his approachability.

A special note of thanks goes to the staff of the Machine Tool Laboratory (Antonio Micozzi, J. Roy Westgate and Andreas Hofmann) for their excellent craftsmanship in machining the various components of my experimental apparatus. I would also like to thank Gary Savard and John Boisvert for going out of their way to help me and particularly, for knowing how to brighten up my day.

I would like to thank the Mechanical Engineering Department Staff, both academic and administrative, for their support and encouragement throughout my university experience.

Finally, I must send my most sincere affection to my loving family for creating an environment where I can freely concentrate on my studies.

TABLE OF CONTENTS

ABSTR	ACT	i
RÉSUM	ıÉ	ii
ACKNO	WLEDGEMENTS	iv
LIST OF	FIGURES	viii
LIST OF	TABLES	xiv
Chapter	1 Introduction	1
1.1	General overview	1
1.2	Literature review	2
1.3	State of the art on detonation limits	11
1.4	Current study	12
Chapter	2 Experimental details	14
2.1	Detonation tube	14
2.2	Ignition system	14
2.3	Explosive mixture selection and preparation	15
2.4	Experimental procedures	15
2.5	Diagnostics	16
Chapter 3 Results and discussion		18
3.1	Detonation velocity	18
3.1	.1 Round tubes	18
3.1	2. Annular channels	21
3.1	.3 Velocity deficit according to Fay's model	23
3.1	.4 ZND induction length analysis	25
3.2	Detonation structure	27
3.2	.1 Cell structure: well within the limit	27
3.2	.2 Cell structure: approaching the limit	28
3.2	.3 Near the limit: spinning structure	31
3.2	.2 Track angle	33
3.3	Pressure traces	35

3.3.1	Well within the limit	35
3.3.2	Near the limit: spinning	35
3.3.3	Outside the limit	36
Chapter 4	Conclusion	37
Appendix	A: Fay's model	38
Appendix	B: Acoustic theory	41
Reference	S.	49

LIST OF FIGURES

Figure 1a: Schematic of the experimental apparatus	55
Figure 1b: Photograph of the experimental apparatus	55
Figure 2: Typical pressure trace of a detonation	56
Figure 3: Photoprobe circuit	57
Figure 4: Typical photoprobe signals	58
Figure 5: Typical trajectory of a detonation ($C_2H_2 + 2.5O_2 + 70\%Ar$, 9.525 mr	n
annular channel)	59
Figure 6: Typical smoked foil record of a detonation ($C_2H_2 + 2.5O_2 + 70\%Ar$,	p ₀
=10 kPa, 58 mm diameter round tube).	60
Figure 7: Typical trajectory of a detonation within the limit of detonation (C_2H_2	₂ +
2.5O ₂ + 70%Ar, 65 mm diameter round tube)	61
Figure 8: Typical trajectory of a detonation outside the limit of detonation (C_2 l	H ₂ +
2.5O ₂ + 70%Ar, 3.175 mm annular channel)	62
Figure 9: Normalized detonation velocity as a function of initial pressure in Ca	₂ H ₂
+ 2.5O ₂ + 70%Ar mixtures for round tubes.	63
Figure 10: Normalized detonation velocity as a function of initial pressure in 0	CH₄
+ 2O ₂ mixtures for round tubes.	64
Figure 11: Normalized detonation velocity as a function of initial pressure in 0	C ₂ H ₂
+ 5N ₂ O + 50%Ar mixtures for round tubes	65

Figure 12: Normalized detonation velocity as a function of initial pressure in C ₂ H ₂
+ 2.5O ₂ + 70%Ar mixtures for annular channels66
Figure 13: Normalized detonation velocity as a function of initial pressure in CH ₄
+ 2O ₂ mixtures for annular channels67
Figure 14: Normalized detonation velocity as a function of initial pressure in C_2H_2
+ 5N ₂ O + 50%Ar mixtures for annular channels
Figure 15: Normalized detonation velocity computed using Fay's model in C ₂ H ₂ +
2.5O ₂ + 70%Ar mixtures in annular channels69
Figure 16: Normalized detonation velocity computed using Fay's model in CH ₄ +
2O ₂ mixtures in annular channels70
Figure 17: Comparison of Fay's curvature model with experimental results for
C ₂ H ₂ +2.5 O ₂ +70%Ar in a 9.525 mm annular gap71
Figure 18: Comparison of Fay's curvature model with experimental results for
C ₂ H ₂ +2.5 O ₂ +70%Ar in a 3.175 mm annular gap72
Figure 19: Comparison of Fay's curvature model with experimental results for
CH ₄ +2O ₂ in a 9.525 mm annular gap73
Figure 20: Comparison of Fay's curvature model with experimental results for
CH ₄ +2O ₂ in a 3.175 mm annular gap74
Figure 21: Normalized detonation velocities as a function of $1/\Delta_{ZND}$ in C_2H_2 +2.5
O ₂ +70%Ar mixture in annular channels and round tubes

Figure 22: Normalized detonation velocities as a function of L/Δ_{ZND} in $C_2H_2 + 2$.	.5
O ₂ +70%Ar mixture in annular channels and round tubes	.76
Figure 23: Normalized detonation velocities as a function of L/Δ_{ZND} in CH ₄ + 20	O ₂
mixture in annular channels and round tubes.	.77
Figure 24: Normalized detonation velocities as a function of L/Δ_{ZND} in C_2H_2 +	
5N ₂ O + 50%Ar mixture in annular channels and round tubes	.78
Figure 25: Sketch of an idealized two-dimensional detonation front superimpos	sed
on triple point tracks	.79
Figure 26: Smoked foil record of a detonation (C_2H_2 +2.5 O_2 +70%Ar, p_0 = 30 kl	Pa,
65 mm diameter round tube)	.80
Figure 27: Smoked foil record of a detonation (C_2H_2 +2.5 O_2 +70%Ar, p_0 = 25 kl	Pa,
9.525 mm channel gap)	.81
Figure 28: Smoked foil record of a detonation (CH ₄ +2O ₂ , p ₀ = 35 kPa, 44 mm	
diameter round tube)	.82
Figure 29: Smoked foil record of a detonation (C_2H_2 +5 N_2O +50%Ar, p_0 = 20 kF	Pа,
51 mm diameter round tube)	.83
Figure 30: Variation of cell size as a function of initial pressure in C ₂ H ₂ +2.5O ₂	
+70%Ar for different diameter round tubes.	.84
Figure 31: Variation of cell size as a function of initial pressure in CH ₄ + 2O ₂	
mixture for different diameter round tubes	85

Figure 32: Variation of cell size as a function of initial pressure in C ₂ H ₂ + 5N ₂ O	+
50%Ar mixture for different diameter round tubes	.86
Figure 33: Variation of cell size with initial pressure in C ₂ H ₂ +2.5O ₂ +70%Ar in	
annular channels	.87
Figure 34: Variation of cell size with initial pressure in CH ₄ +2O ₂ mixtures in	
annular channels	.88
Figure 35: Variation of cell size with initial pressure in C ₂ H ₂ +5N ₂ O +50%Ar in	
annular channels	.89
Figure 36: Smoked foil record of a detonation (C ₂ H ₂ +2.5O ₂ +70%Ar, p ₀ = 6 kP	a,
51 mm diameter round tube)	.90
Figure 37: Smoked foil record of a detonation ($C_2H_2 + 2.5O_2 + 70\%Ar$, $p_0 = 8 \text{ kF}$	ра,
6.35 mm channel gap)	.91
Figure 38: Smoked foil of a detonation ($C_2H_2 + 2.5O_2 + 70\%Ar$, p_0 = 10 kPa, 3.1	75
mm channel gap).	.92
Figure 39: Smoked foil record of a detonation (CH ₄ +2O ₂ , p ₀ = 7.5 kPa, 44 mm	
diameter round tube)	.93
Figure 40: Smoked foil record of a detonation (CH ₄ +2O ₂ , p ₀ = 4 kPa, 44 mm	
diameter round tube)	.94
Figure 41: Smoked foil record of a detonation (CH ₄ +2O ₂ , p ₀ = 7.5 kPa, 6.35 mi	m
channel)	.95

Figure 42: Smoked foil record of a detonation (CH ₄ +2O ₂ , p ₀ = 8 kPa, 3.175 mm
channel)96
Figure 43: Smoked foil record of a detonation ($C_2H_2 + 5N_2O + 50\%Ar$, $p_0 = 17.5$
kPa, 3.175 mm channel)97
Figure 44: Smoked foil record of a spinning detonation (CH ₄ +20 ₂ , p ₀ = 5 kPa, 65
mm diameter round tube)98
Figure 45: Smoked foil of a spinning detonation (CH ₄ +20 ₂ , p ₀ = 3.25 kPa, 44 mm
diameter round tube)99
Figure 46: Smoked foil records of a spinning detonation (C ₂ H ₂ +5N ₂ O +50%Ar,
p ₀ = 3.5 kPa, 6.35 mm channel)100
Figure 47: Comparison between measured and computed values of α from
acoustic theory in $C_2H_2 + 2.5O_2 + 70\%$ Ar for round tubes101
Figure 48: Comparison between measured and computed values of α from
acoustic theory in CH ₄ + 2O ₂ for round tubes
Figure 49: Comparison between measured and computed values of α from
acoustic theory in C ₂ H ₂ + 5N ₂ O +50%Ar for round tubes103
Figure 50: Variation of angle with mode n in C_2H_2 + 2.5 O_2 +70%Ar mixture in
annular channels104
Figure 51: Variation of angle α with mode n in CH_4 + $2O_2$ mixtures in annular
channels

Figure 52: Variation of track angle α with mode n in C ₂ H ₂ + 5N ₂ O +50%Ar
mixtures in annular channels
Figure 53: Typical pressure trace well within the limit (C_2H_2 +2.5 O_2 +70% Ar,
9.525 mm channel)
Figure 54: Pressure trace of a spinning detonation (CH $_4$ +2O $_2$, p $_0$ = 4 kPa, 65 mm
diameter tube)108
Figure 55: Pressure trace outside the limits of detonation ($C_2H_2+5N_20+50\%Ar$, 65
mm diameter tube, p_0 = 1.25 kPa)109
Figure 56: Theoretical and experimental values of track angle α in hydrogen-
oxygen mixtures in round tube110

LIST OF TABLES

Table 1: Range of initial pressures at which spinning detonations were observed	d
in round tubes	32
Table 2: Range of initial pressures at which spinning detonations were observed	d
in annular channels	33
Table 3: Values of k _{m1} for the circumferential mode	43
Table 4: Dimensions of the three annular channels	45
Table 5: Roots of the cross product Bessel functions	46

Chapter 1

Introduction

1.1 General overview

The present thesis describes a study on the near-limit propagation of detonation. Detonation limits refer to the conditions where a detonation wave can no longer propagate. For example, given an explosive mixture, excessive amount of inert dilution, too rich or too lean mixture composition, too low an initial pressure or too small a tube diameter will result in the detonation limits. Consider the case of reducing the tube diameter. Well within the limit, the detonation generally propagates at a steady velocity close to the theoretical Chapman-Jouguet (CJ) value. As the limit is approached by reducing the tube diameter, the detonation velocity is observed to decrease and deviate from the CJ value. The structure of the detonation also tends towards lower unstable modes. Near the limit, the detonation can also become unstable and the detonation velocity can fluctuate. Further approach towards the limits leads to larger velocity deficit and fluctuations. Near the limit there exists a continuous spectrum of unstable behaviour before failure occurs. The following literature review presents the past studies on detonation limits.

1.2 Literature review

The first systematic study on detonation limit was carried out by Wendlandt (1924,1925) who measured the detonation velocity in a 5 m long 20 mm diameter tube for hydrogen-air and carbon monoxide-oxygen mixtures for different mixture composition at atmospheric pressure. It was observed that, for example, above 18% of hydrogen concentration in hydrogen-air mixture a constant detonation velocity is measure along the tube while the velocity continuously decreases along the tube in leaner mixtures. The concentration limit was determined when a drop in detonation velocity was observed in the tube.

Breton (1936a, 1936b) measured the detonation velocity in a small diameter tube for various explosive mixtures as the mixture composition was varied from rich to lean. A limit of detonation was determined when no stable detonation was observed. Breton's study reported the concentration limit for a dozen of explosive mixtures.

Zeldovich (1940) was perhaps the first to develop a detonation limit theory which considered the effect of heat and momentum losses to the tube wall. The model predicts that the velocity deficit is proportional to the total losses to the wall divided by the total momentum of the detonation. Viscous drag is proportional to the circumference of the tube multiplied by the reaction zone length while the total momentum of the detonation is proportional to the tube area

multiplied by the reaction zone thickness. Thus the model predicts that the detonation velocity decreases as the tube diameter is reduced. Manson and Guénoche (1956) also proposed a model based on heat losses to the wall that result in quenching of a layer of mixture adjacent to the tube walls. Therefore, the total chemical energy supplied to support the propagation of the detonation is reduced which leads to velocity deficit.

Belles (1958) attempted to define the limits based on the chemical kinetics of hydrogen-oxygen mixtures. A minimum detonation velocity can be computed based on the critical temperature where chain termination dominates chain branching reactions. The chemical kinetic condition for chain-branching is first defined in terms of pressure, temperature and mixture composition. The temperature and pressure of the shocked but unreacted mixture is determined using shock equations while the Mach number is determined from the shock velocity. The expressions are then combined with the explosion conditions in terms of Mach number and mixture composition in order to determine the critical shock strength required for explosion to occur. Detonation limit is reached if the mixture cannot support the shock strength required for explosion.

Fay (1959) later argued that Zeldovich's interpretation of the losses as uniformly distributed across the detonation cross section was incorrect. Fay pointed out that the boundary layer causes the streamlines to diverge in the

reaction zone and reduce the detonation velocity. The effect of the boundary layer can be modeled by the flow of an inviscid fluid through an expanding nozzle. The fractional area increase is proportional to the tube circumference multiplied by the displacement thickness and divided by the cross-sectional area of the tube. The velocity deficit becomes proportional to the displacement thickness divided by the tube diameter. If the limit is approached by reducing the initial pressure the reaction zone length increases and consequently increases the displacement thickness. More mass would then leak into the boundary layer resulting in larger velocity deficit. For a given initial pressure, if the tube diameter is reduced the effect of the boundary layer is more dominant and results into larger velocity deficits. Fay mentioned that a consequence of the effect of boundary layer is to cause a curved detonation wave.

Gordon et al. (1959) studied detonation limits in a 12 m long 20 mm diameter tube by reducing the initial pressure and varying the mixture composition in hydrogen-air, hydrogen-oxygen and hydrogen-oxygen-diluent mixtures. Single head spinning detonations were observed over a wide range of conditions near the limit. Both the pressure and composition limit was determined when no steady velocity can be observed. Particularly in hydrogen-air mixtures, the detonation became unstable and velocity fluctuations became larger near the limit. For different diameter tubes (ranging from 1.5 to 12 mm), Pusch and

Wagner (1962) varied the mixture composition of methane-oxygen from rich to lean and determine the limiting tube diameter. The detonation was recorded using a rotating drum camera. The detonation velocity was determined from the slope of the luminous trace. As the limit was approached, the detonation became unstable. The limit was defined when no steady velocity can be measured from the photographs. The smallest limiting tube diameter was found near stoichiometric conditions.

For different diameter tubes (ranging from 12 to 52 mm), Manson et al. (1962) approached the limit in propane-oxygen mixtures at atmospheric pressure by adding nitrogen diluents. From streak schlieren photographs of the detonation, the frequency of vibration in the burnt gas was observed to decrease and the amplitude of oscillation increased as the limit was approached. Manson et al. measured the local and average detonation velocity. Detonation limit was defined as the deviation of the local velocity from the average velocity by 0.4%.

Moen et al. (1981) studied detonation limits in ethylene mixtures by varying the mixture composition in tubes of 28, 48 and 145 mm in diameter. The detonation velocity and the frequency of pressure oscillations were measured. Well within the limits the frequency was high and was observed to decrease as the limit was approached. Single head spinning detonation was observed over a wide range of mixture compositions near the limit and the limit was defined as the

onset of single head spin. Donato (1982) studied detonation limits by varying the composition of ethylene-air mixtures in different diameter tubes. It was observed that past the onset of single head spin the detonation was unable to recover its structure if perturbed and failed. Therefore, conditions past the onset of single head spin are outside of the detonation limit.

Lee (1984) proposed a limit criterion for circular tubes as $\lambda = \pi d$, λ representing the cell size or transverse wave spacing and d being the tube diameter. The parameter corresponds to the first onset of single-head spin. It was obtained from equating the longest characteristic time of the transverse vibration to the characteristic time for the chemical reactions. Dupré et al. (1986) studied limits by varying the composition of lean hydrogen-air mixtures at atmospheric pressure in tubes of decreasing diameter (from 152 to 38 mm). The detonation velocity was measured and smoked foil records were taken. It was observed that past $\lambda = \pi d$ the detonation was unstable and exhibited large velocity fluctuation. On the basis of wave stability, the work of Dupré et al. validated the limit criterion of $\lambda = \pi d$ for round tubes.

Laberge et al. (1993) studied the propagation of detonations in bundles of small diameter tubes (1.69, 5.46 and 11.55 mm in diameter). The detonation velocity was measured as the initial pressure of the mixture is reduced. For equimolar acetylene-oxygen and stoichiometric methane-oxygen mixtures, a

maximum velocity deficit of 15% CJ values was observed before the detonation failed. In acetylene-nitrous oxide mixtures a large fluctuation in velocity deficit ranging from 4 to 13% was measured.

Lee et al. (1995) studied near-limit propagation of detonations in various explosive mixtures. Using a 38 mm diameter 10 m long tube, the limit was approached by reducing the initial pressure. The detonation velocity was continuously measured using a Doppler interferometer. Near the limit, highly unstable detonations with large velocity fluctuations were observed. Based on the magnitude and frequency of the fluctuations, Lee et al. classified six different behaviours: stable (constant velocity close to CJ values), rapid fluctuation, stuttering, galloping, low-velocity stable and failure. Acetylene-oxygen mixtures with high argon dilution were observed to only exhibit rapid fluctuations before failure while most mixtures were observed to exhibit a wider range of unstable behaviours.

Glassman (1996) revisited Belle's theory and argues that Belle's approach to determine the limit was questionable and that agreement between experiments and Belles' theory may be fortuitous. He criticizes that a given Mach number specifies the pressure and temperature behind the shock while the explosion condition expression also specifies temperature and pressure. It is

argued that it is unlikely that there is a direct correspondence of the two conditions from shock and explosion relationships.

More recent studies explored the influence of different boundary conditions on detonation limits. For example, Radulescu and Lee (2002) studied limits of detonation propagating in tubes with porous walls. The limit was approached by decreasing the initial pressure of various mixtures. The detonation velocity was measured using streak photographs and open shutter photography. The detonation velocity decreased as the limit was approached. For most mixtures, a sudden decrease in velocity was observed when d/λ , the tube diameter over the transverse wave spacing ratio, reached a value of 4. A maximum velocity deficit of 30% was measured before the detonation failed. Radulescu and Lee claimed that failure was caused by the attenuation of transverse waves. In mixtures highly diluted with argon, the detonation velocity precipitously decreased when d/λ reached a value of 11. A maximum velocity deficit of about 20% CJ value was measured. For this type of mixture, Radulescu and Lee state that failure was caused by curvature.

Ishii et al. (2002) investigated the propagation of detonations in narrow rectangular channels. The limit was approached by reducing the channel height for various hydrogen-oxygen-argon mixtures. The detonation velocity was measured and soot covered foils were used to record the detonation structure

near the limit. As the limit was approached, the detonation velocity was observed to fluctuate and fluctuations were larger near the limit. Near the limit, a zig-zag detonation, analogous to spinning detonation in circular tubes, was observed.

Chao et al. (2009) studied detonation limits of hydrogen-oxygen and acetylene-oxygen mixtures with over 50% of argon dilution in 360 mm long annular channels. The detonation velocity was measured as the limit was approached by reducing the initial pressure. A maximum velocity deficit of about 25% CJ value was measured before failure of the detonation occurred.

Jackson et al. (2009) criticizes that Lee et al. (1995) used a single tube diameter of 38 mm to study the different regimes of velocity fluctuation near the limit. Therefore, Jackson et al. investigated the propagation of detonations of propane and hydrogen mixtures in smaller diameter tubes (1.27 and 6.35 mm diameter). The detonation velocity was measured using a high speed camera. As the limit was approached by reducing the initial pressure the detonation velocity was observed to decrease. In the largest diameter tube, a sharp decrease in the velocity was observed near the limit while a more gradual decrease in observed in the smallest diameter tube. In hydrogen mixtures, a velocity deficit of 20% CJ value was observed near the limit whereas a velocity deficit of up to 50% was measured in propane mixtures. The detonation velocity normalized by the CJ value was found to decrease linearly as the induction zone length normalized by

the tube radius increased. Near the limit, the detonation velocity was observed to fluctuate. Based on the frequency and magnitude of the fluctuations four out of six velocity regimes classified by Lee et al. (1995) were observed in smaller diameter tubes: steady, stuttering, galloping and failure.

Kitano et al. (2009) studied the propagation of detonations in various small diameter tubes. The detonation limit in hydrogen-oxygen mixture was approached by reducing the initial pressure. The detonation velocity was measured and smoke foil records were taken. The detonation velocity decreased as the limit was approached and a velocity deficit of 15% was measured near the limit. Near the limit, single head spinning detonations were observed over a wide range of initial pressures. In methane-oxygen mixtures, galloping detonations were observed near the limit. Fischer et al. (2009) studied detonation limits of stoichiometric ethene-oxygen mixtures in capillary tubes. The limit was approached by reducing the initial pressure. The detonation velocity was measured and was observed to decrease as the limit was approached. A velocity deficit as high as 50% CJ value was measured near the limit.

Camargo et al. (2010) studied the near-limit propagation of detonations of different mixtures in small diameter tubes. The limit was approached by reducing the initial pressure. The detonation velocity was measured and streak photographs of the detonation were taken. As the limit was approached, the

detonation velocity decreased and was observed to fluctuate near the limit. In stoichiometric acetylene-oxygen and stoichiometric acetylene-oxygen with high argon diluted mixtures a velocity deficit of 15% was measured near the limit. Spinning detonations were observed near the limit. Galloping detonations were observed near the limit in stoichiometric methane-oxygen mixtures.

Ishii and Monwar (2011) studied detonation limits of hydrogen-oxygen mixtures with argon or nitrogen dilution in narrow channels. The limit was approached by reducing the channel gap. The detonation velocity was measured and smoked foil records were taken. The detonation velocity decreased as the limit was approached. A maximum velocity deficit of 15% was measured for stable propagation of detonations. The limit was defined when no steady velocity can be measured. Galloping detonations were observed in nitrogen diluted mixtures.

1.3 State of the art on detonation limits

Based on the previous studies, detonation limits were found to depend on both initial conditions (mixture composition, amount of inert diluents, initial pressure) and boundary conditions (tube dimension, geometry, wall surface). However, detonation limit is not a sharp boundary which separates the propagation of detonations from failure. There exists a range of initial and boundary conditions where the propagation of the detonation is uncertain. It is

not possible to precisely determine the limits experimentally since an operational definition of the limit does not exist. For this reason, detonation limit has generally been defined arbitrarily. For example, detonation limit have been determined based on the stability of the detonation velocity (Manson et al. 1962). Limits have also been determined based on the onset of spinning detonation (Moen et al. 1981). The state of the art on detonation limit is that a limit criterion is lacking and a quantitative theory for predicting the limit does not exist. As the limit is approached, it becomes increasingly difficult to initiate a detonation. Failure to initiate a detonation due to experimental limitations may be mistaken as the detonation limits. For this reason, it is important to focus on describing the near-limit propagation of detonation.

1.4 Current study

Most of the studies on detonation limits have been carried out in circular tubes and studies in other geometries are superficial. The current study concentrates on describing the near-limit propagation of detonations in both circular tubes and annular channels. By having the annular channel gap small compared to the radius, curvature effects may be neglected and an ideal two-dimensional geometry can be achieved. The near-limit propagation of detonations in two-dimensional annular channels will be compared to that in circular tubes to elucidate the effect of geometry on the near-limit propagation of

detonations. A wide range of explosive mixtures are considered to investigate any difference in the near-limit propagation of detonations.

Chapter 2

Experimental details

2.1 Detonation tube

The experimental apparatus consists of a 0.3 m long, 25.4 mm diameter steel driver section followed by a steel detonation tube totalling 4.16m in length with an inner diameter of 65 mm. The annular channel test section is created by inserting a brass tube supported by fins into the end of the detonation tube. The leading edge of the brass tube is chamfered to prevent any wave process from affecting the propagation of the detonation wave. Three brass tubes are used to create three annular channel gaps: w = 3.175, 6.35 and 9.525 mm. A schematic of the experimental apparatus is shown in Fig. 1a. Experiments are also conducted in the 65 mm diameter detonation tube without brass tubes for comparison.

2.2 Ignition system

Ignition of the detonation is achieved through a high energy spark by discharging a high voltage capacitor. To help initiate a detonation wave, a sensitive mixture of equimolar acetylene and oxygen was released into the driver section seconds before ignition. Shchelkin spirals are placed in the driver section and in the detonation tube to facilitate the establishment of a detonation wave.

2.3 Explosive mixture selection and preparation

Three explosive mixtures are studied. A stoichiometric mixture of acetylene and oxygen diluted with 70% of argon is chosen for its regular cellular pattern characteristics (Stehlow 1968, Radulescu and Lee 2002, Lee 2008) and its piecewise laminar detonation structure (Pintgen 2003). A stoichiometric mixture of methane and oxygen and a stoichiometric composition of acetylene and nitrous oxide diluted with 50% of argon are used for their irregular cellular pattern (Stehlow 1968, Laberge et al. 1993, Lee 2008) and a rather turbulent reaction zone structure (Lee 2008, Shepherd 2009). An equimolar mixture of acetylene and oxygen is used as a driver mixture. The explosive mixtures are prepared in separate vessels by the method of partial pressure. They are left to mix for at least 24 hours to ensure homogeneity.

2.4 Experimental procedures

The detonation tube is first vacuumed. The detonation tube is filled with the explosive mixture through a manifold. The detonation tube is initially overfilled to ensure a uniform distribution of the mixture in the experimental apparatus. The mixture is then slowly evacuated to the desired initial pressure. In a 500 cc pressure vessel connected to the driver section through a valve, a certain amount of driver mixture is filled. Prior to ignition, the driver mixture is released

into the driver section. For a given annular channel gap, the limit is approached by reducing the initial pressure of the explosive mixture.

2.5 Diagnostics

PCB pressure transducers are used to monitor the pressure rise and pressure profile of the detonation wave. A typical pressure trace is shown in Fig.2. Up to 4 pressure transducers can be used in the test section. In the annular test section, a total of 12 optics fibres, roughly 130 mm apart, are mounted flush to the inner diameter of the detonation tube and connected to a circuit of photoprobes shown in Fig.3. Typical photoprobe traces are shown in Fig. 4. These diagnostics provide the time of arrival of the combustion wave from which the trajectory of the detonation can be determined. The detonation velocity is determined by taking the slope of the trajectory as shown in Fig. 5. For additional detonation velocity data in round tubes, the average velocity of the detonation propagating inside the brass tube was measured using an additional PCB pressure transducer mounted on the end flange. All pressure transducers and optic fibre signals where recorded on a LeCroy oscilloscope.

Smoked foil technique is used to study the structure of the detonation wave. Clear Mylar sheets are uniformly covered with soot using a kerosene lamp.

The sheets are cooled using a wet cloth to prevent warping from heat, and to

facilitate the deposition of soot. To obtain records of the detonation structure in a 65 mm diameter round tube, the Mylar sheet was placed along the detonation tube. To obtain records of the detonation structure in annular channels, the Mylar sheet is placed either around the brass tube or along the detonation tube. A Mylar sheet is also placed inside the brass tube to simultaneously collect records of the detonation structure in round tubes. Figure 6 shows a typical smoke foil record of a detonation. Cell size measurements are obtained by first hand tracing the main transverse wave trajectories. Several transverse wave spacing measurements of dominant bands were taken and averaged to obtain a characteristic representation of the cell size.

Chapter 3

Results and discussion

3.1 Detonation velocity

The detonation velocity is obtained from the slope of the trajectory in both round tubes and annular channels. Figure 7 shows an example of the trajectory of the detonation wave in a 65 mm diameter round tube. The x-axis indicates the position of the various photoprobes and the y-axis indicates the time of arrival of the wave. At an initial pressure of p₀= 15 kPa the detonation is found to propagate at 1717 m/s. Using the Chemical Equilibrium and Applications (CEA) program to calculate the CJ velocity, the detonation is found to propagate at about 98% of CJ value. At a lower initial pressure, p₀= 3 kPa, the detonation propagates at about 95% of CJ value. When outside of the limit no steady velocity can be measured from the trajectory and Fig. 8 shows an example of this.

3.1.1 Round tubes

Figure 9, Figure 10 and Figure 11 show the variation of the detonation velocity normalized with CJ value as a function of initial pressure in round tubes for $C_2H_2 + 2.5O_2 + 70\%Ar$, $CH_4 + 2O_2$ and $C_2H_2 + 5N_2O + 50\%Ar$ mixtures, respectively. The trends of the experimental results are also shown. Well within

the limits of detonation in round tubes, the detonation velocity is within a few percent of theoretical CJ values. As the limit is approached by reducing the initial pressure the detonation velocity progressively decreases and deviates from the CJ value. It is well knows that as the initial pressure is reduced the reaction zone length increases allowing more losses, either by boundary layer divergence according to Fay (1959) or by quenching of the reaction as proposed by Manson and Guénoche (1956), which results in larger velocity deficit.

For a given initial pressure the detonation velocity decreases as the tube diameter is reduced. For example, at an initial pressure of p_0 = 5 kPa, the detonation velocity is about 95% of CJ in the larger tubes and about 90% of CJ value in the smaller diameter tube. For a given initial pressure, as the tube diameter is reduced the effect of the boundary layer is more dominant and results into larger velocity deficits. Note that experimental results for $C_2H_2 + 2.5O_2 + 70\%$ Ar, $CH_4 + 2O_2$ do not indicate a significant difference in detonation velocity between a 65 and 44 mm diameter tube.

Near the limit, a sharp decrease in the detonation velocity is observed while a more gradual decrease in velocity is observed in smaller diameter tube for $C_2H_2 + 2.5O_2 + 70\%$ Ar and $C_2H_2 + 5N_2O + 50\%$ Ar mixtures. Experimental results from Fischer et al. (2009) and Jackson et al. (2009) also indicate a gradual decrease in velocity for smaller diameter tubes.

The minimum detonation velocity observed in round tubes depends on both the mixture and the tube diameter. For $C_2H_2 + 2.5O_2 + 70\%$ Ar and and $C_2H_2 + 5N_2O + 50\%$ Ar mixtures, the minimum detonation velocity was found to be about 85% and 88% of the CJ value, respectively, regardless of the tube diameter. In larger diameter tubes, the minimum detonation velocity is about 80% of CJ values in $CH_4 + 2O_2$. In smaller diameter tubes, the minimum detonation velocity is higher; about 85% of CJ value. The obtained results are within reasonable agreement with past observation (Laberge et al. 1993, Lee 2008) where the minimum detonation velocity in smooth round tubes is about 85% CJ value.

In larger diameter tubes the limiting pressure is about p_0 = 1.5 kPa in both $C_2H_2 + 2.5O_2 + 70\%$ Ar and $C_2H_2 + 5N_2O + 50\%$ Ar mixtures and about p_0 = 3 kPa in CH₄ + 2O₂ mixtures. In smaller diameter tubes, the limiting pressure is higher; p_0 = 3 kPa, p_0 = 12 kPa and p_0 = 2.5 kPa for $C_2H_2 + 2.5O_2 + 70\%$ Ar, $CH_4 + 2O_2$ and $C_2H_2 + 5N_2O + 50\%$ Ar mixtures, respectively. Below p_0 = 12 kPa for CH₄ + 2O₂ mixtures pulsating and galloping detonations where observed in the smaller diameter tube. Galloping detonations are only observed in the small-diameter smooth tube where, according to Manzhalei (1992), the boundary layer exerts a greater effect on the flow behind the shock.

3.1.2. Annular channels

Figure 12, Figure 13 and Figure 14 show the variation of the detonation velocity normalized with CJ value as a function of initial pressure in annular channels for $C_2H_2 + 2.5O_2 + 70\%Ar$, $CH_4 + 2O_2$ and $C_2H_2 + 5N_2O + 50\%Ar$ mixtures, respectively. Experimental data from a 44 mm diameter round tube is also included for comparison. Well within the detonation limit in annular channels, the detonation velocity is within 10% of CJ values. This observation indicates that even well within the limit the annular channel geometry has an effect of reducing the detonation velocity. As the limit is approached by decreasing the initial pressure the detonation is subjected to more losses: the detonation velocity progressively decreases and deviates from the CJ values. For a given initial pressure, the detonation velocity decreases with decreasing annular channel gap. As the channel gap is reduced, the detonation is subjected to more losses causing larger velocity deficit. For example, it can be observed from Fig. 12 that at p₀=10 kPa in acetylene-oxygen mixtures diluted with 70% of argon, the velocity deficit is about 10% CJ values in the 9.525 and 6.35 mm channels and about 20% in the 3.175 mm channel. In all mixtures, a sharp decrease in the velocity is observed near the limit in the two larger channels while a more gradual decrease in velocity is observed in the thinnest channel.

An effect of a two-dimensional annular channel is to reduce the minimum measured detonation velocity than in round tubes. In $C_2H_2 + 2.5O_2 + 70\%$ Ar mixtures, the minimum detonation velocity in annular channels is about 70% of the CJ value. A common minimum detonation velocity in annular channels may imply that once the temperature in the reaction zone falls below an auto-ignition value, shock compression is no longer sufficient to support the detonation.

In $C_2H_2 + 5N_2O + 50\%$ Ar mixtures, the minimum detonation velocity is about 80% of CJ values for the larger channels and about 70% in the thinnest channel. In CH₄ + 2O₂ mixtures, the minimum detonation velocity is about 75% CJ value in the larger channel, and can be as low as about 55% CJ values in thinner annular channels. This observation is reminiscent of low-velocity detonations observed in rough-walled tubes (Schelkin 1940) and small diameter tubes (Manzhalei 1992). At such low velocities, the shock strength is too low to cause auto-ignition of the mixture. However, the tube wall roughness produces turbulence and transverse shocks that create local high-temperatures (hot spots) (Lee 2008). Their combined effects can maintain a sufficiently fast reaction rate to sustain the propagation of the detonation. Similarly, in CH₄ + 2O₂ mixtures, although the average propagation velocity may be as low as nearly half CJ values, transverse waves may provide local high-temperatures to ignite the mixture. Once the chemical reactions are initiated, the reaction front spreads to

neighbouring unreacted regions. The turbulent boundary layer would promote rapid mixing to maintain a sufficiently high burning rate in the reaction zone.

Near the limit, experiments become irreproducible. There exists a range of initial pressures where a steady detonation velocity is not always measured in the annular channel test section. In acetylene-oxygen mixtures with high argon dilution, this range corresponds to initial pressures between 4 and 2.75 kPa, and 7 and 5.5 kPa in the 6.35 and 3.175 mm annular channels, respectively. In methane-oxygen mixtures, this range corresponds to between 6 and 4 kPa in the 3.175 mm annular channel. A wider range of limiting pressures is observed in thinner channels.

3.1.3 Velocity deficit according to Fay's model

Assuming velocity deficit is a result of flow divergence in the reaction zone, the detonation velocity was computed based on Fay's model (see Appendix A). Figure 15 and Figure 16 show the variation of the computed normalized detonation velocity with initial pressure from the quasi-steady ZND analysis in annular channels in $C_2H_2 + 2.5O_2 + 70\%$ Ar and $CH_4 + 2O_2$ mixtures, respectively. Well within the limit, the computed detonation velocities in all three annular channels are very close to each other in both mixtures. As the limit is approached, the computed normalized detonation velocity progressively decreases. Near the limit, a precipitous drop in the normalized velocity is

predicted in all three annular channels. In $C_2H_2 + 2.5O_2 + 70\%$ Ar mixture, the model predicts a minimum detonation velocity of about 70% of CJ values, whereas in $CH_4 + 2O_2$ mixture a minimum detonation velocity of about 80 to 85% of CJ value is predicted. The predicted critical pressure is different between the two mixtures. For example, the limiting initial pressure in a 3.175 mm annular channel gap is about $p_0 = 3$ kPa in $C_2H_2 + 2.5O_2 + 70\%$ Ar mixture whereas it is about $p_0 = 34$ kPa in $CH_4 + 2O_2$ mixture.

In reality, a detonation possesses a transient three-dimensional cellular structure. Therefore a quantitative agreement between the Fay's model and experimental results is not expected. Nevertheless, comparisons between the detonation velocities based on Fay's model and experimental results have been made in the past (Fay 1959, Moen et al. 1985, Murray and Lee 1986, Laberge et al. 1993, Radulescu and Lee 2002, Chao et al. 2009, Camargo et al. 2010). A similar comparison is made in this study. Fig. 17 and Fig.18 compare the computed detonation velocity using Fay's model with experimental results for $C_2H_2 + 2.5O_2 + 70\%$ Ar mixture in 9.525 and 3.175 mm annular channels, respectively. The model qualitatively describes the variation of the detonation velocity as the limit is approached in the larger annular channel. The model captures the sharp velocity decrease near the limit in larger channels but fails to capture the gradual velocity decrease near the limit in thinner channels. Fay's

model also quantitatively captures the minimum detonation velocity in annular channels, though the agreement is fortuitous because of the assumptions made in Fay's model.

Figure 19 and Figure 20 compare the computed detonation velocity using Fay's theory with experimental results for $CH_4 + 2O_2$ mixture in 9.525 and 3.175 mm annular channels, respectively. It can be observed that Fay's model is not in agreement with experimental results. The model underestimates the detonation velocity for all initial pressures, fails to predict the minimum detonation velocity and fails to capture the gradual velocity decrease in thinner channels.

3.1.4 ZND induction length analysis

A common feature between the different mixtures is that as the limit is approached by reducing the initial pressure the cell size and reaction zone length increases. Therefore, it is of interest to investigate the variation of the detonation velocity with respect to a reaction zone length to see any correlation between the different mixtures. Figure 21 shows the variation of the normalized detonation velocity in $C_2H_2 + 2.5O_2 + 70\%$ Ar for larger diameter tubes and annular channels with respect to the inverse of the inverse ratio of the theoretical ZND induction zone length, computed using the Konnov chemical kinetic mechanism [24]. The ZND induction zone length is taken as the chemical sensitivity length scale.

Comparing Fig. 21 with Fig. 12 it can be observed that the detonation velocity varies similarly with both initial pressure and the ZND induction length.

A geometrical factor is then introduced by normalizing the induction length by either the channel gap or the tube diameter. Figure 22 show the variation of the normalized detonation velocity in C₂H₂ + 2.5O₂ + 70%Ar mixtures with the parameter L/Δ_{ZND} , where the parameter L denotes either the channel gap or tube diameter. The trends of the experimental results are also included. The parameter L/Δ_{ZND} represents the relative role of the geometry, manifested by wall losses, with respect to the chemical sensitivity of the mixture. The first observation from Fig. 22 is that the results from the different annular channels coalesce onto a single curve. This is also observed in CH₄ +2O₂ and C₂H₂ + 5N₂O + 50%Ar mixtures as shown in Fig. 23 and Fig. 24, respectively. The experimental results indicate that well within the limits of detonation, where the value of the parameter L/Δ_{ZND} is large, boundary conditions do not influence the detonation wave resulting in a small velocity deficit. As the limit is approached and L/Δ_{ZND} decreases boundary conditions start to influence the detonation wave resulting in larger velocity deficits.

3.2 Detonation structure

A detonation typically possesses a cellular structure. The front is composed of Mach stems and incident shocks. Reflected shocks, or transverse waves, are joined to the front and extend well into the burnt gases. The intersection of the Mach stem, incident shock and transverse wave is called the triple point. As the detonation propagates along a soot covered foil, the triple point displaces the soot and leaves markings of its passage. Fig. 25 is a sketch of an idealized two-dimensional detonation, propagating from bottom to top, highlighting the key features of its structure. Note that as the detonation propagates, the Mach stem and incident shock are interchanged. Using smoked foils as a record of the history of the detonation structure, the evolution of the structure is studied as the limit is approached in both round tubes and annular channels. The direction of propagation in all smoked foil records is from bottom to top.

3.2.1 Cell structure: well within the limit

Well within the limit, the structure of the detonation is independent of the geometry. Smoked foil records under the similar initial conditions, for example Fig. 26 and Fig. 27, indicate that the structure in round tubes and annular channels are similar. Typical smoked foil records from $C_2H_2 + 2.5O_2 + 70\%$ Ar

mixtures, such as Fig. 26, show regular transverse wave spacing and transverse wave trajectories may be described as straight lines. Smoked foil records from methane-oxygen and acetylene-nitrous oxide mixture reveal detonations with an irregular cellular pattern, as shown by Fig. 28 and Fig. 29, respectively. The tracks of the transverse waves are thin wavy lines and substructures can be observed. Well within the limit, the transverse wave spacing is small compared to the dimensions of the tube or annular channel. Different experiments conducted under the same initial conditions indicate that the structure of the detonation is globally reproducible.

3.2.2 Cell structure: approaching the limit

3.2.2.1 General observations

As the limit is approached by reducing the initial pressure, the structure of the detonation tends towards lower modes; a progressive increase in transverse wave spacing is observed, as indicated by Fig. 30, Fig. 31 and Fig. 32 for C₂H₂ +2.5O₂ +70%Ar, CH₄ +2O₂ and C₂H₂ +5N₂O +50%Ar mixtures, respectively, in round tubes. Cell size measurements from the detonation database [GALCIT Explosion Dynamics Laboratory Detonation Database] are also included for comparison in Fig. 30 and Fig. 31. Good agreement is observed between the measured cell size and that of the database. The cell size measurements in

annular channels are shows in Fig. 33, Fig. 34 and Fig. 35. Measurements from a round tube are also included for comparison. No significant difference can be observed in the cell size measurement between round tubes and larger annular channels.

3.2.2.2 $C_2H_2 + 2.5O_2 + 70\%$ Ar

As the limit is approached, the detonation structure in $C_2H_2 + 2.5O_2 + 70\%$ Ar mixtures seems to lose its regularity, as illustrated by Fig. 36. Transverse wave trajectories become wavy and the transverse wave spacing is less regular. As the limit is approached, the structure of the detonation becomes irreproducible.

In larger annular channels, the markings left by the passage of the triple point become fainter and it is harder to distinguish the main trajectories from substructures, as exemplified in Fig. 37. Further approaching the limit, the trajectories are observed to become fainter and disappear.

The detonation structure is significantly affected by the boundary layer in the thinnest annular channel. Typical smoked foil records, such as Fig. 38, show wavy transverse wave trajectories and detonations which no longer possess a regular cellular pattern.

3.2.2.3 CH₄ +2O₂

Based on a large number of smoked foils from round tubes, the detonation structure near the limit does not seem to fluctuate significantly for CH₄ +2O₂ mixture. Figure 39 and Figure 40 show typical smoked foil records of the detonation at an initial pressure of 7.5 and 4 kPa in a 44 mm diameter tube. Smoked foil records from this range of initial pressure repeatedly show two transverse waves. In methane-oxygen mixtures, transverse waves disappear and regenerate continuously resulting in the irregular cellular pattern. Perturbation from the boundary layer in large diameter tubes may not significantly alter the decay and regeneration of transverse waves (Gamezo et al. 1999, Lee 2008).

As the limit is approached in annular channels the tracks left by the transverse waves become progressively wider and less defined, as illustrated by Fig. 41, whereas the markings remain thin and faint in round tubes. As the limit is further approached, more soot is removed and the markings become faint and disappear. Particularly in the thinnest channel, larger area of soot removal is observed, as illustrated by Fig. 42. It is possible that the non-uniform flow behind the detonation sweeps the soot resulting in large area of soot removal.

3.2.2.4 $C_2H_2 + 5N_2O + 50\%$ Ar

In C₂H₂ +5N₂O +50%Ar mixtures, the detonation structure is irreproducible near the limit. In annular channels, the main trajectories become more prominent compared to substructures. As the limit is approached in thinner annular channels, the wave trajectories become increasingly wavy and both fine and large substructures are observed, as shown in Fig. 43. The cell size is noticeably larger in the thinnest channel.

3.2.3 Near the limit: spinning structure

Near the limit, the structure of the detonation is that of a spinning detonation in both round tubes and annular channels. Figure 44 shows a typical smoked foil record of spinning detonation in round tubes. Generally, the helical trajectory is observed to be a thin wavy line implying that the transverse wave is unstable. The helical path can also be a wide band, such as in Fig. 45. The finite width the helical track is due to a transverse shock sweeping into the compressed yet unburned gas behind the incident shock. Looking at the internal structure of the band, sets of transverse waves forming diamond patterns can be observed. As the limit is further approached, past the onset of single head spin, the tracks left by the passage of the transverse waves become faint and

disappear. For all mixtures, spinning detonations were observed over a range of pressures in round tubes and is summarized in Table 1.

Mixture Tube diameter	65 mm	44 mm	38 mm
C ₂ H ₂ + 2.5O ₂ + 70% Ar	2 – 1.75 kPa	2 – 1.75 kPa	2.5 – 2
CH ₄ +2O ₂	6 – 3.25 kPa	4 – 3.25 kPa	
C ₂ H ₂ +5N ₂ O +50% Ar	2.5 – 1 kPa	4 – 3 kPa	3

Table 1: Range of initial pressures at which spinning detonations were observed in round tubes

The observation of a single transverse wave propagating around the annulus, analogous to a spinning detonation in round tubes, is in agreement with Campbell and Finch (1928) who were the first to report a spinning detonation in an annular geometry. In contrast with round tubes, spinning detonations in annular channels are not repeatedly observed prior to failure. It is possible that the spinning structure is only observed in a very narrow range of conditions. Table 2 summarizes the initial pressures where spinning detonations were observed in annular channels. Figure 46 shows an example of a spinning detonation in annular channels for $C_2H_2 + 5N_2O + 50\%$ Ar mixtures. Substructures

generated by the transverse shock can be observed behind the main track and larger substructures generated by the Mach stem are visible ahead of the track.

Mixture annular channel	9.525 mm	6.35 mm	3.175 mm
C ₂ H ₂ + 2.5O ₂ + 70% Ar		4 kPa	7 kPa
CH ₄ +2O ₂	4 kPa		7 kPa
C ₂ H ₂ +5N ₂ O +50% Ar	3.5 – 3 kPa	3.5 kPa	

Table 2: Range of initial pressures at which spinning detonations were observed in annular channels.

3.2.2 Track angle

3.2.2.1 Round tube

Well within the limit, the angle between the transverse wave trajectory and the tube axis is about 33 degrees, regardless of mixture composition, and is in agreement with the acoustic theory (See Appendix). As the limit is approached, the detonation structure tends to lower vibrational modes and the track angle increases. Figure 47 to Figure 49 shows the measured track angle near the limit for $C_2H_2 + 2.5O_2 + 70\%$ Ar, $CH_4 + 2O_2$ and $C_2H_2 + 5N_2O + 50\%$ Ar mixtures,

respectively. The track angle computed from the acoustic theory is also shown. In $C_2H_2 + 2.5O_2 + 70\%$ Ar, and $C_2H_2 + 5N_2O + 50\%$ Ar mixtures, the trend of the variation of the measured track angle with mode number is similar to the acoustic theory. Duff (1961) measured the track angle in $2H_2+O_2$ mixtures and observed a similar trend with the acoustic theory. Near the limit, a wider range of angles is measured for a given mode number. In methane-oxygen mixtures (Fig. 48), no definite trend can be observed.

3.2.2.2 Annular channels

Well within the limits, the angle between the wave trajectory and the tube axis is about 30 to 32 degrees and is in reasonable agreement with the acoustic theory. Figure 50 to Figure 52 show the variation of track angle with mode near the limit for $C_2H_2 + 2.5O_2 + 70\%$ Ar, $CH_4 + 2O_2$ and $C_2H_2 + 5N_2O + 50\%$ Ar mixtures, respectively, in annular channels. According to the acoustic theory, the track angle, for all practical purpose, remains invariant with mode number. In general, a wide range of track angle is obtained for lower modes, and a conclusive experimental trend cannot be obtained. Track angles as high as about 40 degrees have been measured when a single transverse wave is observed to propagate around the annulus. Deviation from the acoustic theory near the limit has also been reported in Fickett and Davis (1979) for rectangular

geometries. Disagreement with the acoustic theory indicates strong non-linear wave interactions near the limit.

3.3 Pressure traces

3.3.1 Well within the limit

Figure 53 show typical pressure profile behind a detonation at various locations in annular channels. In both round tube and annular channels, a sharp pressure rise is observed across the leading shock, followed by a progressive decrease in pressure due to Taylor expansion waves behind the detonation. The amplitude of the pressure oscillations behind the detonation front are relatively small compared to the initial pressure rise and are of relatively high frequency.

3.3.2 Near the limit: spinning

Near the limit, spinning detonations are observed both in round tubes and annular channels. Figure 54 shows a typical pressure profile of a single head spinning detonation. In both geometries a sharp spike in pressure is followed by smaller amplitude periodic pressure oscillations. The frequency of the pressure oscillations of spinning detonations corresponds approximately to the acoustic spin frequency. For example, the measured oscillation frequency in Fig. 54 is about 10 kHz while acoustic theory predicts about 11 kHz.

3.3.3 Outside the limit

When outside the limit, the pressure profile of the combustion wave is different from a detonation wave. A small gradual rise in pressure is observed following by large pressure oscillations can also be observed, such as in Fig. 55.

Chapter 4

Conclusion

The present research investigated the near-limit propagation of detonations in both circular tubes and annular channels. Varying the tube diameter from 65 to 13 mm does not significantly affect the measured minimum detonation velocity in $C_2H_2 + 2.5O_2 + 70\%Ar$ and $C_2H_2 + 5N_2O + 50\%Ar$ mixtures. In CH₄ + 2O₂ mixtures, the minimum detonation velocity in the smaller diameter tube is about 85% of the CJ value whereas it is about 80% of the CJ value in the larger diameter tubes. From the present study, it may be concluded that an effect of annular channels, compared to circular tubes, is to reduce the minimum detonation velocity. When the channel gap is normalized with the ZND induction length, it was observed that the normalized detonation velocity curves for the different channels coalesce onto a single curve. This implies that the detonation velocity depends on the relative role of losses to the channel wall to the chemical sensitivity of the mixture. Near the limit in annular channels, the detonation becomes unstable and the structure is less reproducible. Particularly in the thinnest channel, the detonation becomes highly unstable due to the effect of the thinner geometry and the more dominant boundary layer.

Appendix A: Fay's model

To compute the detonation velocity based on Fay's model, the detonation is modeled according to the one-dimensional ZND structure. According to the classical ZND model, the structure of a detonation is composed of a planar leading shock which adiabatically compresses the reactants to auto-ignition temperatures, followed by a reaction zone which converts the reactants into products. The chemical reactions release an amount of energy which increases the temperature. The pressure and density drop in the reaction zone. The expansion in the reaction zone provides a forward thrust to maintain the leading shock. The quasi-one-dimensional ZND structure equations including a flow divergence term and detailed chemical kinetics must be solved numerically to seek an eigenvalue solution for the detonation velocity. Flow divergence is modeled as flow of an inviscid fluid through an expanding nozzle. Assuming a quasi-one dimensional flow behind the leading shock, the conservation equations are written as:

$$\frac{d}{dx}(\rho uA) = 0$$

$$\rho u A \frac{du}{dx} + A \frac{dp}{dx} = 0$$

$$\frac{d}{dx}\bigg(h + u^2/2\bigg) = 0$$

$$u\frac{dy_i}{dx} = \frac{W_i\omega_i}{\rho} \qquad (i = 1, ... N_s)$$

where ρ , u, A, h, N_s , y_i W_i and ω_i are density, velocity, cross-sectional area, enthalpy, total number of species, mass fraction, molar mass and molar rate of production of species i, respectively. The effective cross-sectional area of the annular channel being $A = w + 2\delta^*$ at any given point the fractional area increase in an annular channel can be expressed as:

$$\xi(x) = \frac{1}{A} \frac{dA}{dx} = \frac{2}{w + 2\delta^*} \frac{d\delta^*}{dx},$$

where w is the channel height. The mass displacement thickness δ^* is obtained from Gooderum's (1958) boundary layer measurements in shock tubes:

$$\delta^* = 0.22x^{0.8} \left(\frac{\mu}{\rho D}\right)^{0.2}$$

where x, μ , ρ and D denote the distance from the shock (reaction zone length), viscosity of the gas in the boundary layer, initial density and detonation velocity, respectively.

The following represent the ZND model equations:

$$\frac{dp}{dt} = -\rho u^2 \frac{\dot{\sigma} - u\xi}{\eta}$$

$$\frac{d\rho}{dt} = -\rho \frac{\dot{\sigma} - uM^2 \xi}{\eta}$$

$$\frac{du}{dt} = u \frac{\sigma - u\xi}{\eta}$$

$$\frac{dy_i}{dt} = \frac{W_i \omega_i}{\rho} \qquad (i = 1, ... N_s)$$

$$\frac{dA}{dt} = Au\xi$$
with $\eta = 1 - M^2$

$$\dot{\sigma} = \sum_{i=1}^{N_s} \left(\frac{W}{W_i} - \frac{h_i}{c_n T}\right) \frac{dy_i}{dt}$$

where M, W, c_p and h_i are the Mach number, mean molar mass of the mixture, specific hear at constant pressure and the specific enthalpy of species i. The above equations along with the flow divergence term in the conservation of mass equation and detailed chemistry model are solved numerically using the CHEMKIN II package. Above a certain maximum velocity deficit (or curvature of the front) no steady ZND solution can be obtained.

Appendix B: Acoustic theory

In a detonation confined to a tube, the frequency of the transverse vibrations can be described by the linear acoustic theory and is dictated by the tube geometry. By solving the acoustic wave equation for a given geometry a spectrum of possible vibration modes is obtained.

Circular tubes

For a circular tube case, the wave equation in cylindrical form is

$$\frac{\partial^2 \Phi}{\partial r^2} + \frac{1}{r} \frac{\partial \Phi}{\partial r} + \frac{1}{r^2} \frac{\partial^2 \Phi}{\partial \theta^2} = \frac{1}{C^2} \frac{\partial^2 \Phi}{\partial t^2},\tag{1}$$

where ϕ is the potential function and \mathcal{C} is the sound speed. Using the separation of variables method, the potential function is assumed to have a solution of the following form:

$$\Phi(r,\theta,t) = R(r)\Theta(\theta)T(t). \tag{2}$$

Substituting the above into the differential equation and expanding, the following is obtained:

$$\frac{c^2}{R} \left(\frac{d^2 R}{dr^2} + \frac{1}{r} \frac{dR}{dr} \right) + \frac{c^2}{r^2 \theta} \frac{d^2 \theta}{d\theta^2} = \frac{1}{T} \frac{d^2 T}{dt^2} = -\omega^2$$
 (3)

Solving for the temporal component:

$$\frac{d^2T}{dt^2} + \omega^2 T = 0 \tag{4}$$

we obtain:

$$T(t) = A\sin(\omega t) + B\cos(\omega t). \tag{5}$$

Solving for the spatial component

$$\frac{r^2}{R} \left(\frac{d^2 R}{dr^2} + \frac{1}{r} \frac{dR}{dr} \right) + \frac{\omega^2}{c^2} r^2 = -\frac{1}{\theta} \frac{d^2 \Theta}{d\theta^2} = m^2$$
 (6)

$$\begin{cases} \frac{d^2\Theta}{d\theta^2} + m^2\theta = 0\\ \frac{d^2R}{dr^2} + \frac{1}{r}\frac{dR}{dr} + \left(\frac{\omega^2}{c^2} - \frac{m^2}{r^2}\right)R = 0 \end{cases}$$
 (7)

the following is obtained:

$$\Theta(\theta) = C\sin(m\theta) + D\cos(m\theta) \tag{8}$$

and

$$R(r) = EJ_m(\beta r) + FY_m(\beta r), \tag{9}$$

where J_m and Y_m are the Bessel function of the first and second kind respectively. The Bessel function of second kind must vanish by setting F to zero since the potential function must be finite at r=0. Applying the boundary conditions where the particle velocity normal to the wall vanishes gives:

$$u = \left(\frac{\partial \Phi}{\partial r}\right)_{r=R} = 0. \tag{10}$$

Thus,

$$J_m'(\beta r) = J_m'(k_{mn}) = 0, (11)$$

where k_{mn} is the root of the first derivative of the Bessel function. The integer m and n denote the number of circumferential and radial modes, respectively.

Considering only the circumferential mode, we take n = 1 and the numerical values of the first few modes of km1 are given in Table 3 below.

m	1	2	3	4	5
k _{m1}	1.84	3.05	4.20	5.32	6.41

Table 3: Values of k_{m1} for the circumferential mode

The frequency of vibration is given as

$$N = \frac{C * k_{mn}}{2\pi Rn}. (12)$$

The linear velocity of the transverse wave at the wall is given as

$$v_n = \frac{C * k_{mn}}{n}.$$
 (13)

Equating the time required for the transverse wave to travel around the circumference to the time needed to propagate the pitch (the longitudinal wave spacing), the following expression can be obtain

$$\frac{\pi d}{v_n} = \frac{p_n}{D}.$$
 (14)

Rearranging, an expression for the pitch to diameter is obtained as

$$\frac{p_n}{\mathrm{d}} = \frac{n\pi}{k_{mn}} \left(\frac{D}{C} \right). \tag{15}$$

The track angle can be related to the pitch to diameter expression by

$$\frac{p_n}{d} = \frac{\pi}{\tan \mathbb{R}\alpha}.$$
 (16)

Combining equation (15) and (16) to solve for α , the track angle is predicted by acoustic theory as

$$\alpha = tan^{-1}(\frac{Ck_{mn}}{nD}). \tag{17}$$

An equivalent expression for the track angle is

$$\alpha = tan^{-1} \left(\frac{\rho_0 k_{mn}}{\rho n}\right),\tag{18}$$

where ρ_0/ρ is the density ratio across the detonation wave. Duff (1961) obtained good agreement between the acoustic theory and experimental values of the track angle for detonations in hydrogen-oxygen mixtures propagating in round tubes. Experiments in hydrogen-oxygen mixtures were performed and compared to acoustic theory to validate the angle measurements in the current research. As shown in Fig.109, experiment results follow a similar trend with acoustic theory.

Annular channels

The solution to solve for the frequency of vibration in an annular geometry follows the same steps as the circular tube. Applying the boundary conditions to equation (9) where the particle velocity vanishes at the wall at $r = r_1$ and $r = r_2$, the following expression is obtained:

$$\begin{cases} 0 = EJ'_{m}(\beta r_{1}) + FY'_{m}(\beta r_{1}) \\ 0 = EJ'_{m}(\beta r_{2}) + FY'_{m}(\beta r_{2}) \end{cases}$$
(19)

Solving for E and F, the above equations can be combined and manipulated to obtain:

$$J'_{m}(\beta r)Y'_{m}(r) - J'_{m}(r)Y'_{m}(\beta r) = 0$$
(20)

where $r = \frac{\omega}{c} r_2$ and $\beta = \frac{r_1}{r_2}$. The roots for the above equation are tabulated by Helmut F. Bauer (1964). Table 4 summarizes the dimensions of the three annular channels considered in this research.

Annular gap (mm)	3.175	6.35	9.525	
r ₁ (mm)	28.575	25.4	22.225	
r ₂ (mm)	31.75	31.75	31.75	
r ₁ /r ₂	0.9	0.8	0.7	

Table 4: Dimensions of the three annular channels.

Letting β_1 =0.9, β_2 =0.8 and β_3 =0.7, we obtain the roots tabulated in Table 5. Following the same procedure as in circular tubes, the vibration frequency and track angle can be obtained.

		Roots					
	m						
	n	0	1	2	3	4	5
	0	31.42923	1.05314	2.10622	3.15933	4.21234	5.26835
	1	62.83849	31.4469	31.50001	31.58836	31.71153	31.8693
	2	94.25221	62.84733	62.87589	62.91809	62.97991	63.05929
β_1	3	125.66702	94.2581	94.27578	94.30525	94.34651	94.39941
	4	157.08228	125.76144	125.68471	125.7068	125.73774	125.77756
	5	188.49777	157.08582	157.09642	157.11411	57.13886	157.17062
	0	15.73755	1.11337	2.22646	3.339	4.45074	5.56194
	1	31.43083	15.77771	15.89762	16.09557	16.36888	16.7145
	2	47.13383	31.45076	31.51055	31.60989	31.74843	31.927576
β_2	3	62.82931	47.14711	47.18691	47.25324	47.34583	47.46467
	4	78.54578	62.84927	62.87912	62.92886	62.99841	63.08768
	5	94.25276	78.55375	78.57762	78.61741	78.67308	78.7446
β_3	0	10.52203	1.18237	2.36285	3.53961	4.71085	5.86629
	1	20.96939	10.59184	10.79885	11.13634	11.59433	12.22983
	2	31.43294	21.00371	21.10636	21.27642	21.51241	21.81256
	3	41.90067	31.45574	31.5241	31.63759	31.79591	31.99842
	4	52.3701	41.91775	41.96895	42.05416	42.17317	42.32573
	5	62.84041	52.38376	52.4247	52.49288	52.58819	52.71052

Table 5: Roots of the cross product Bessel functions.

Rectangular tubes

Acoustic theory can also be extended to rectangular tubes by solving the wave equation in Cartesian coordinates. The wave equation for a 2-dimensional Cartesian coordinate is

$$\frac{\partial^2 \Phi}{\partial x^2} + \frac{\partial^2 \Phi}{\partial y^2} = \frac{1}{C^2} \frac{\partial^2 \Phi}{\partial t^2} \,. \tag{21}$$

Assuming a solution of the following form exists

$$\Phi(x, y, t) = X(x)Y(y)T(t), \tag{22}$$

the temporal and special component of the differential equation can be expanded as the following equations:

$$\frac{\partial^2 T}{\partial x t^2} + \omega^2 T = 0 , \qquad (23)$$

$$\frac{1}{X}\frac{\partial^2 X}{\partial x^2} = \frac{1}{Y}\frac{\partial^2 Y}{\partial y^2} - \frac{\omega^2}{C^2} = -k_x^2, \qquad (24)$$

$$\frac{\partial^2 X}{\partial x^2} + k_x^2 X = 0 , \qquad (25)$$

and

$$\frac{\partial^2 Y}{\partial x v^2} + k_y^2 Y = 0$$
(26)

Applying the boundary conditions of zero particle velocity at the walls, the solution is given as a combination of harmonic functions:

$$\Phi(x, y, t) = A\sin(k_x x)\sin(k_y y)\cos(t \omega t). \tag{27}$$

Assuming the rectangular tube has dimensions of a and b,

$$k_x a = l\pi, l = 1,2,3....$$
 (28)

and

$$k_y$$
b = m π , m = 1,2,3 (29)

to satisfy the boundary conditions. The wave number is expressed as

$$k = (k_x^2 + k_y^2)^{1/2} = \frac{\omega}{c}$$
 (30)

Since $f=\omega/2\pi$, the frequencies of the various modes of vibrations in rectangular tubes are

$$N = \frac{C}{2} \left[\left(\frac{l}{a} \right)^2 + \left(\frac{m}{b} \right)^2 \right]^{1/2} . \tag{31}$$

References

- Bauer, H. F. (1964) Tables of zeros of cross product Bessel functions $J_{\rho}(\xi) Y_{\rho}(k\xi) J_{\rho}(k\xi) Y_{\rho}(\xi) = 0. \text{ Mathematics of computation, } 18 (85):128-135.$
- Belles, F.E. (1958) Detonability and chemical kinetics: Prediction of limits of detonability of hydrogen, 7th Symposium (International) on Combustion p. 745-751.
- Breton, J. (1936a) Ann. office natl. combustible liquids 11:487.
- Breton, J. (1936b). Theses faculté des science, Univ. Nancy.
- Camargo, A., Ng, H. D., Chao, J. And Lee, J. H. S. (2010) Propagation of near-limit gaseous detonations in small diameter tubes. Shock waves 20: 499-508.
- Campbell, C. and Finch, A.C. (1928) Striated photographic records of explosion waves. part II. An explanation of the striae. J. Chem. Soc. p. 2094-2106.
- Chao, J., Ng, H. D. and Lee, J. H. S. (2009) Detonability limits in thin annular channels. Proc. Combust. Inst. 32: 2349.
- Donato, M. (1982) The influence of confinement on the propagation of near limit detonation waves. Ph.D. Thesis, McGill University, Montreal.
- Dove, J. E., Scroggie, B. J. and Semerjian, H. (1974) Velocity deficits and detonability limits of hydrogen–oxygen detonations. Acta Astro. 1: 345.

- Dove, J. E. and Tribbeck, T.D. (1970) Computational study of the kinetics of the hydrogen-oxygen reaction behind steady state shock waves. Application to the composition limits and transverse stability of gaseous detonations, Astronautica Acta, Vol. 15: 387-397.
- Duff, R.E. (1961) Investigation of spinning detonation and detonation stability,

 The physics of fluids: 4,11: 1427-1433.
- Dupré, G., Knystautas, R., and Lee, J.H. (1986) Near-limit propagation of detonation in tubes. Progress in Astronautics and Aeronautics,106:244-259.
- Fay, J. A. (1959) Two-dimensional gaseous detonations: velocity deficit. Phys. Fluids 2: 283.
- Fickett, W. and Davis, W.C. (1979) Detonation, University of California Press.
- Fischer, J., Liebner, C., Hieronymus, H. and Klemn, E. (2009) Maximum safe diameters of microcapillaries for a stoichiometric ethene/oxygen mixture.

 Chemical Engineering Science, 64:2951-2956.
- Gamezo, V.N., Desbordes, D. and Oran, E.S. (1999) Formation and Evolution of two-dimensional cellular detonations, Combustion and Flame 116:154-165.
- Glassman, I. (1996) Combustion 3rd Ed. Academic Press.
- Gooderum, P.B. (1958) NACA Technical Note 4243.

- Gordon, W.E., Mooradian, A.J. and Harper, S.A. (1959) Limit and spin effect in hydrogen-oxygen detonations. Proc. 7th Sym. Int. on Combust. 7: 752.
- Ishii, K., Itoh, K. and Tshuboi, T. (2002) A study on velocity deficits of detonation waves in narrow gaps, Proc. Combust. Inst. 20: 2789-2794.
- Ishii, K. and Monwar, M. (2011) Detonation propagation with velocity deficits in narrow channel. Proc. Combust. Inst. 33:2359–2366.
- Jackson, S., Lee, B.J., Huang, W., Pintgen, F., Karnesky, J., Liang, Z. and Shepherd, J.E. (2009) Experimental detonation propagation under high loss conditions. Proc. 22nd Int. Colloq. Dynamics Expl. Reac. Sys., Minsk, Belarus.
- Kitano, S., Fukao, M., Susa, A., Tsuboi, N., Hayashi, A.K. and Koshi, M. (2009)

 Spinning detonation and velocity deficit in small diameter tubes. Proc.

 Combust. Inst. 32(2), 2355–2362.

Kistiakowsky, G., Kwight, H., and Malin, M. J. (1952) Chem. Phys. 20, 594.

Knystautas, R., Lee, J. H. S. and Guirao, C. (1982) Comb. and Flame 48: 63-82.

Konnov AA. Detailed reaction mechanism for small hydrocarbons combustion.

Release 0.5

- Laberge, S., Atanasov, M., Knystautas, R. and Lee, J. (1993) Propagation and extinction of detonation waves in tube bundles. Prog. Astronaut.Aero. 153, 381–396.
- Lee, J.H. (1984) Dynamic parameters of gaseous detonations. Ann. Rev. Fluid Mech. 16: 311-336.
- Lee, J.H. (1986) On the transition from deflagration to detonation. Dynamics of explosions 106: 3-18.
- Lee, J.J., Dupré, G., Knystautas, R. and Lee, J.H. (1995) Doppler interferometry study of unstable detonations. Shock Waves 5:175-181.
- Lee, J. H. S. (2003) "The universal role of turbulence in the propagation of strong shocks and detonation waves" Chapter 3 in "High pressure shock compression of solids." Vol VI ed. Y. Horie, L. Davidson and N. N. Thadhani, Springer Verlag NY, 121-144.
- Lee, J. H. S. (2008) The Detonation Phenomenon, Cambridge University Press.
- Manson, N. and Guénoche H. (1956) Sixth Sym. (Int'l) on Combustion p. 631-639
- Manson, N., Brochet, C.H., Brossard, J.and Pujol, Y. (1962) 9th Symp. (Int'l) on Combustion, 461-469.
- Manzhalei, V. I. (1992) Detonation regimes of gases in capillaries. Fiz. Goreniya Vzryva, Vol 28 (3): 93-99.

- Moen, I. O., Donato, M., Knystautas, R. and Lee, J.H. (1981) The influence of confinement on the propagation of detonation near the detonability limits, 18th Symp. (Int'l) on Combustion, 1615-1622.
- Moen I.O., Sulmistras A., Thomas G.O., Bjerketvedt D. and Thibault P. (1985)

 Dynamics of explosion" ed. Bower J.R., Reyer J.C., and Soloukhin R.I.

 Prog. in Astro. and Aero. Vol 106.
- Murray S.B., and Lee J.H.S. (1986) Prog. Astro. and Aero. Vol. 106 pp 329-355.
- Murray, S. B. (2008) Numa Manson on velocity deficits and detonation stability.

 Shock Waves, Vol. 18, number 4, 255-268.
- Pintgen, F., Eckett, C. A., Austin, J. M. and Shepherd, J.E. (2003) Direct observations of reaction zone structure in propagating detonations.

 Combust. Flame 133:211–229.
- Pusch W., and Wagner H.Gg. (1962) Investigation of the dependence of the limits of detonatability on tube diameter. Combustion and Flame 6: 157-162.
- Radulescu, M. I. and Lee, J. H. S. (2002) The Failure Mechanism of Gaseous

 Detonations: Experiments in Porous Wall Tubes. Combustion and Flame

 131: 29-46.

- Radulescu, M. I., Ng. H. D., Lee, J. H. S. and Varatharajan, B. (2002) The hydrodynamic structure of unstable cellular detonations. Proc. Combust. Inst., 29,2825–2831.
- Saint-Cloud, J.P. (1971) Contribution a l'étude de la propagation des détonations autonomies instables dans le melange C3H8+5O2+10N2. These 3e cycle, Poitiers, France.
- Schelkin, K. I. (1940) Influence of the wall roughness on initiation and propagation of detonation in gases, Zh. Eksp.Teor. Fiz. Vol. 10, pp.823-827.

Wendlandt, R. (1924) Z. Phys. Chem., vol.110, p. 637.

Wendlandt, R. (1925) Z. Phys. Chem., vol.116, p. 227.

Zel'dovich,Y. B. (1940) J. Exp. Theo. Phys. 10, pp. 542–568 available in translation as NACA TM 1261 (1950)

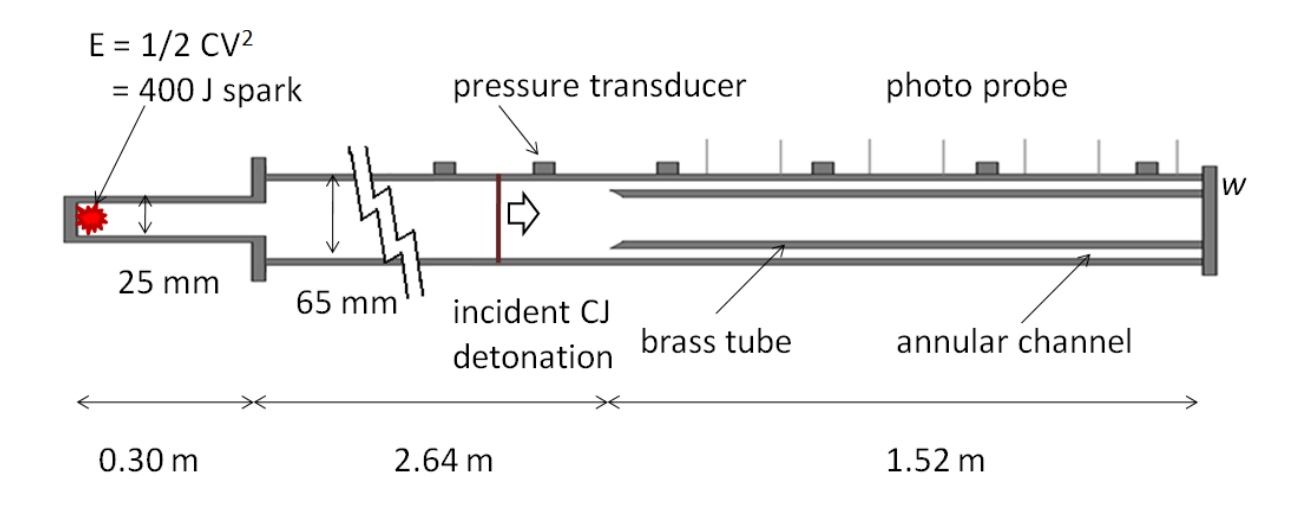


Figure 1a: Schematic of the experimental apparatus.

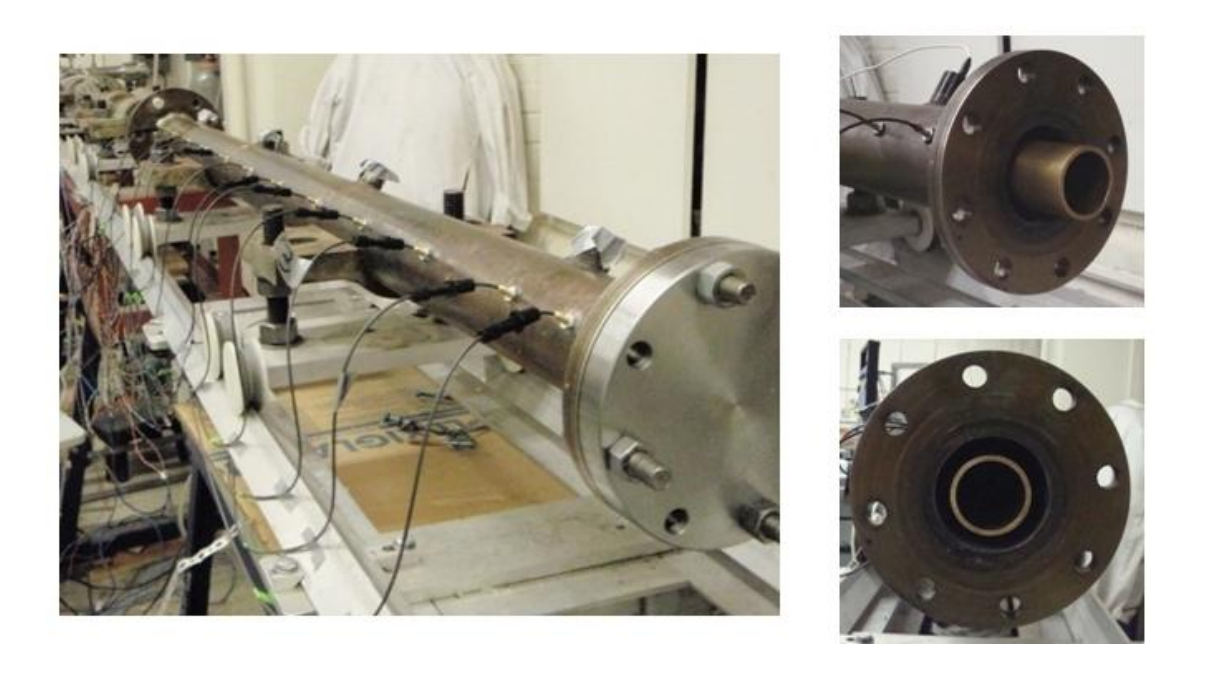


Figure 1b: Photograph of the experimental apparatus.

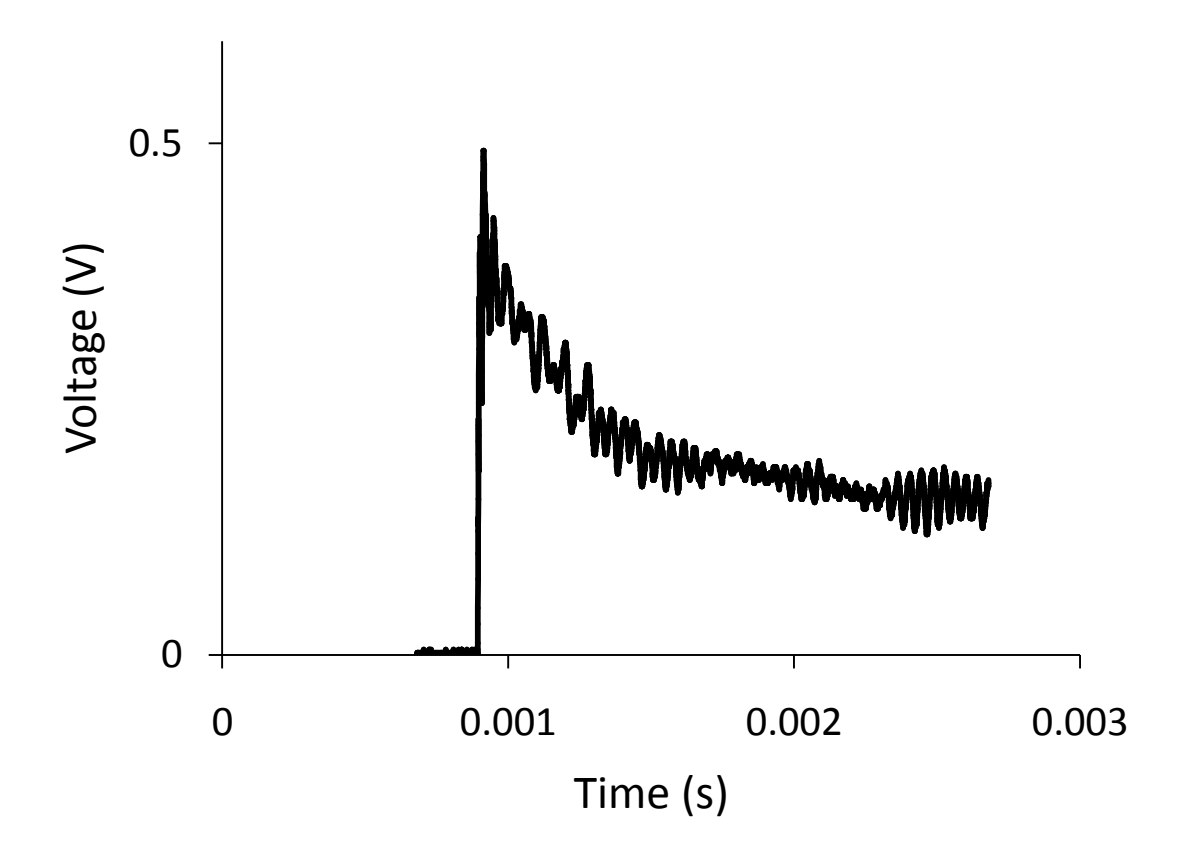


Figure 2: Typical pressure trace of a detonation.

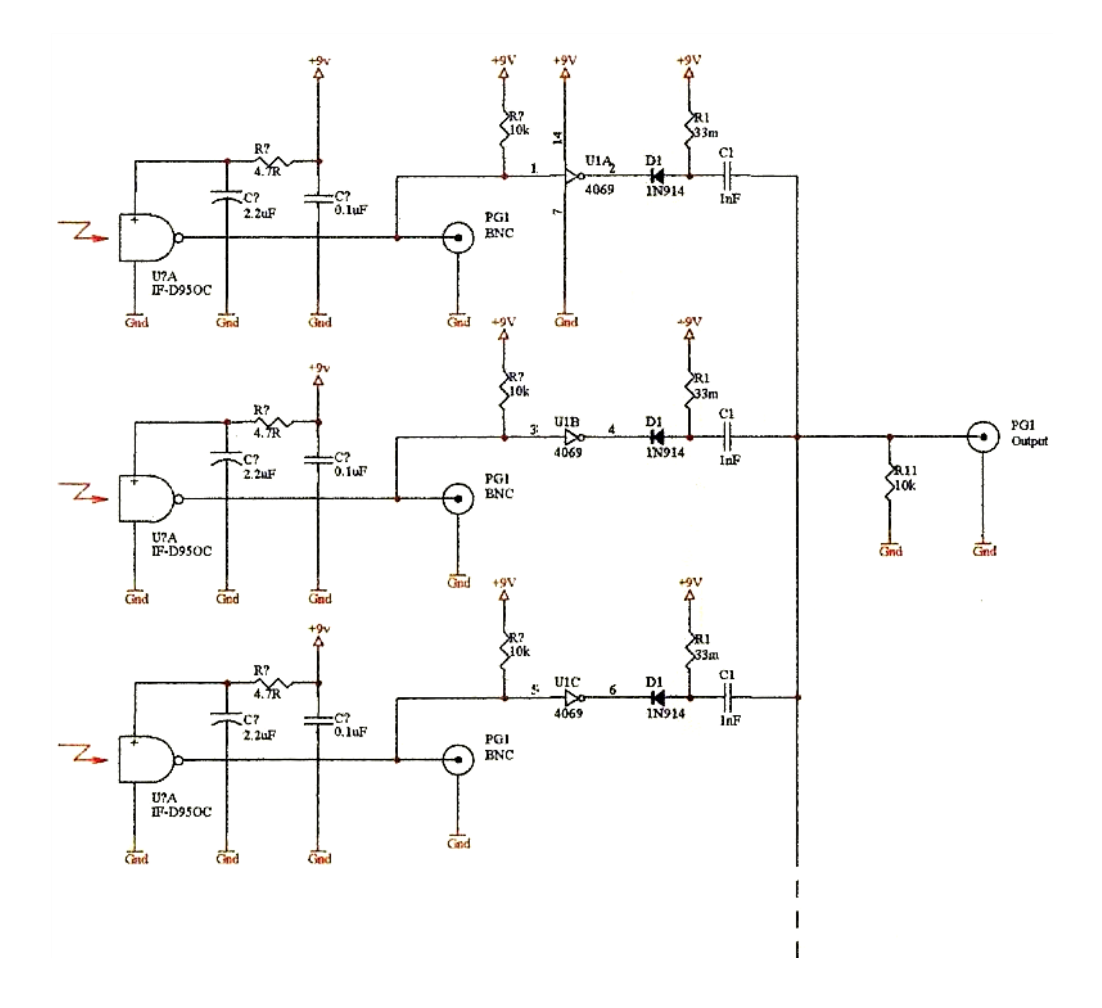


Figure 3: Photoprobe circuit.

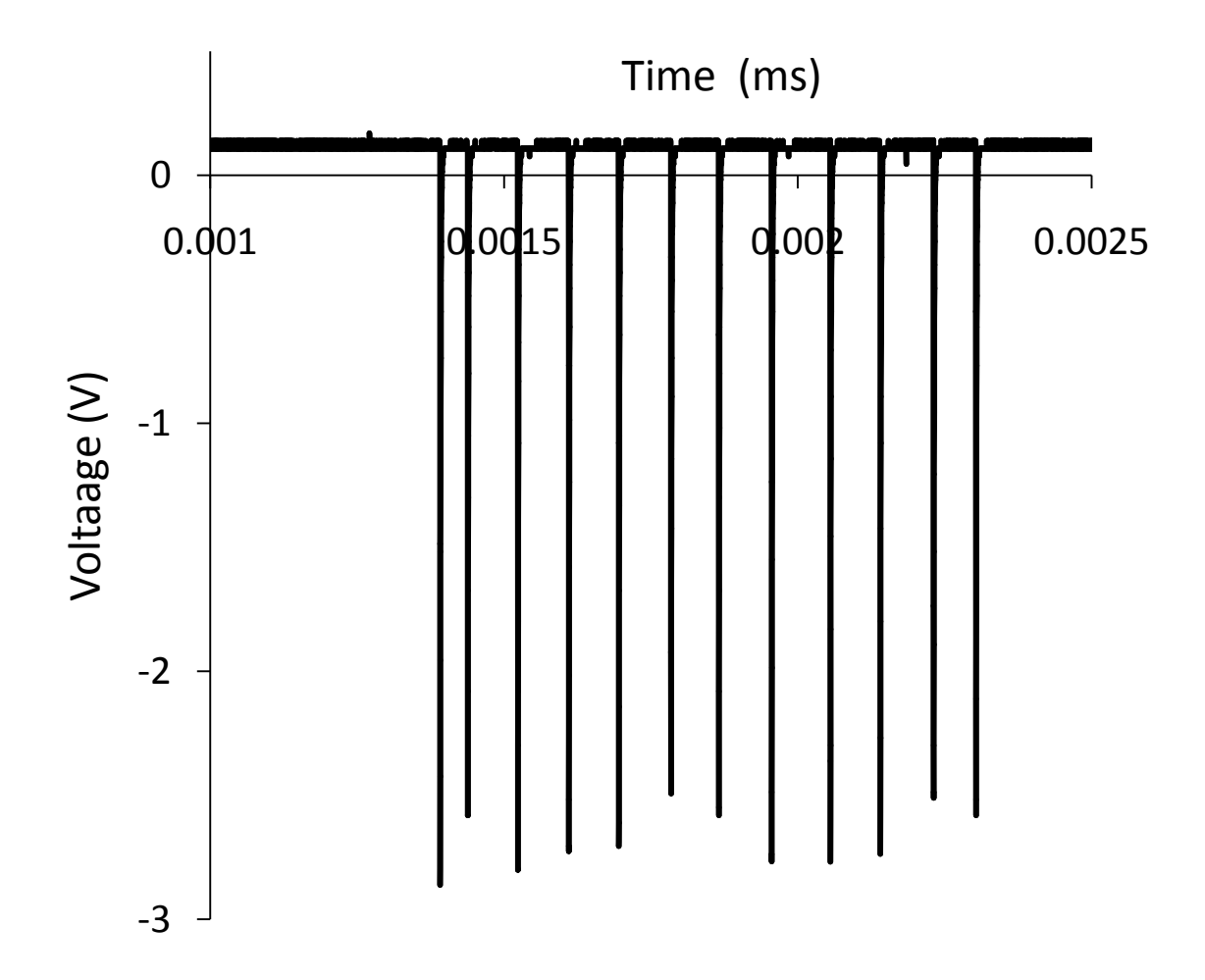


Figure 4: Typical photoprobe signals.

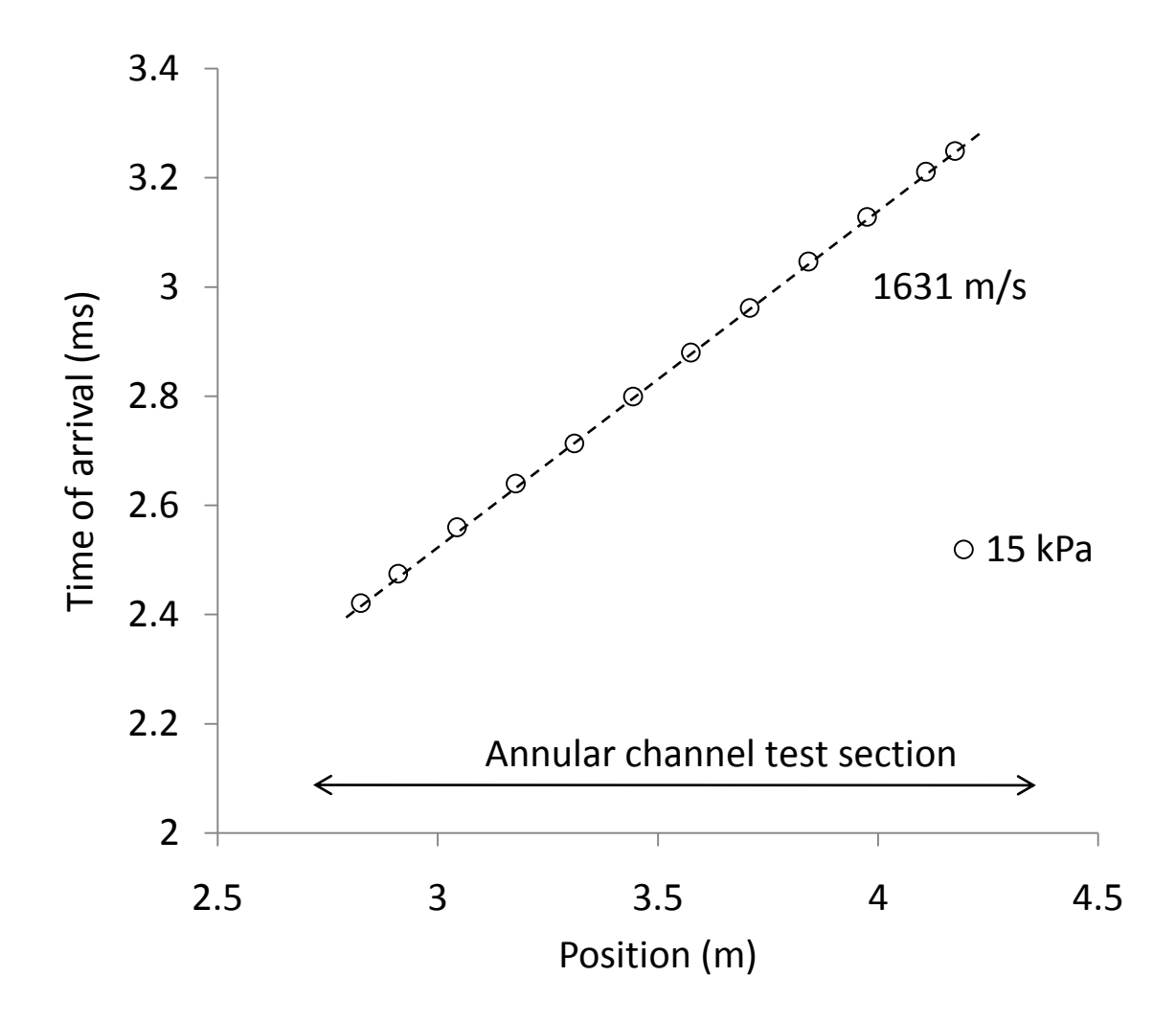


Figure 5: Typical trajectory of a detonation ($C_2H_2 + 2.5O_2 + 70\%$ Ar, 9.525 mm annular channel).

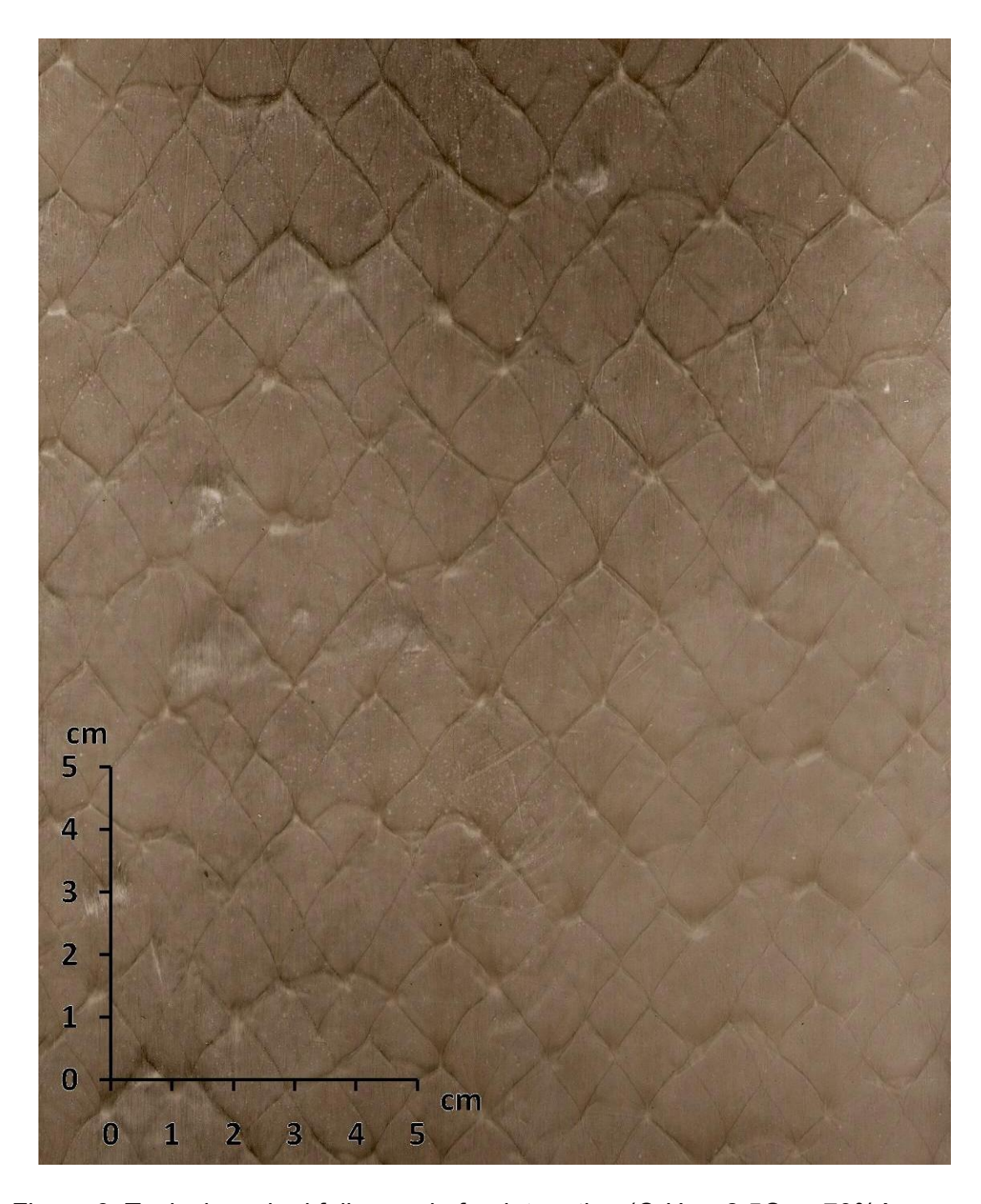


Figure 6: Typical smoked foil record of a detonation ($C_2H_2 + 2.5O_2 + 70\%$ Ar, p_0 =10 kPa, 58 mm diameter round tube).

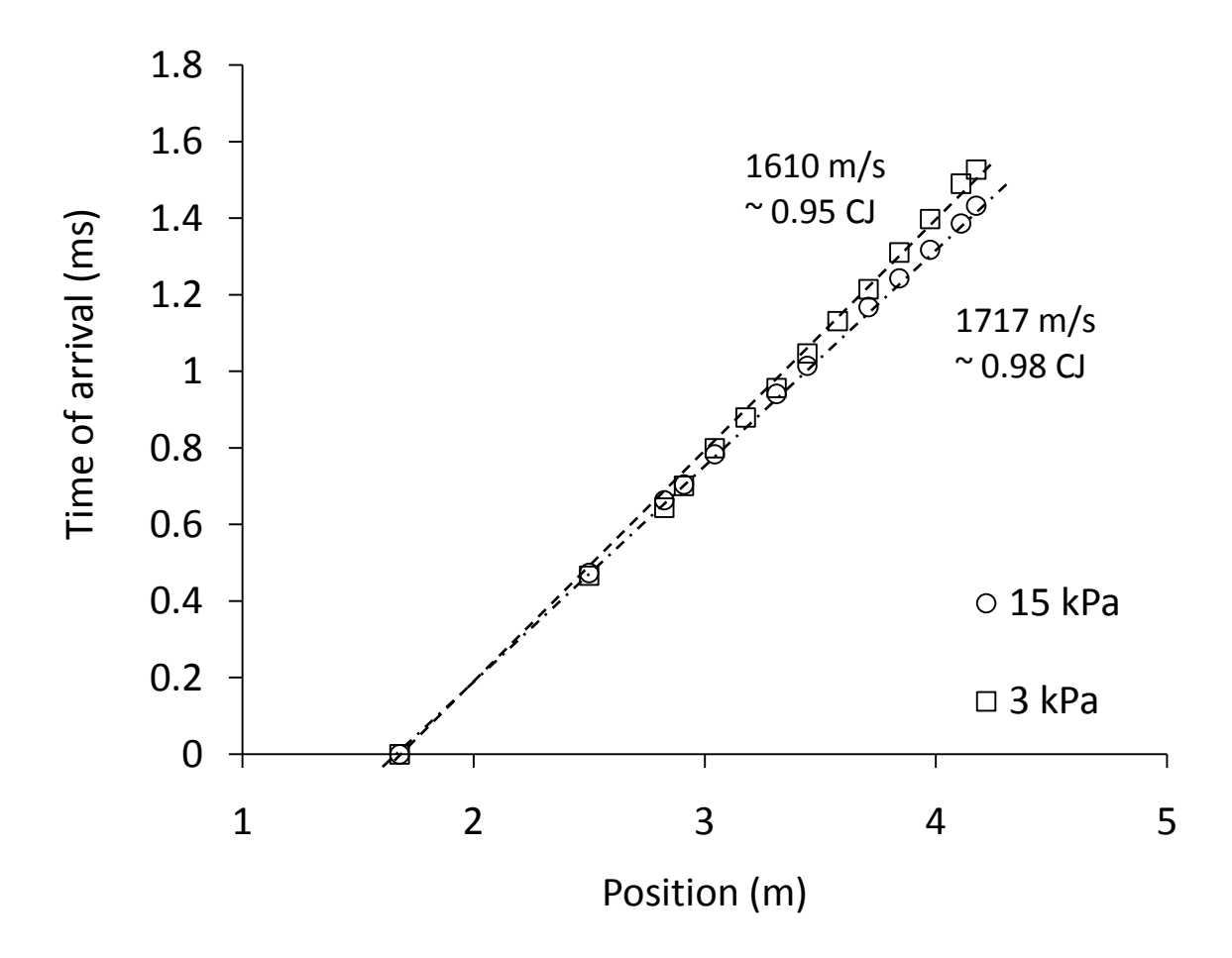


Figure 7: Typical trajectory of a detonation within the limit of detonation ($C_2H_2 + 2.5O_2 + 70\%$ Ar, 65 mm diameter round tube).

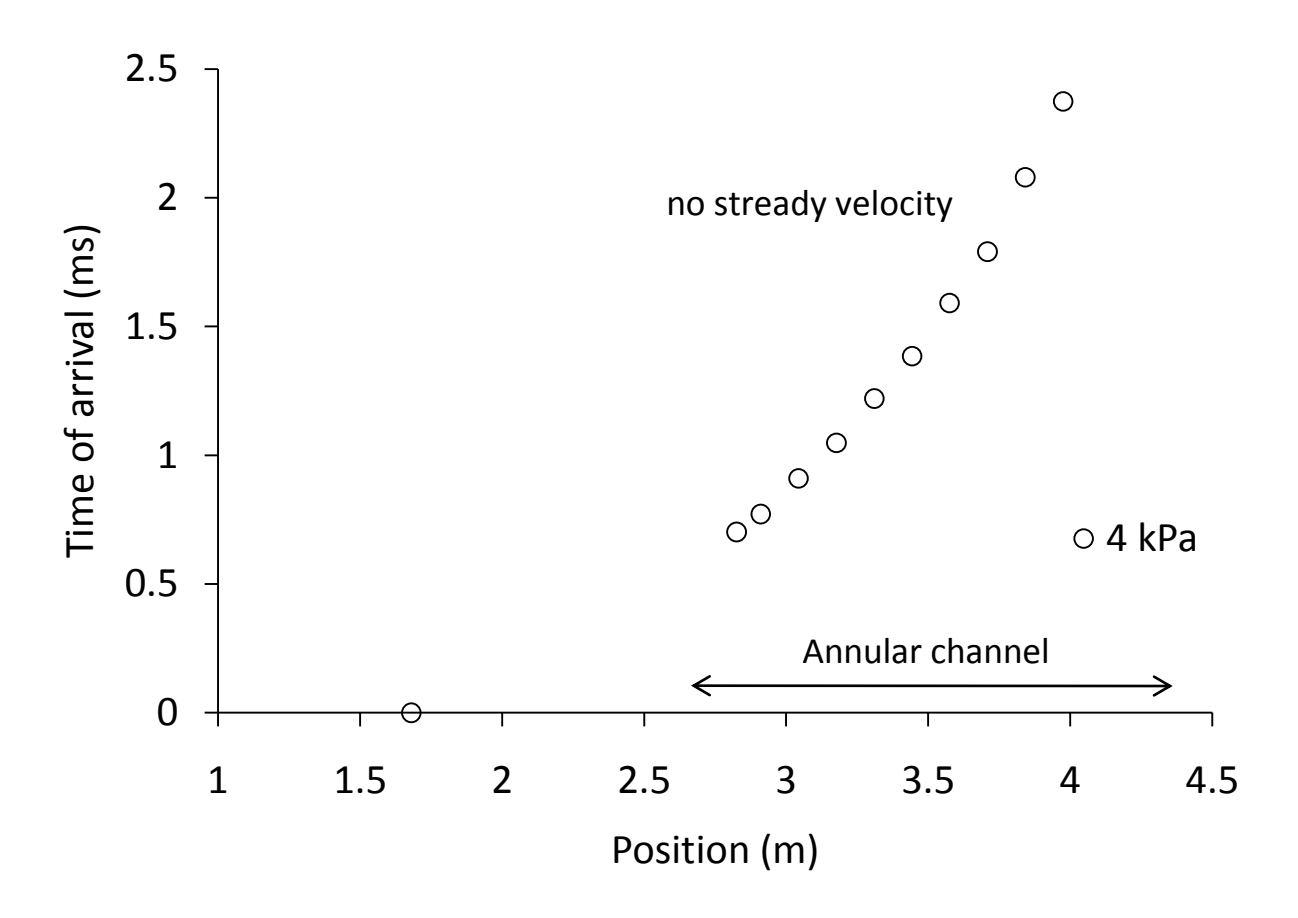


Figure 8: Typical trajectory of a detonation outside the limit of detonation ($C_2H_2 + 2.5O_2 + 70\%$ Ar, 3.175 mm annular channel).

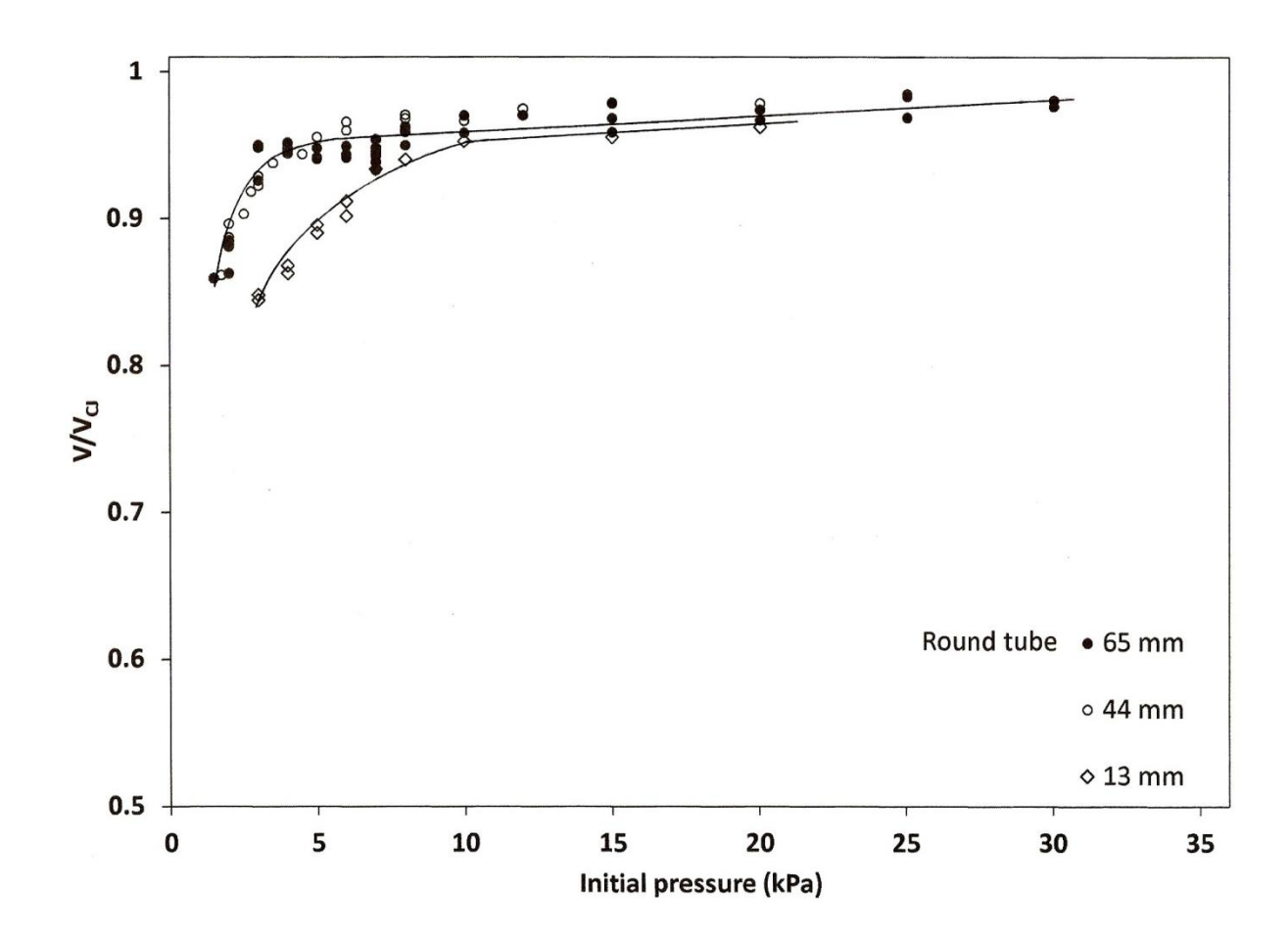


Figure 9: Normalized detonation velocity as a function of initial pressure in C_2H_2 + $2.5O_2$ + 70%Ar mixtures for round tubes.

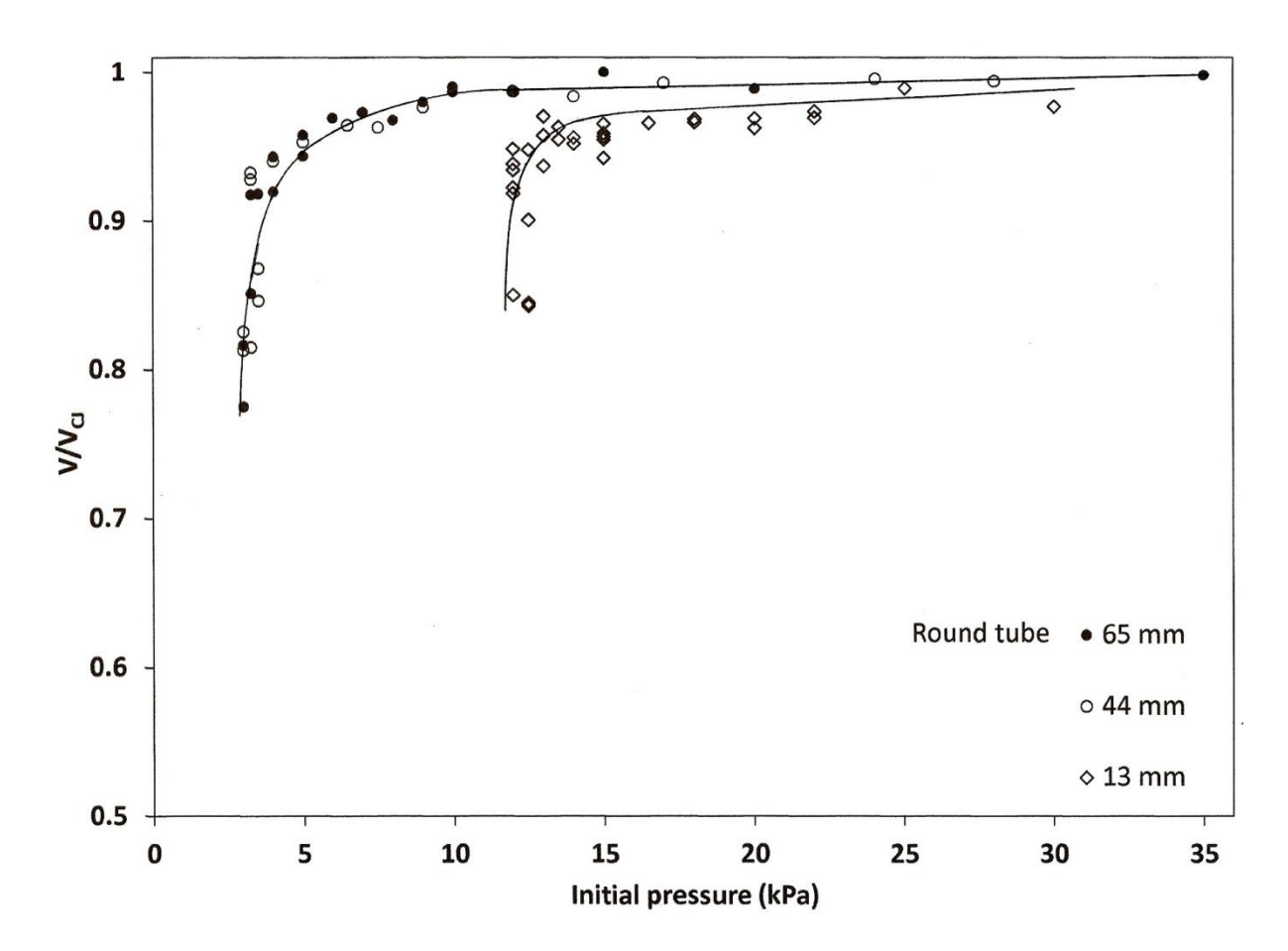


Figure 10: Normalized detonation velocity as a function of initial pressure in CH₄ + 2O₂ mixtures for round tubes.

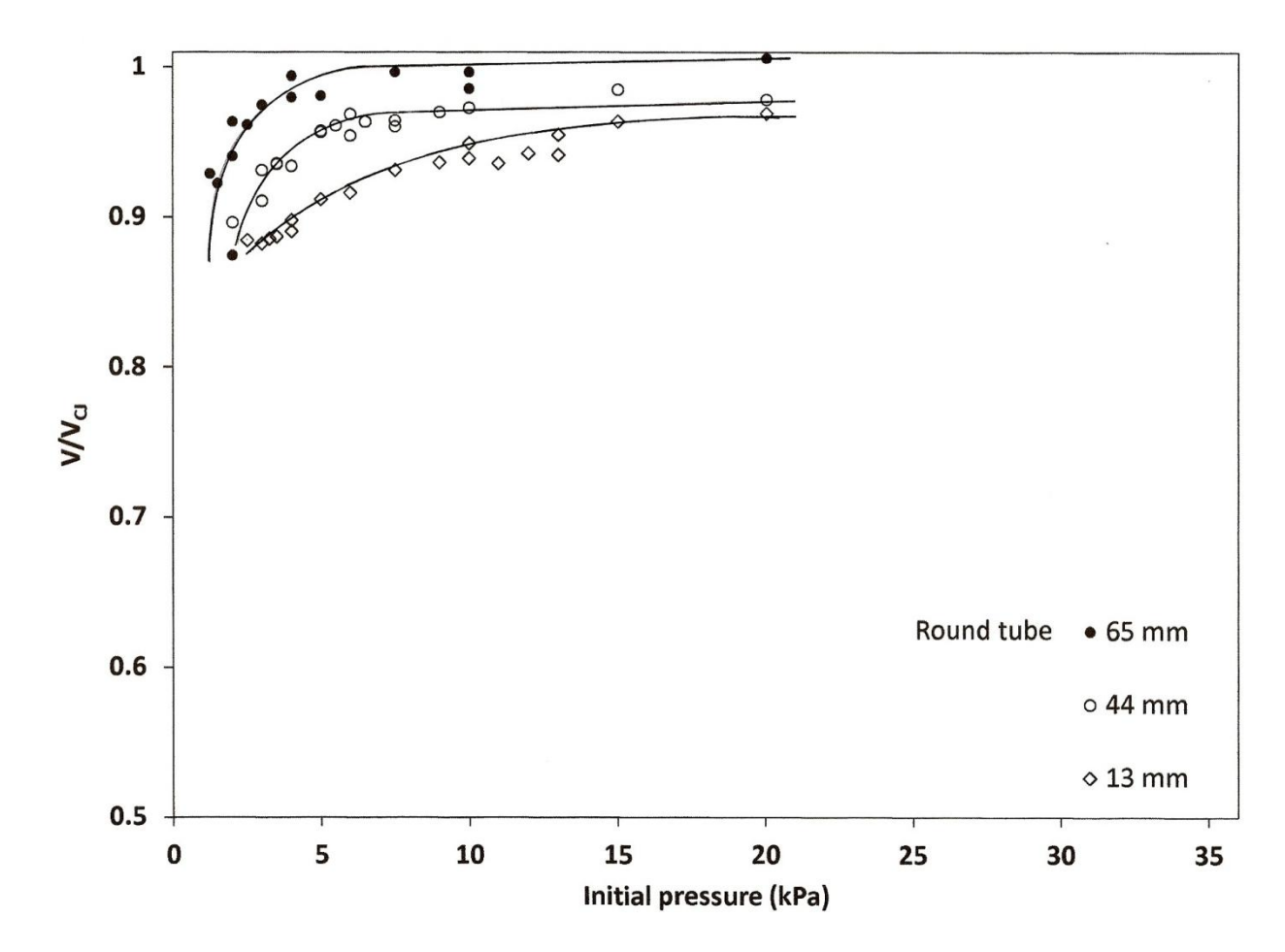


Figure 11: Normalized detonation velocity as a function of initial pressure in C_2H_2 + $5N_2O$ + 50%Ar mixtures for round tubes.

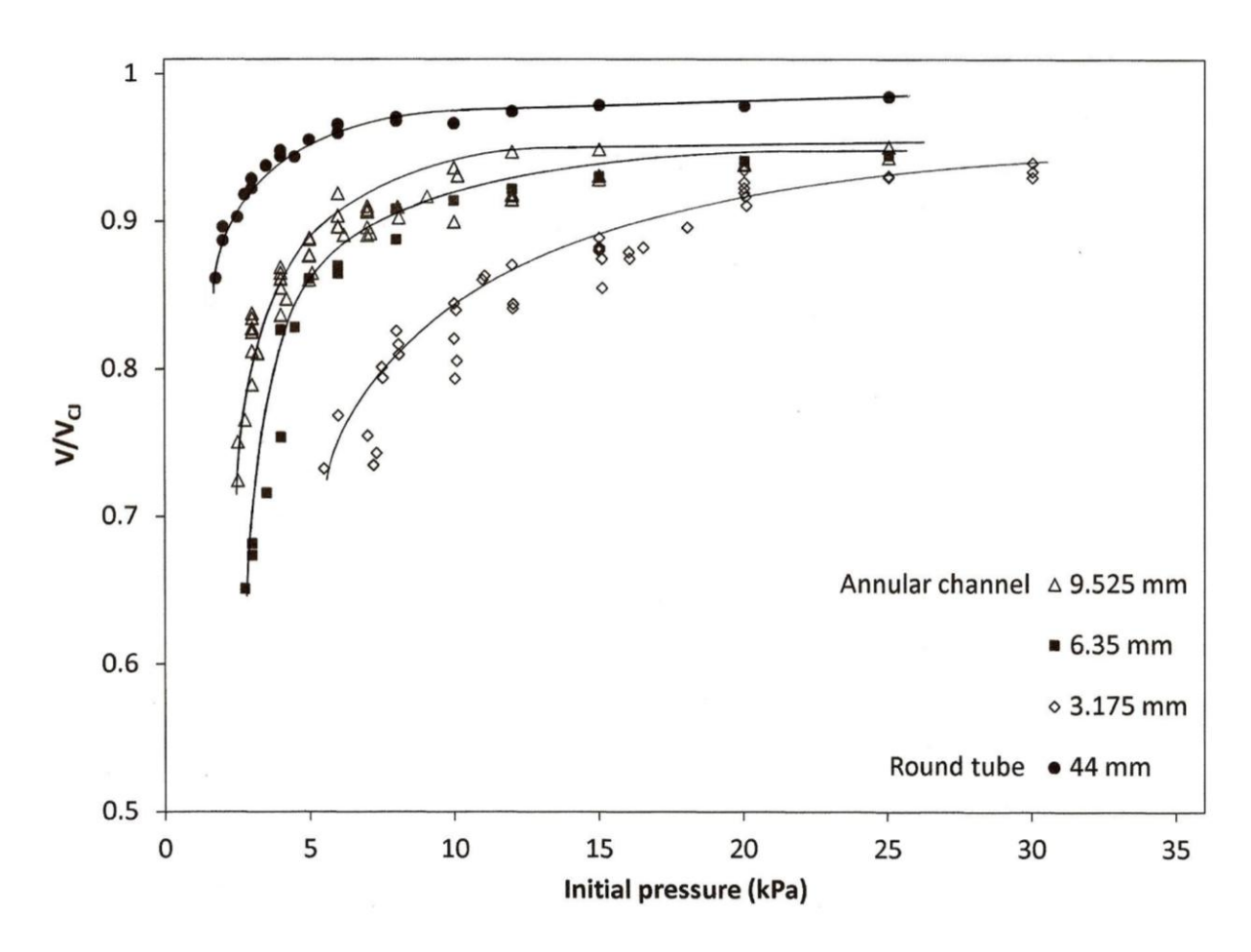


Figure 12: Normalized detonation velocity as a function of initial pressure in C_2H_2 + $2.5O_2$ + 70%Ar mixtures for annular channels.

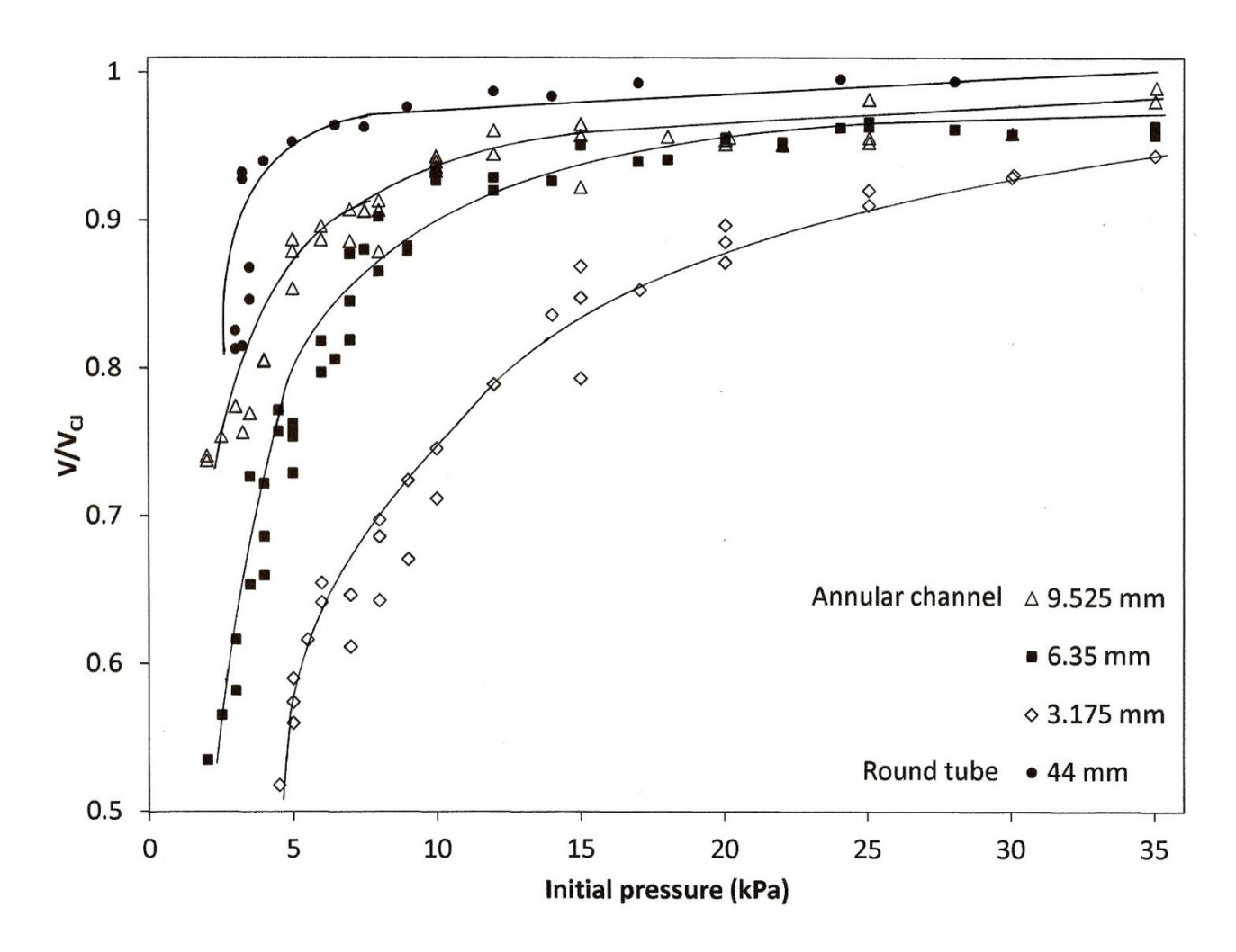


Figure 13: Normalized detonation velocity as a function of initial pressure in CH₄

+ 2O₂ mixtures for annular channels.

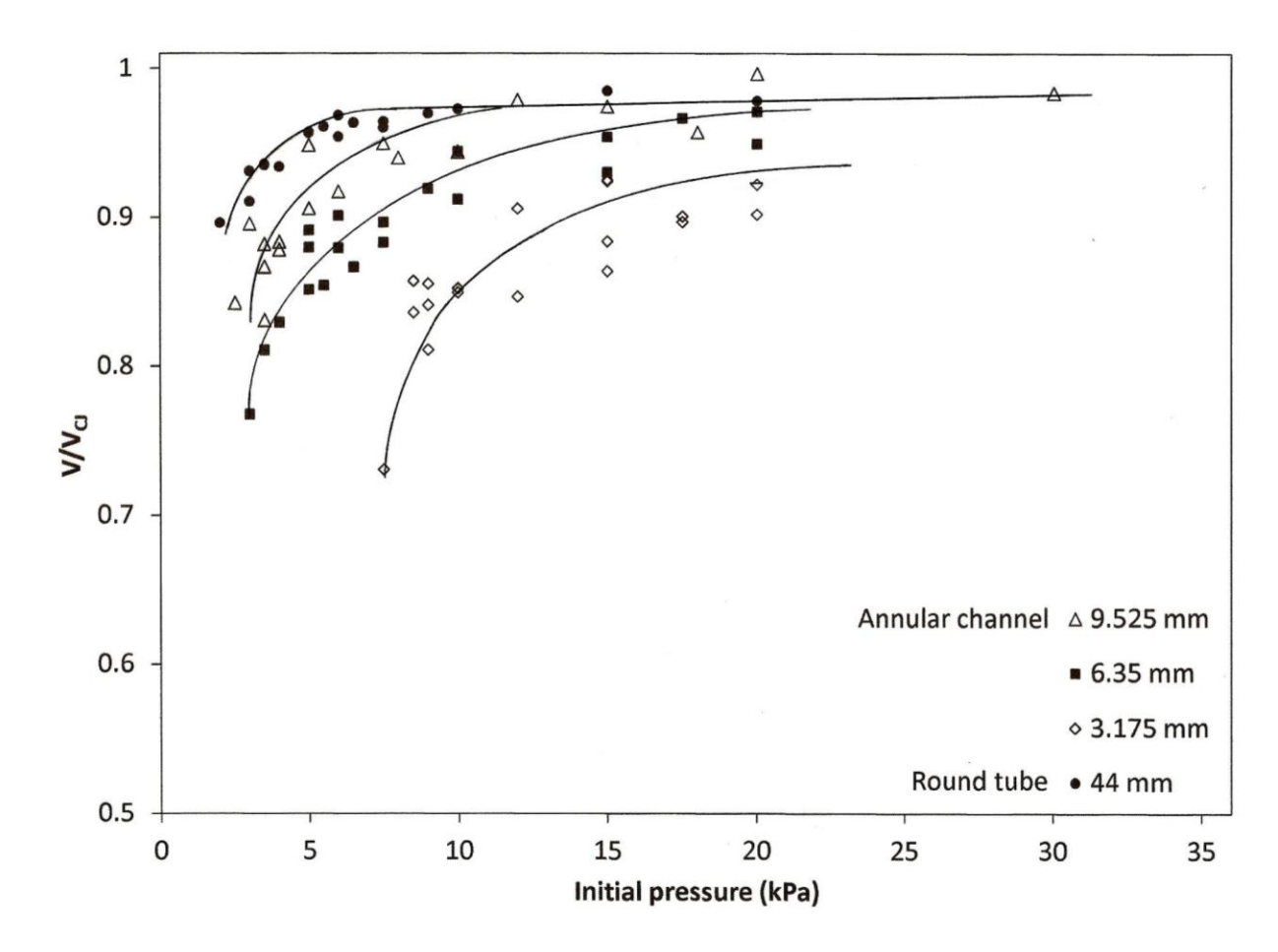


Figure 14: Normalized detonation velocity as a function of initial pressure in C_2H_2 + $5N_2O$ + 50%Ar mixtures for annular channels.

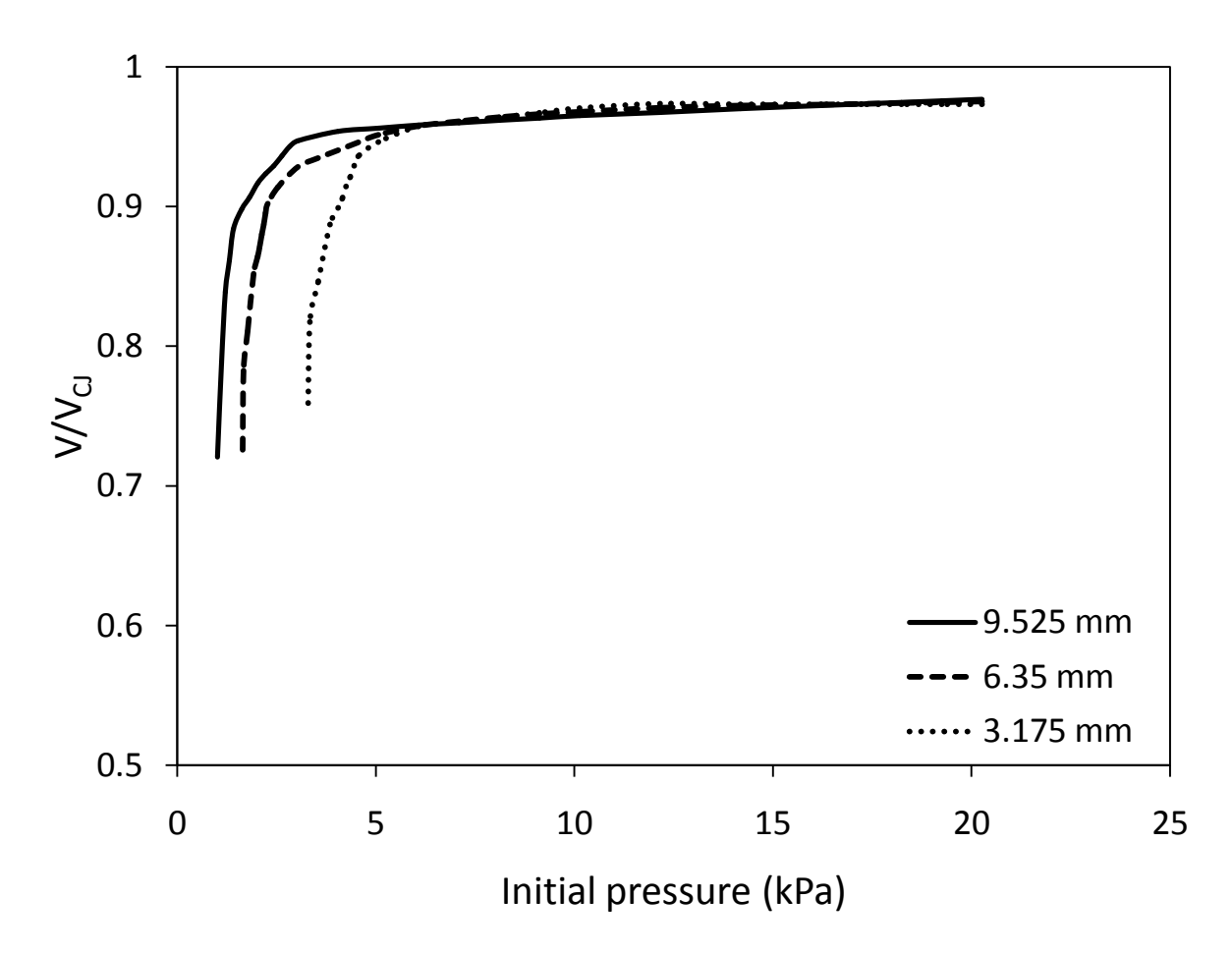


Figure 15: Normalized detonation velocity computed using Fay's model in C_2H_2 + $2.5O_2$ + 70%Ar mixtures in annular channels.

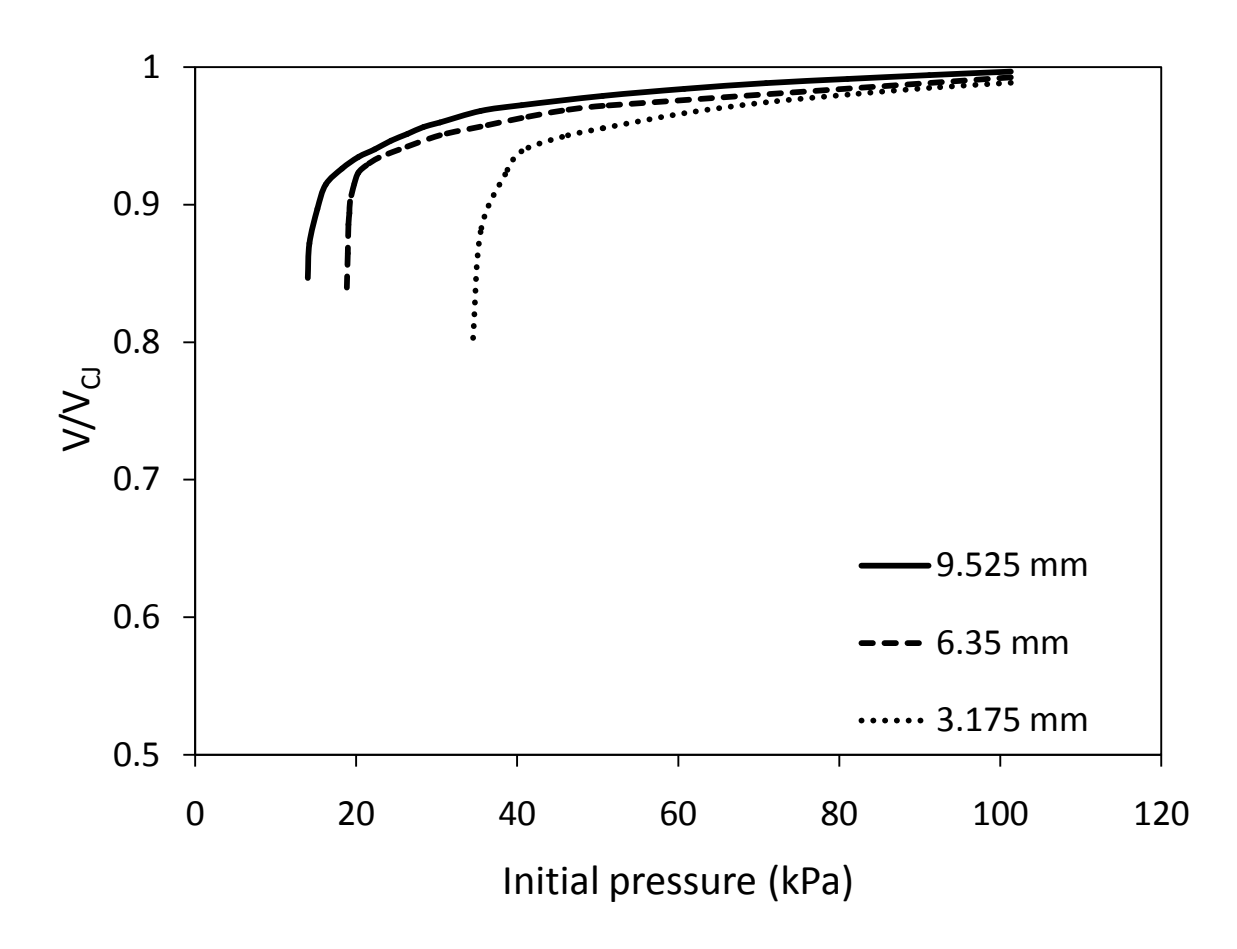


Figure 16: Normalized detonation velocity computed using Fay's model in CH_4 + $2O_2$ mixtures in annular channels.

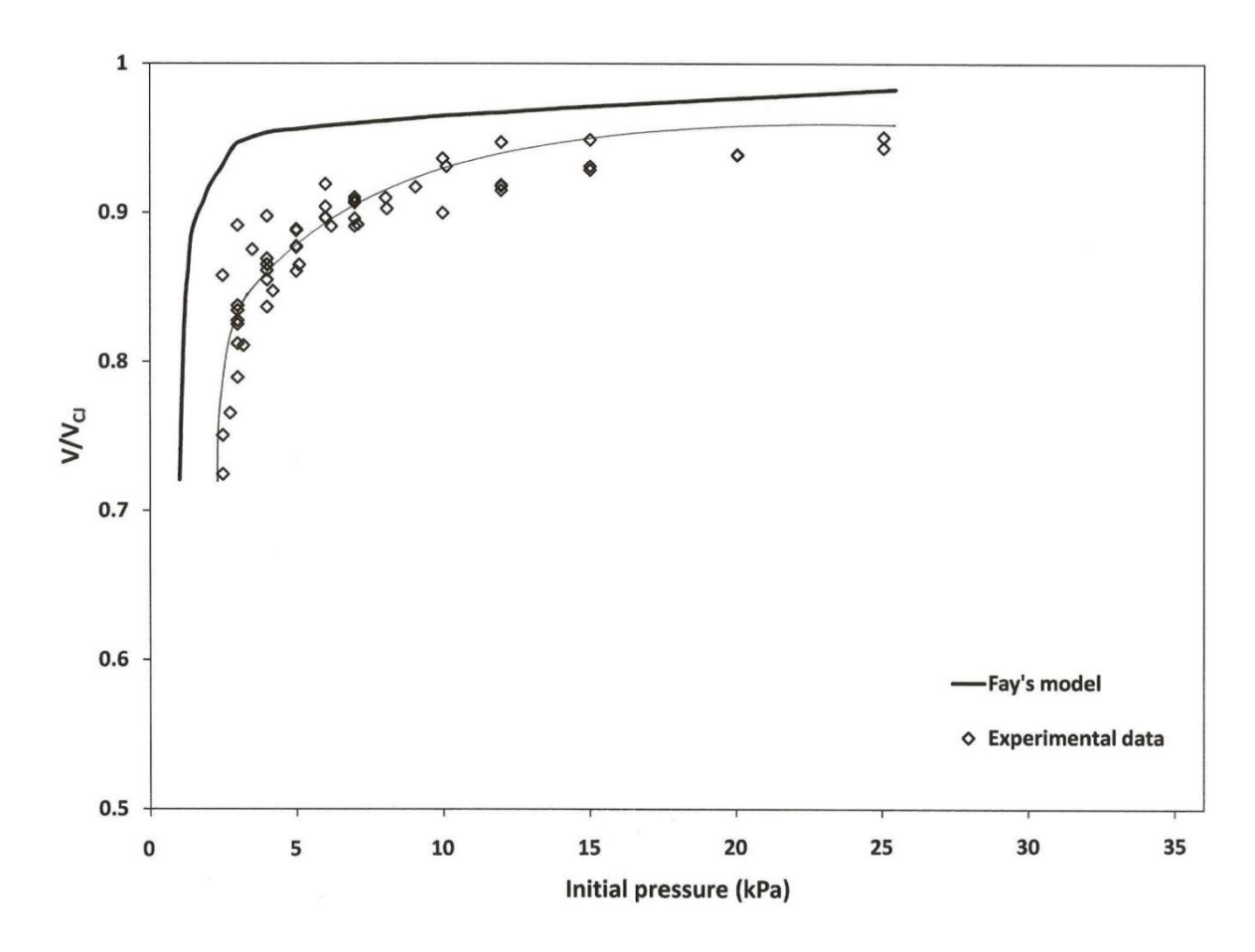


Figure 17: Comparison of Fay's curvature model with experimental results for C_2H_2 +2.5 O_2 +70%Ar in a 9.525 mm annular gap.

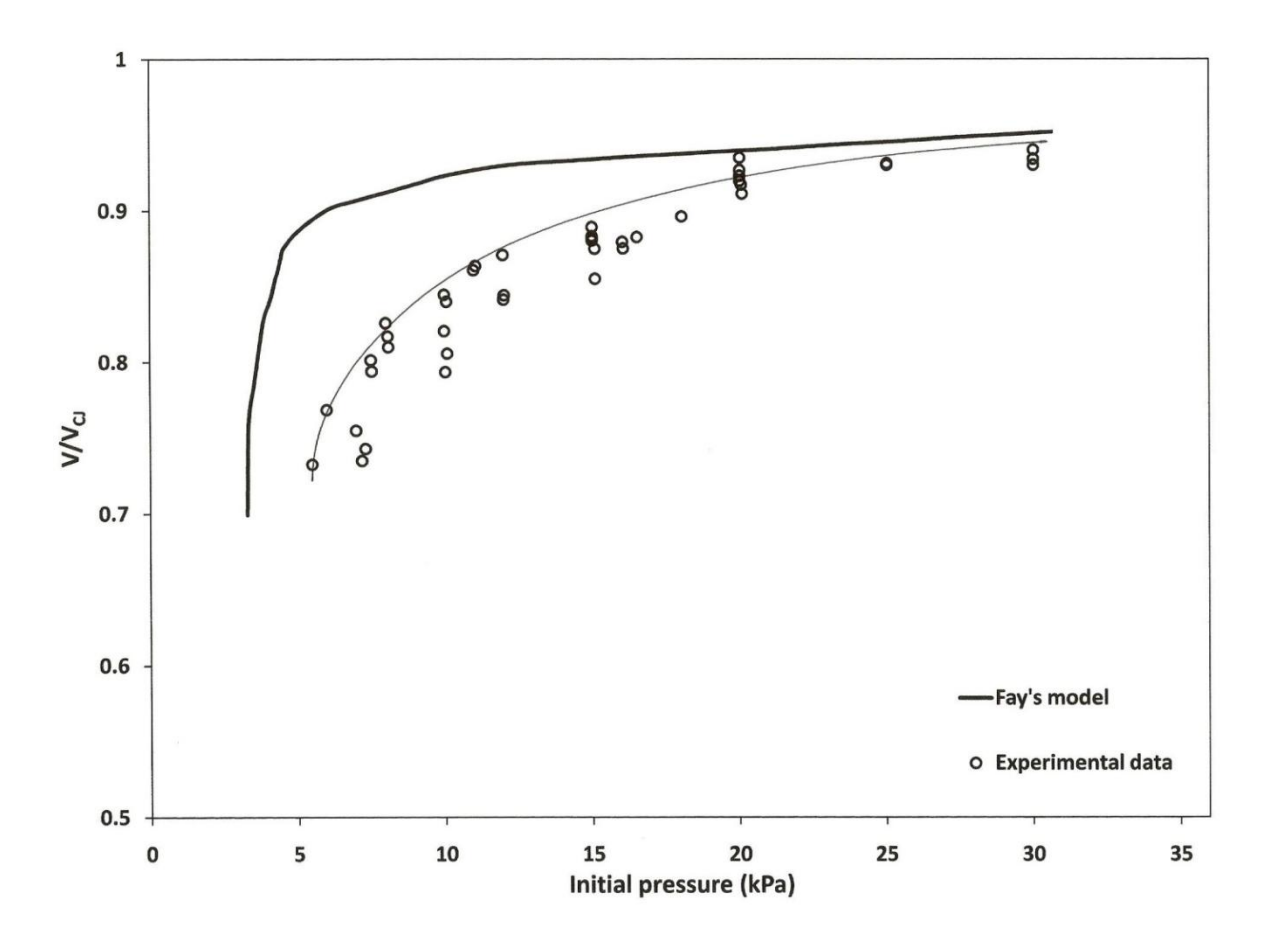


Figure 18: Comparison of Fay's curvature model with experimental results for C_2H_2 +2.5 O_2 +70%Ar in a 3.175 mm annular gap.

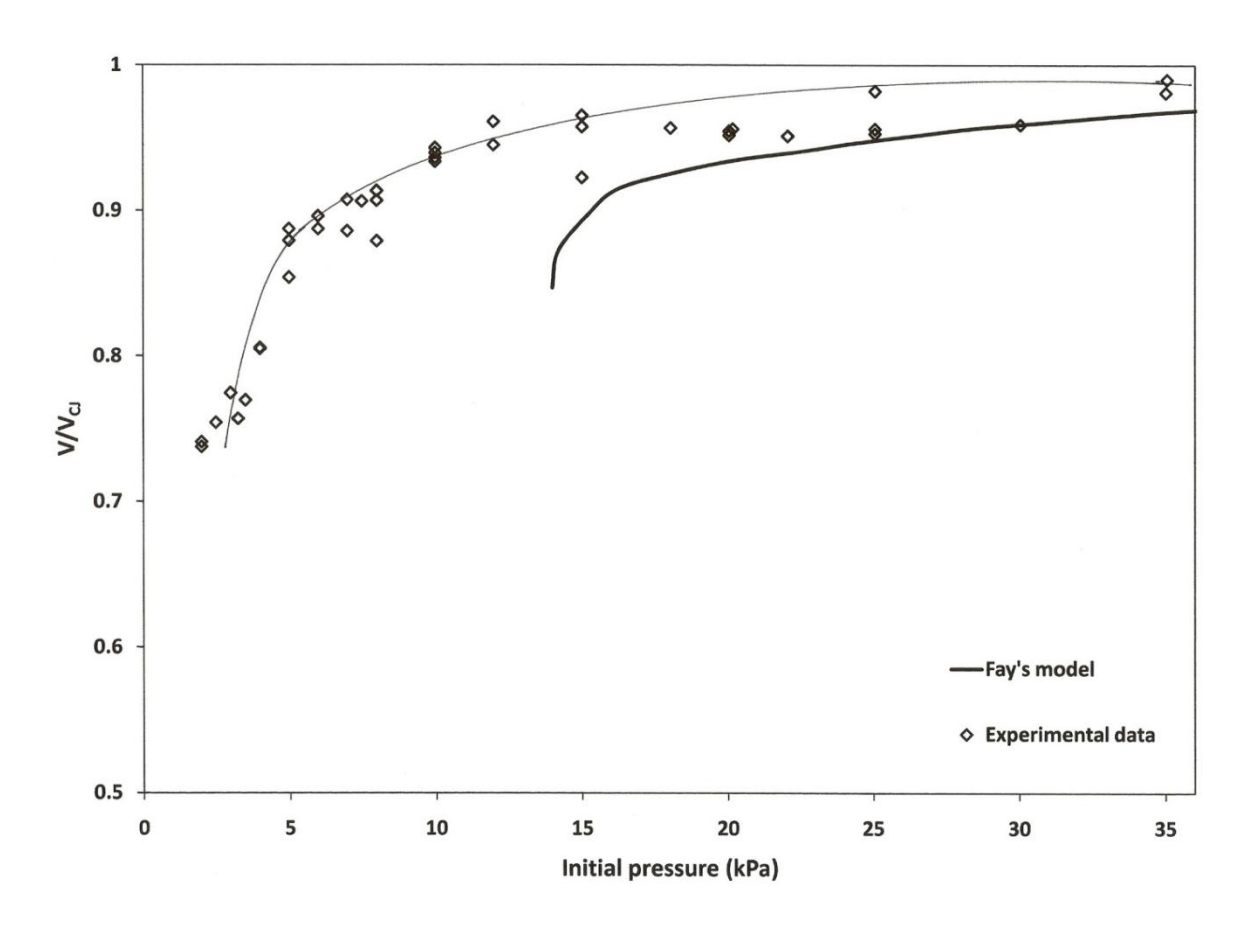


Figure 19: Comparison of Fay's curvature model with experimental results for CH_4 +2O₂ in a 9.525 mm annular gap.

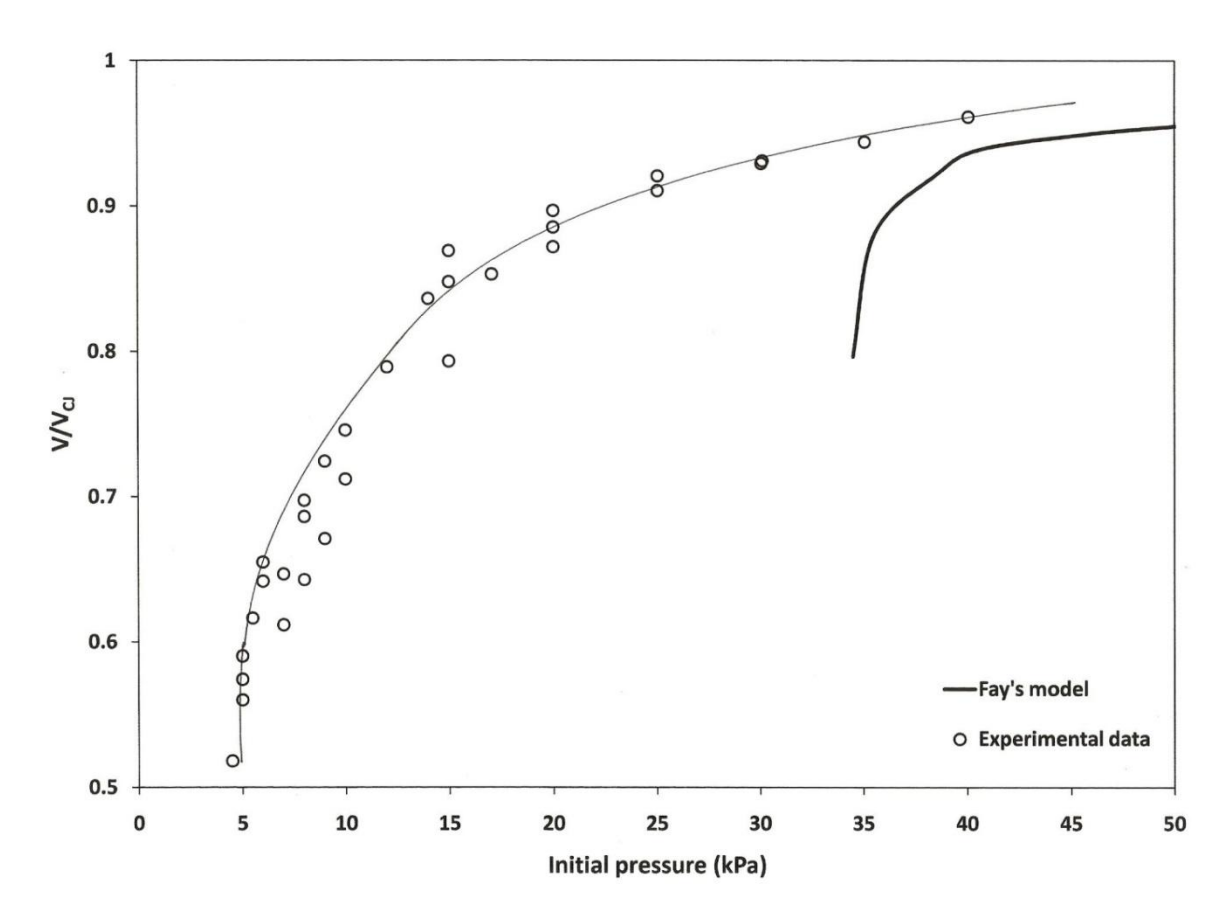


Figure 20: Comparison of Fay's curvature model with experimental results for $CH_4 + 2O_2$ in a 3.175 mm annular gap.

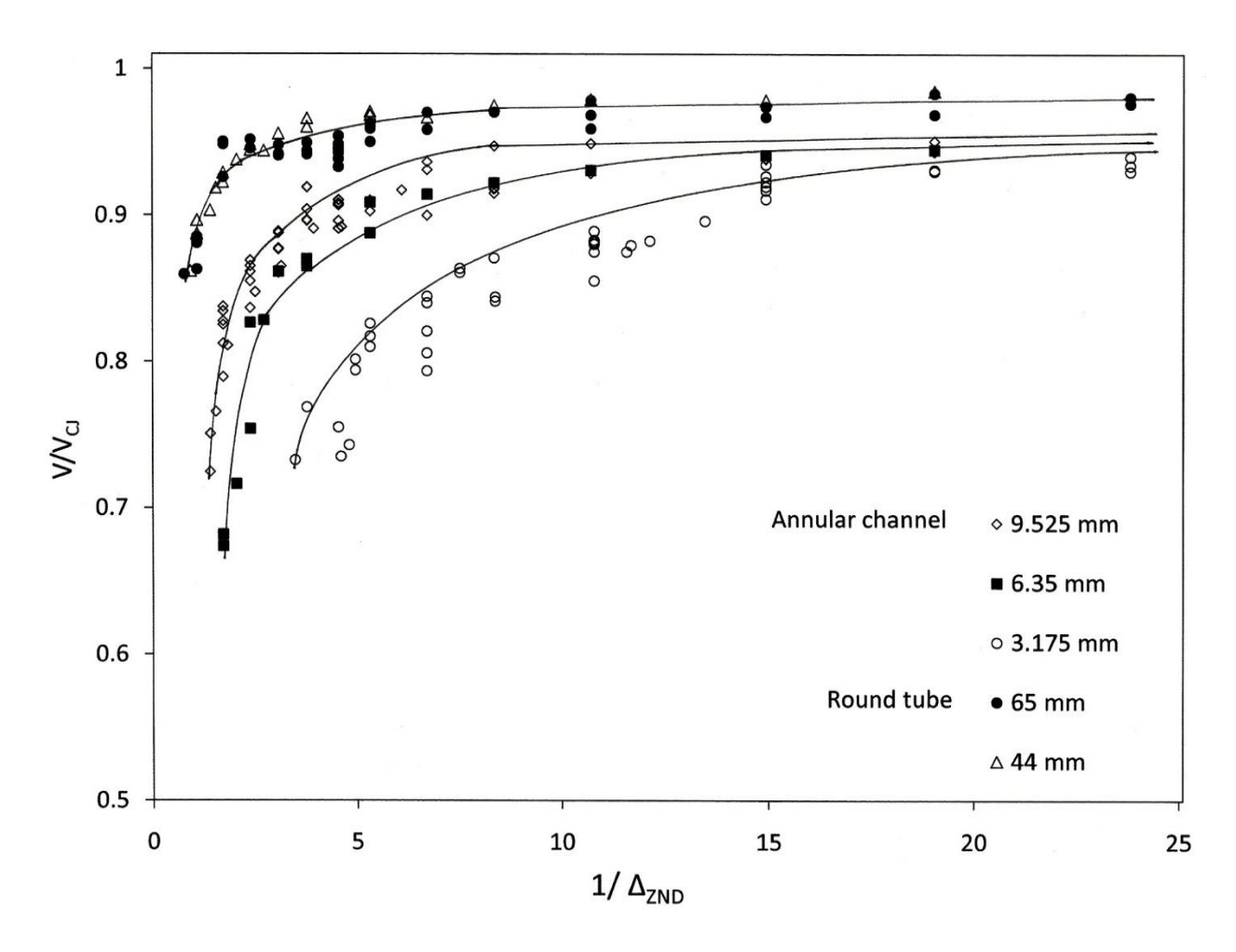


Figure 21: Normalized detonation velocities as a function of $1/\Delta_{ZND}$ in C_2H_2 +2.5 O_2 +70%Ar mixture in annular channels and round tubes.

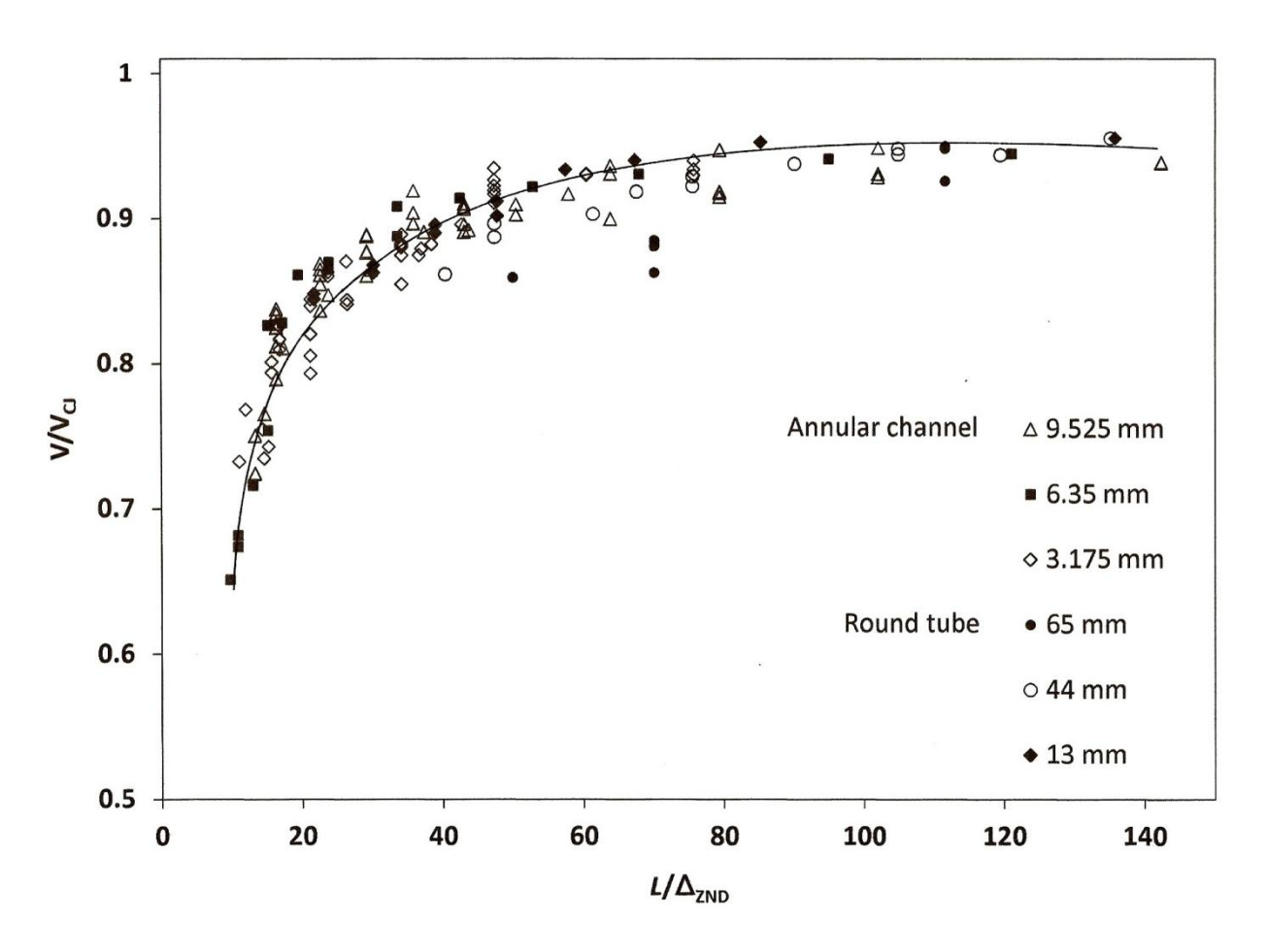


Figure 22: Normalized detonation velocities as a function of L/Δ_{ZND} in C_2H_2 +2.5 O_2 +70%Ar mixture in annular channels and round tubes.

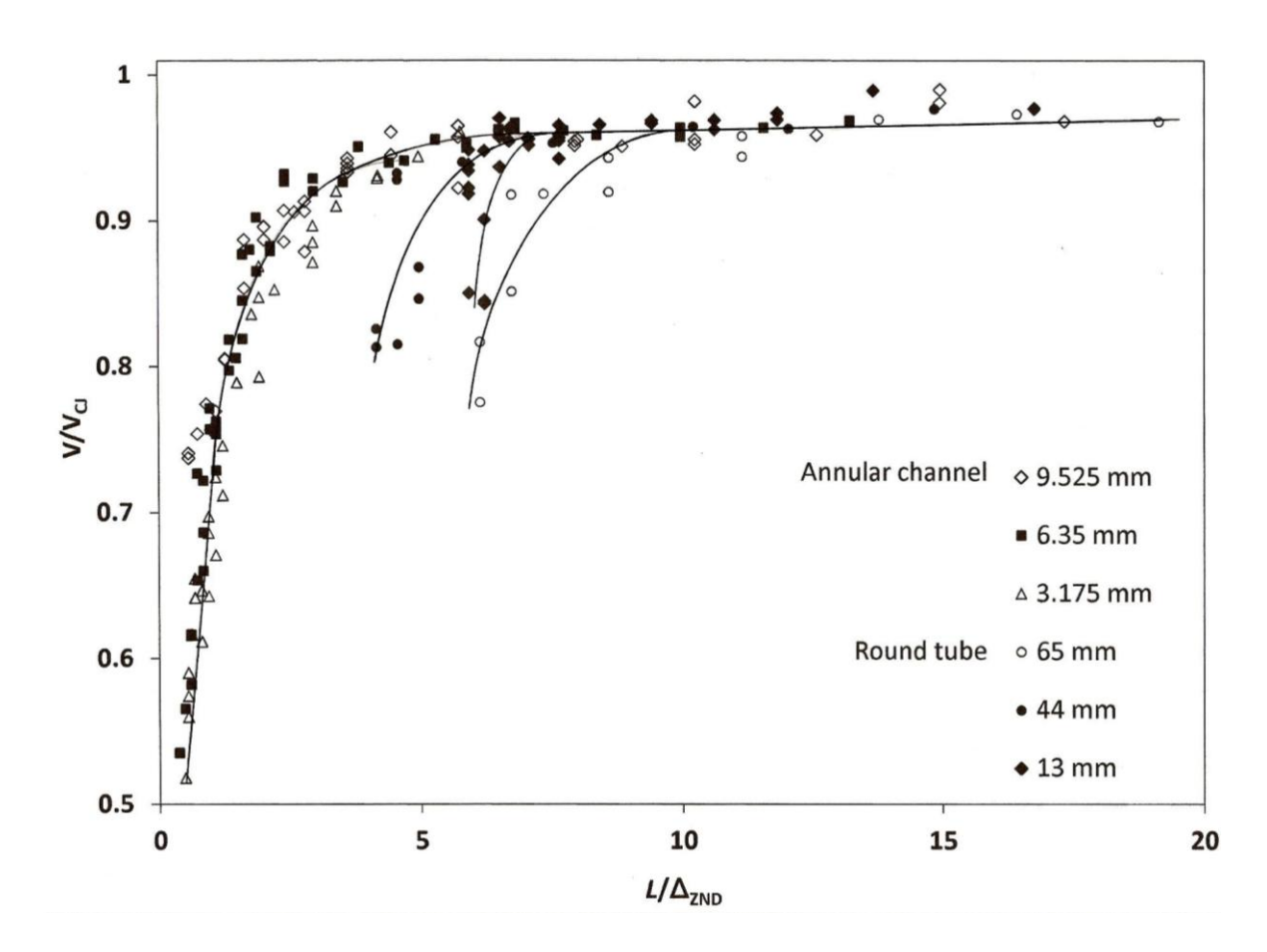


Figure 23: Normalized detonation velocities as a function of L/Δ_{ZND} in CH₄ + 2O₂ mixture in annular channels and round tubes.

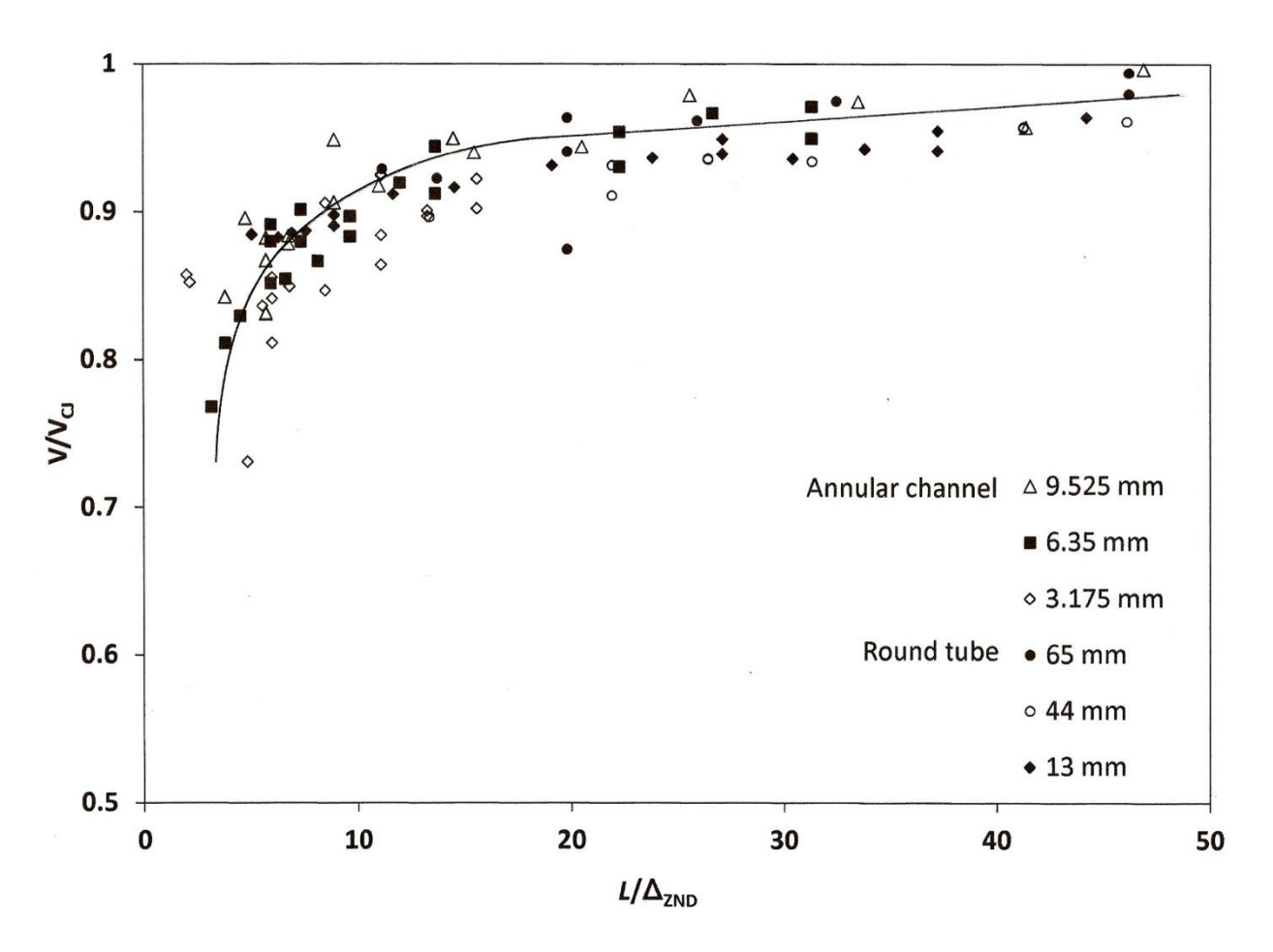


Figure 24: Normalized detonation velocities as a function of L/Δ_{ZND} in C_2H_2 + $5N_2O$ + 50%Ar mixture in annular channels and round tubes.

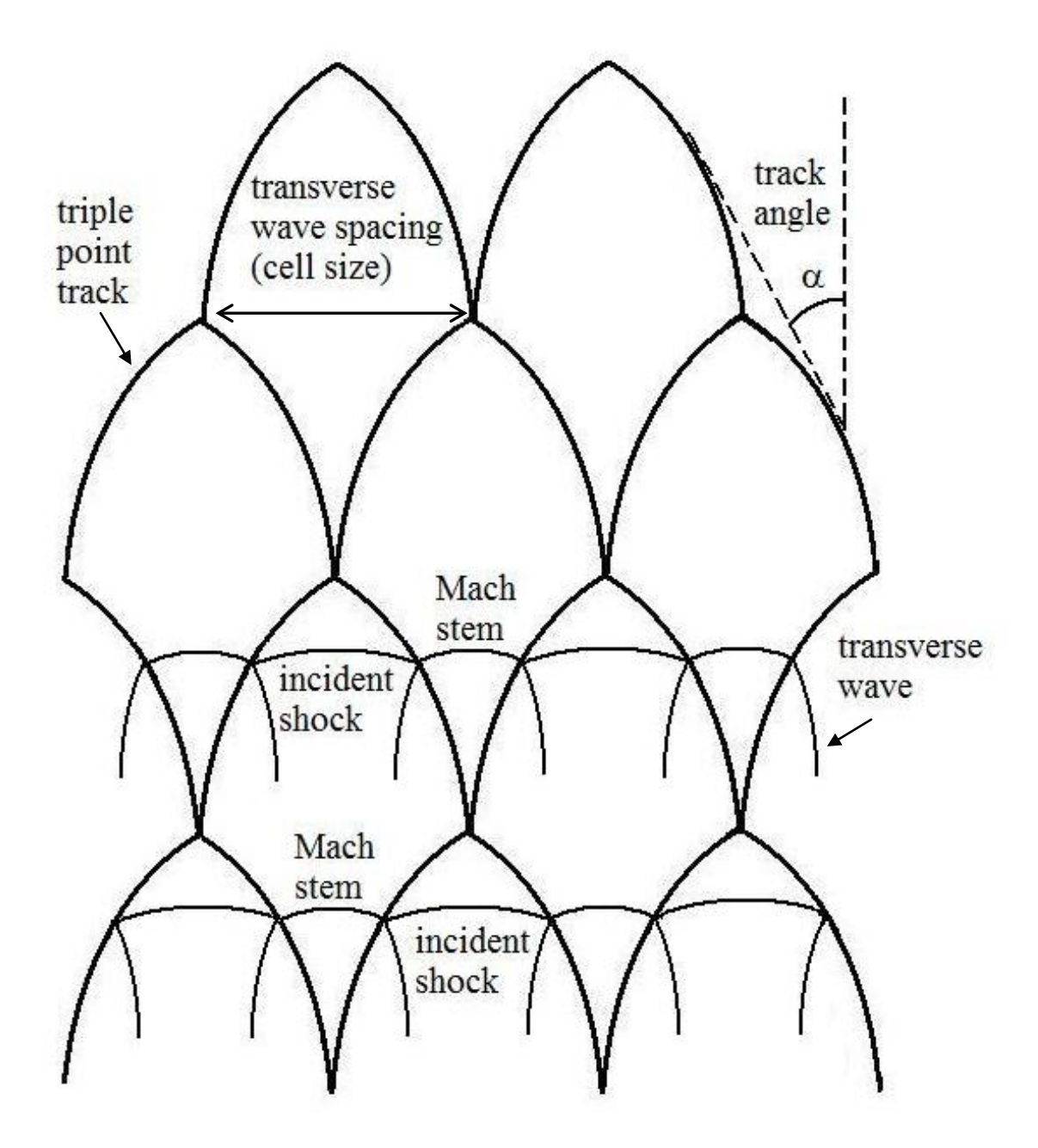


Figure 25: Sketch of an idealized two-dimensional detonation front superimposed on triple point tracks.

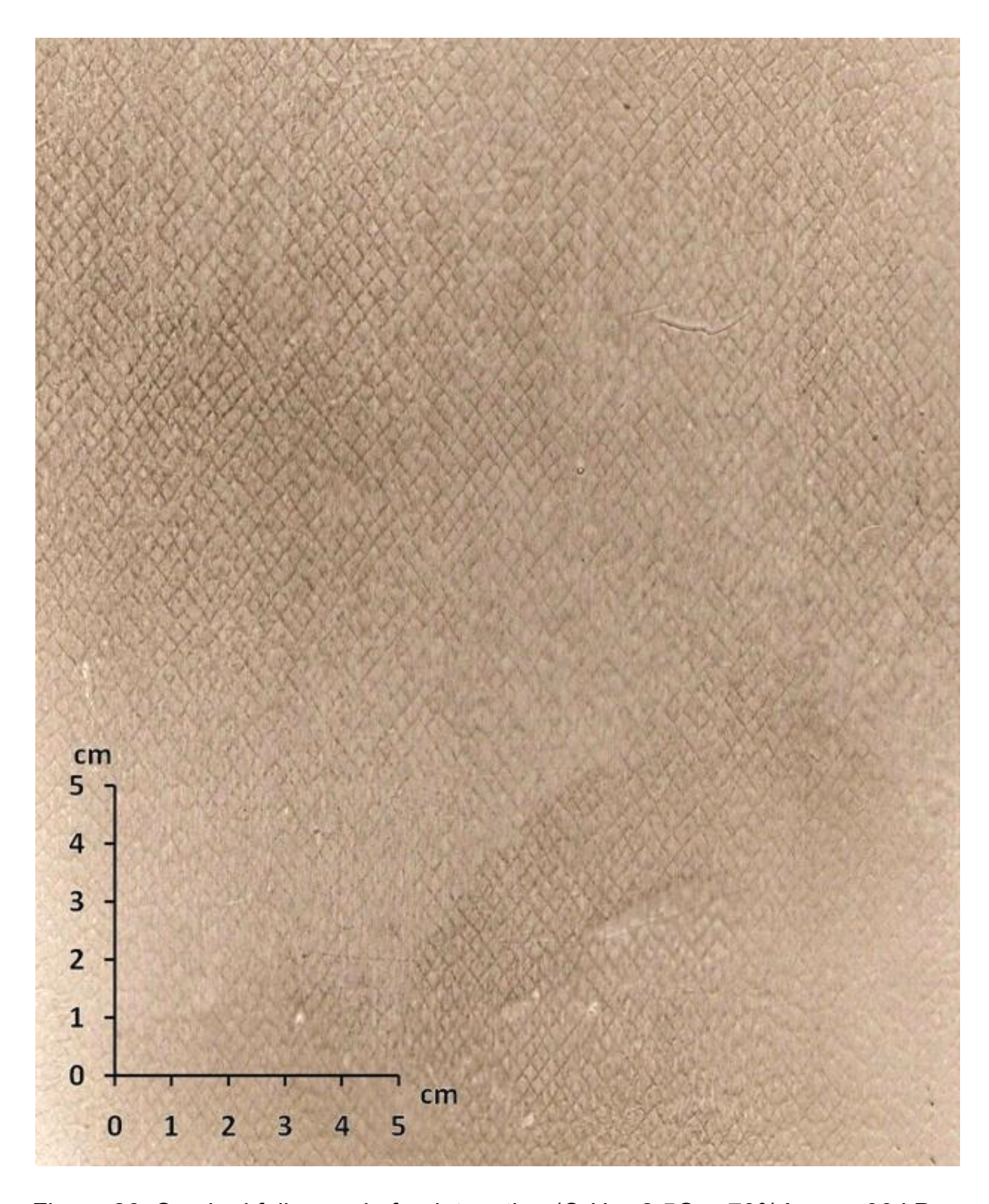


Figure 26: Smoked foil record of a detonation ($C_2H_2 + 2.5O_2 + 70\%$ Ar, p_0 = 30 kPa, 65 mm diameter round tube).

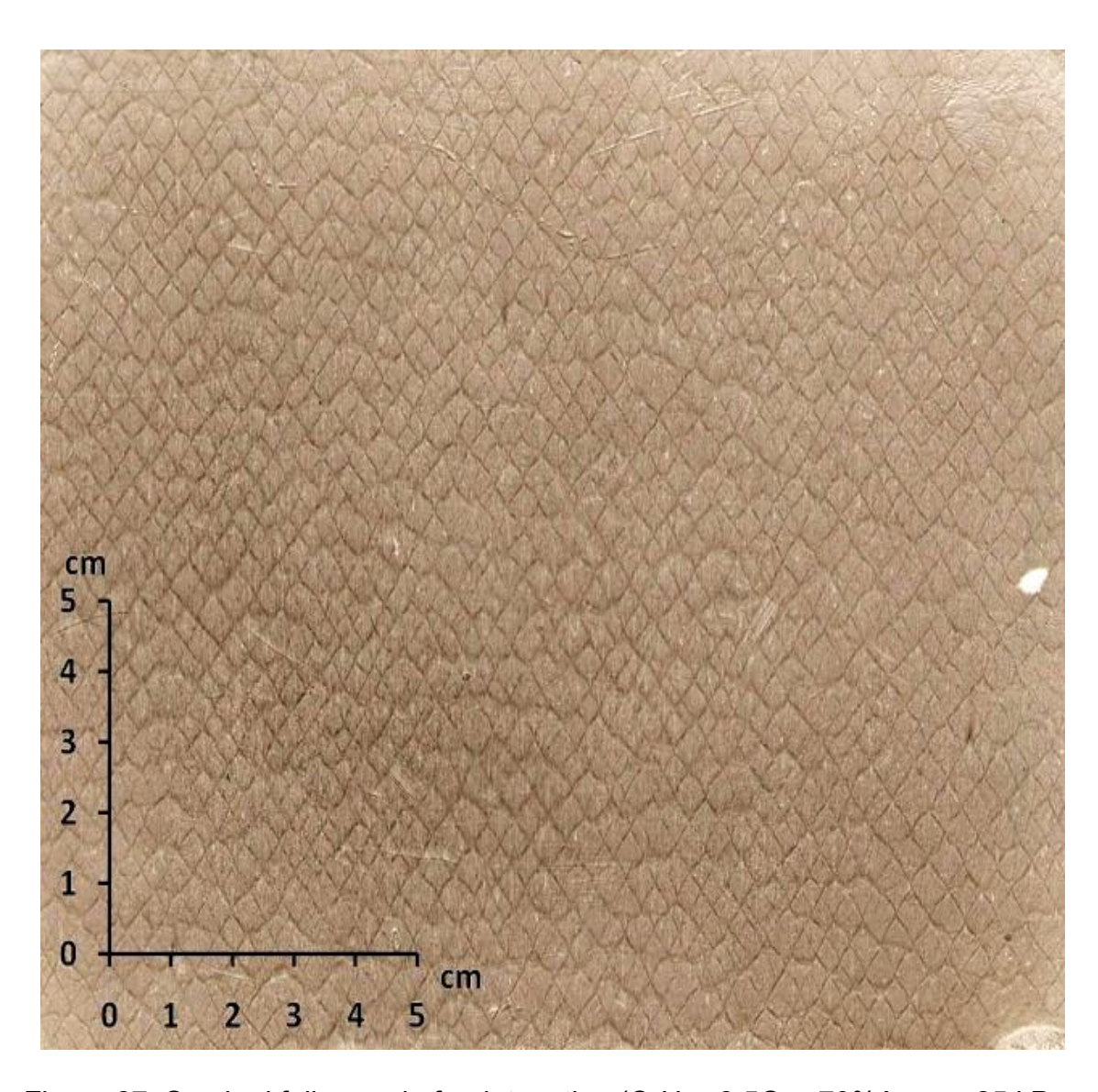


Figure 27: Smoked foil record of a detonation ($C_2H_2 + 2.5O_2 + 70\%$ Ar, p_0 = 25 kPa, 9.525 mm channel gap).

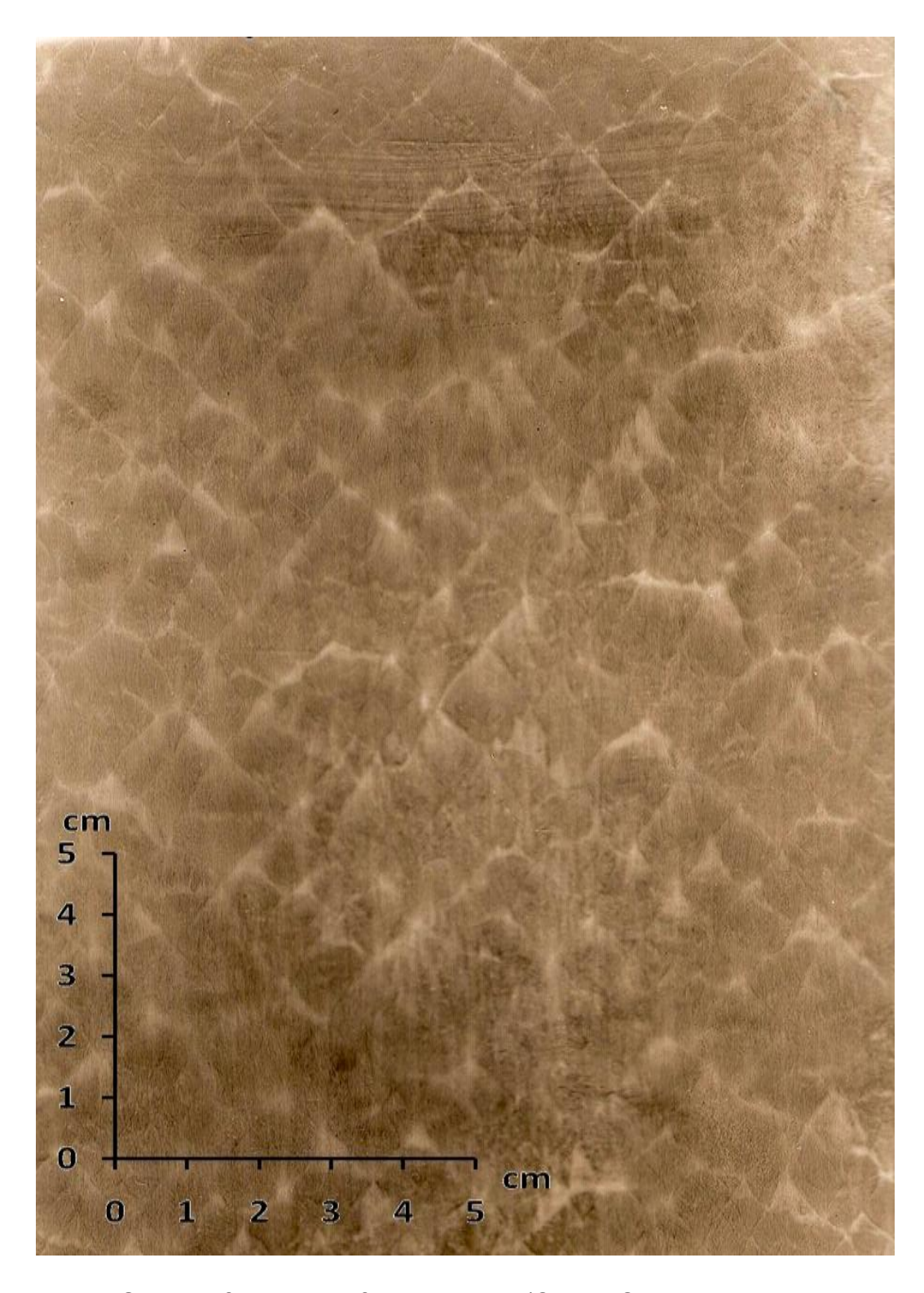


Figure 28: Smoked foil record of a detonation (CH $_4$ +2O $_2$, p $_0$ = 35 kPa, 44 mm diameter round tube).

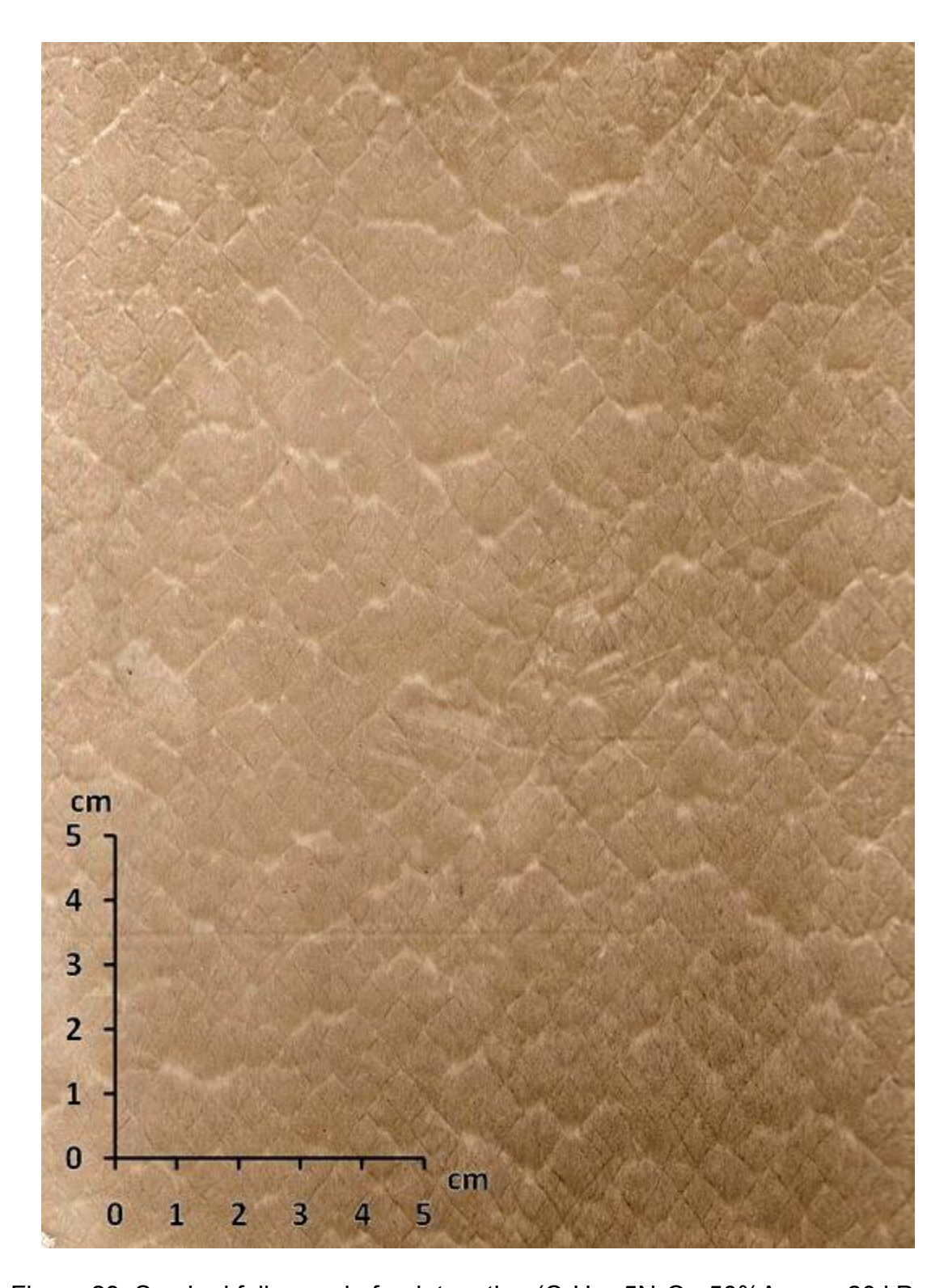


Figure 29: Smoked foil record of a detonation (C_2H_2 +5 N_2O +50%Ar, p_0 = 20 kPa, 51 mm diameter round tube).

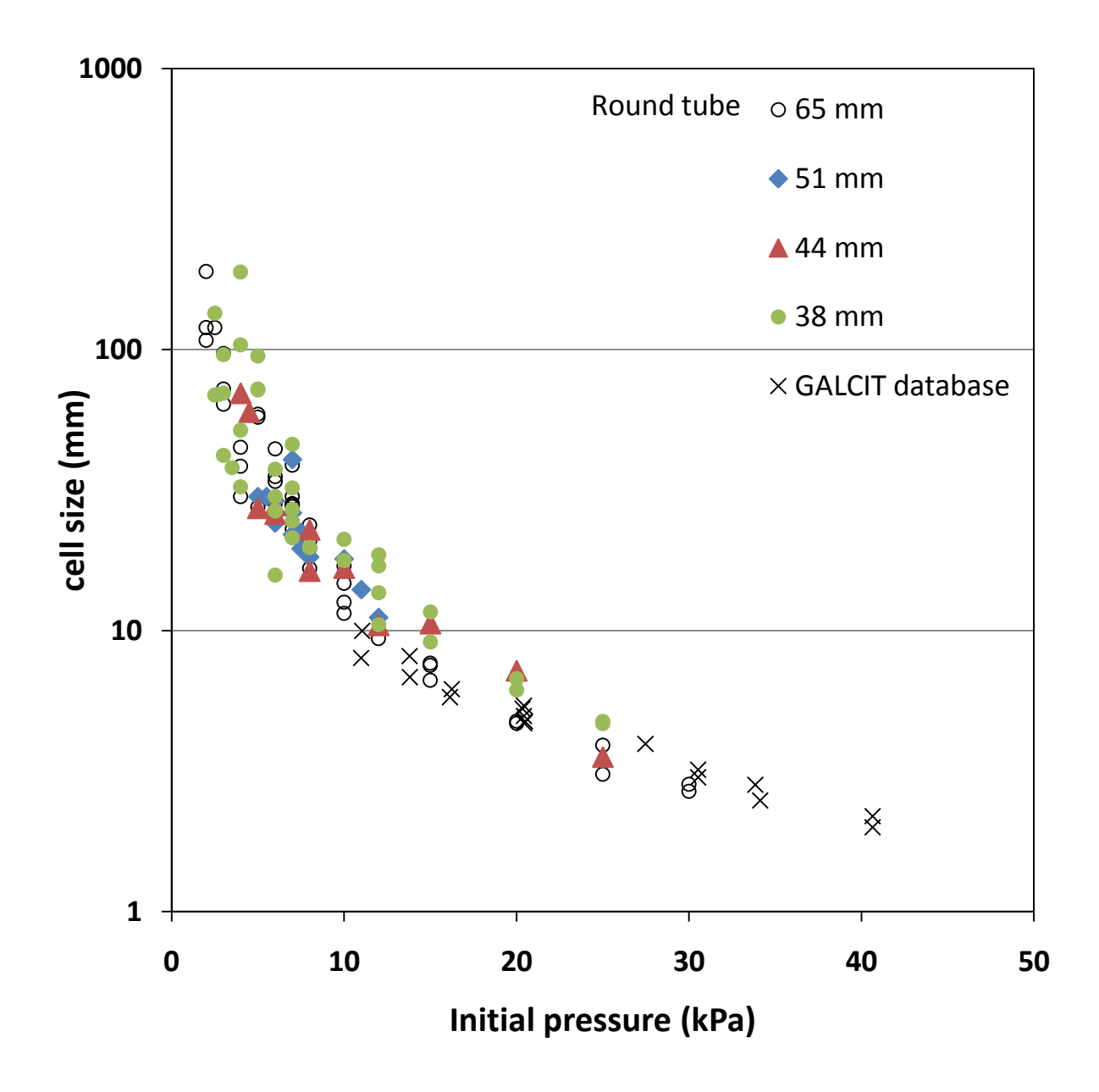


Figure 30: Variation of cell size as a function of initial pressure in C_2H_2 +2.5 O_2 +70%Ar for different diameter round tubes.

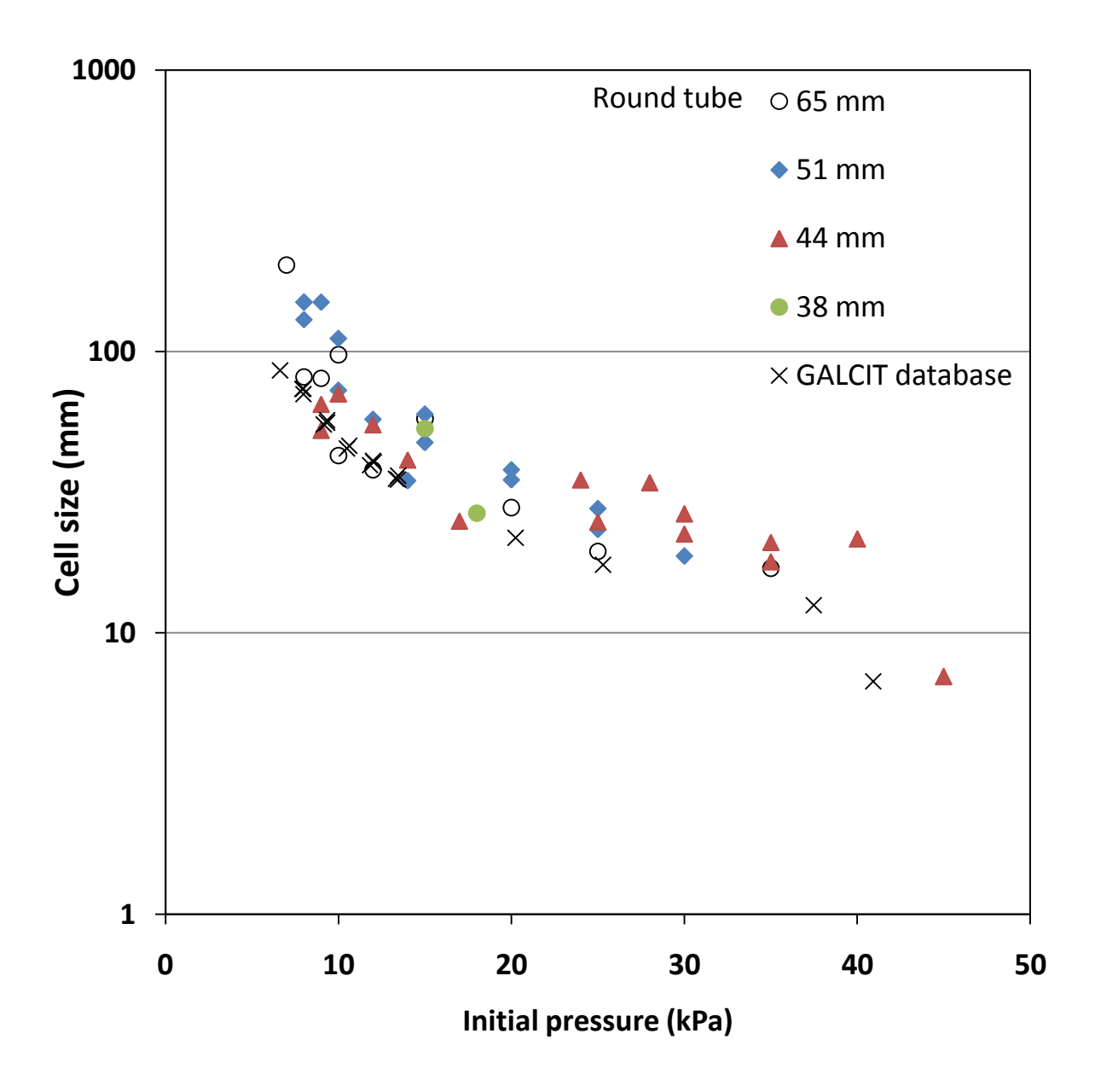


Figure 31: Variation of cell size as a function of initial pressure in $CH_4 + 2O_2$ mixture for different diameter round tubes.

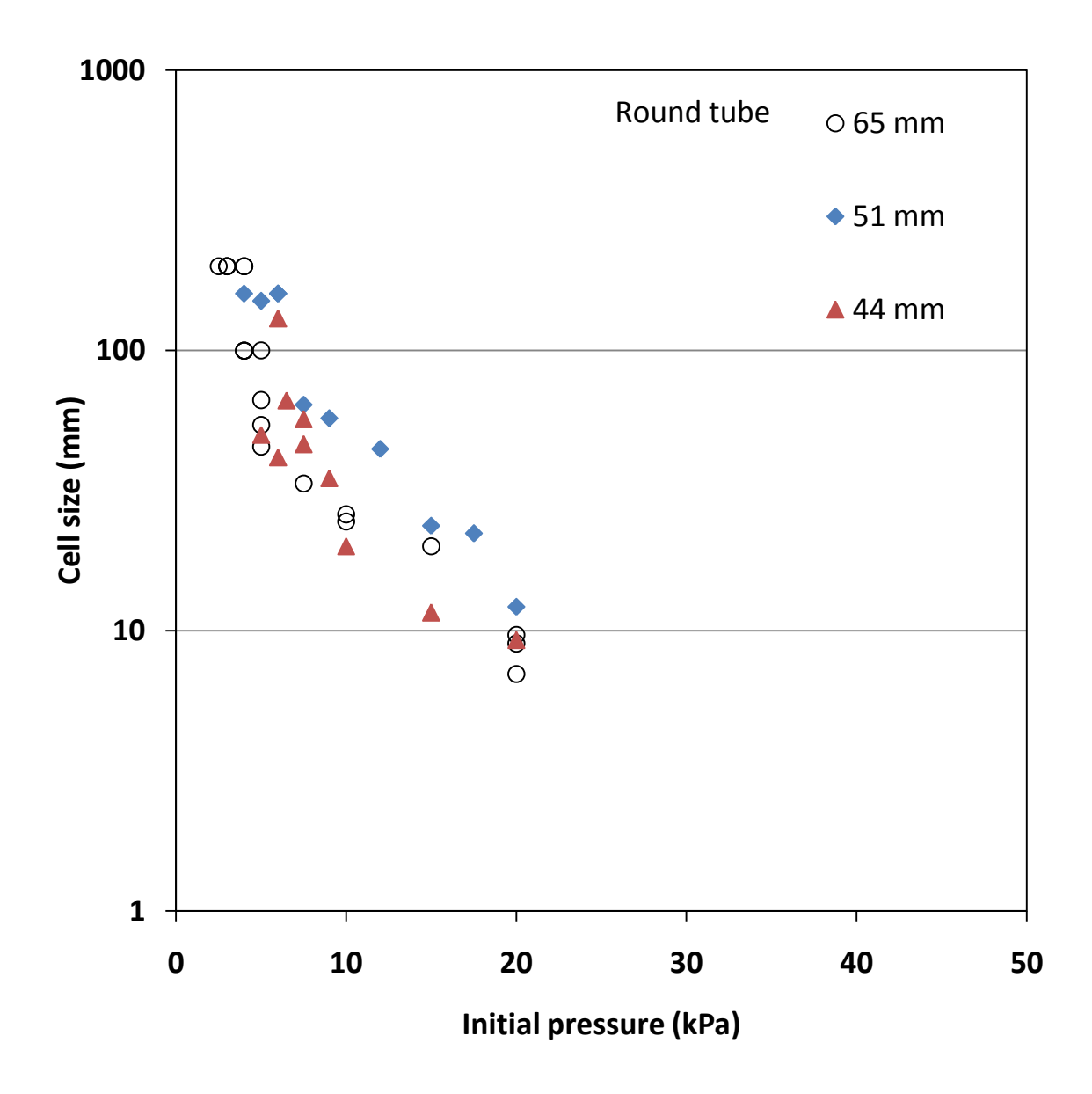


Figure 32: Variation of cell size as a function of initial pressure in $C_2H_2 + 5N_2O + 50\%$ Ar mixture for different diameter round tubes.

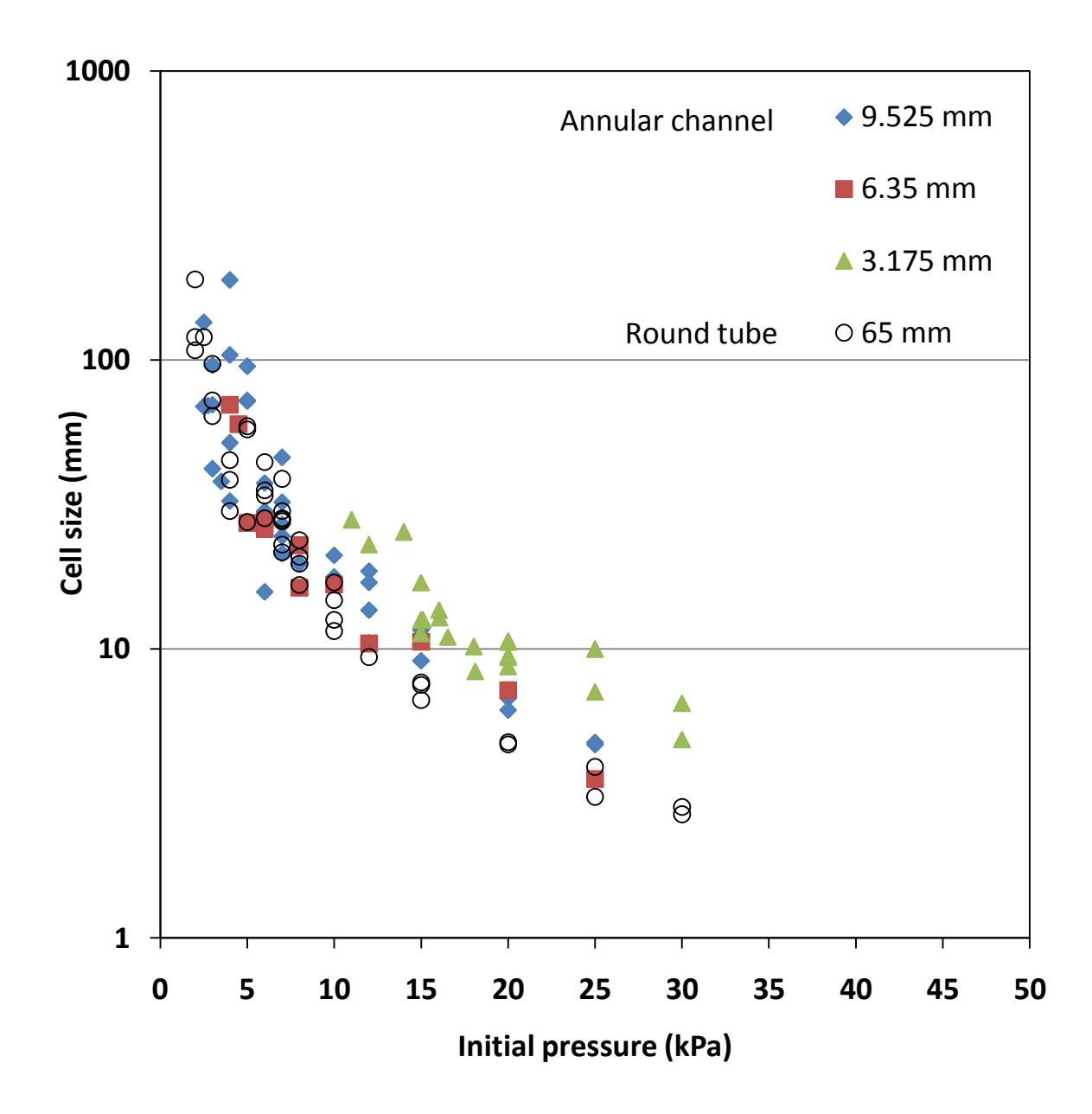


Figure 33: Variation of cell size with initial pressure in C_2H_2 +2.5 O_2 +70%Ar in annular channels.

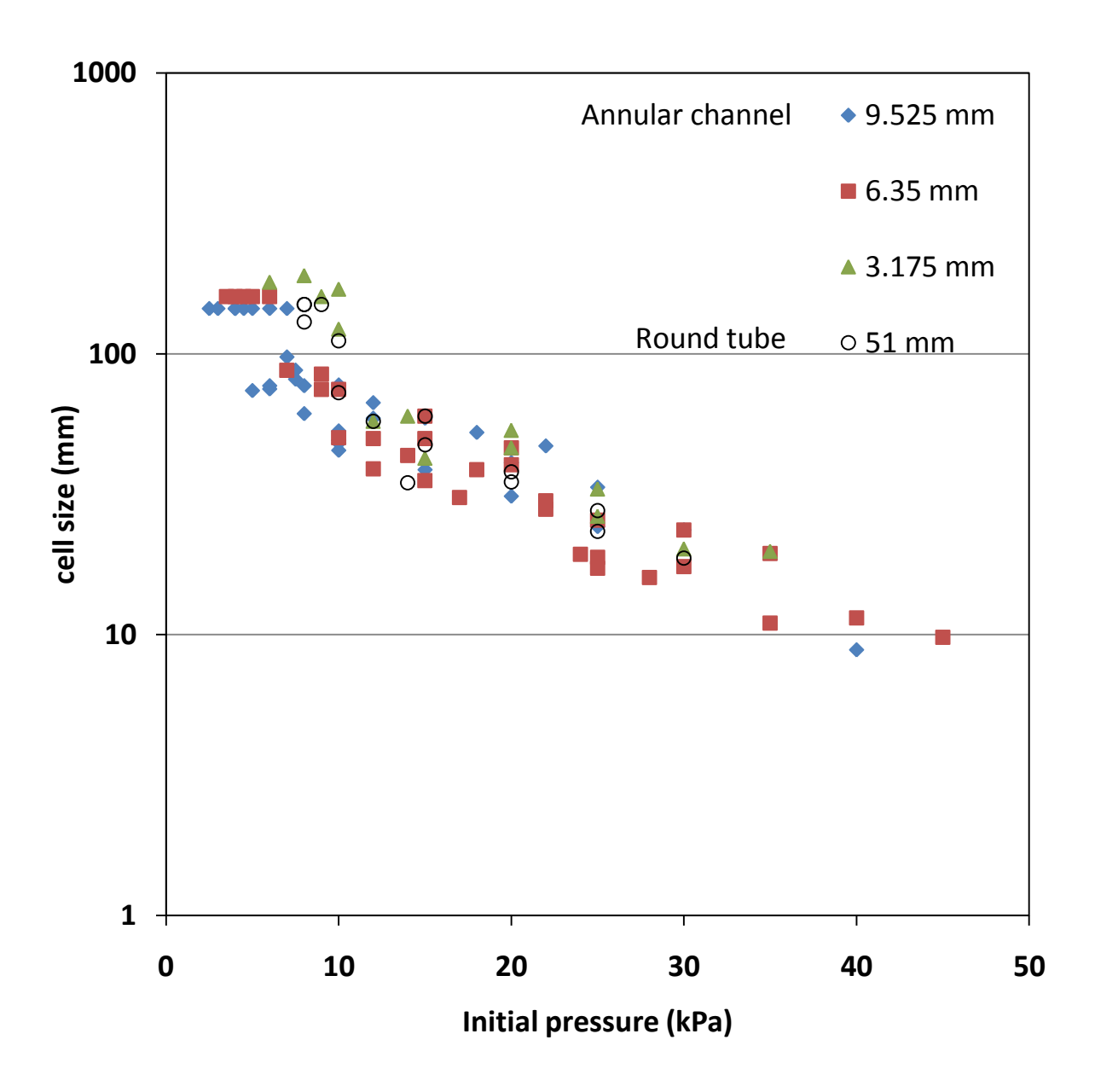


Figure 34: Variation of cell size with initial pressure in CH_4 +2 O_2 mixtures in annular channels.

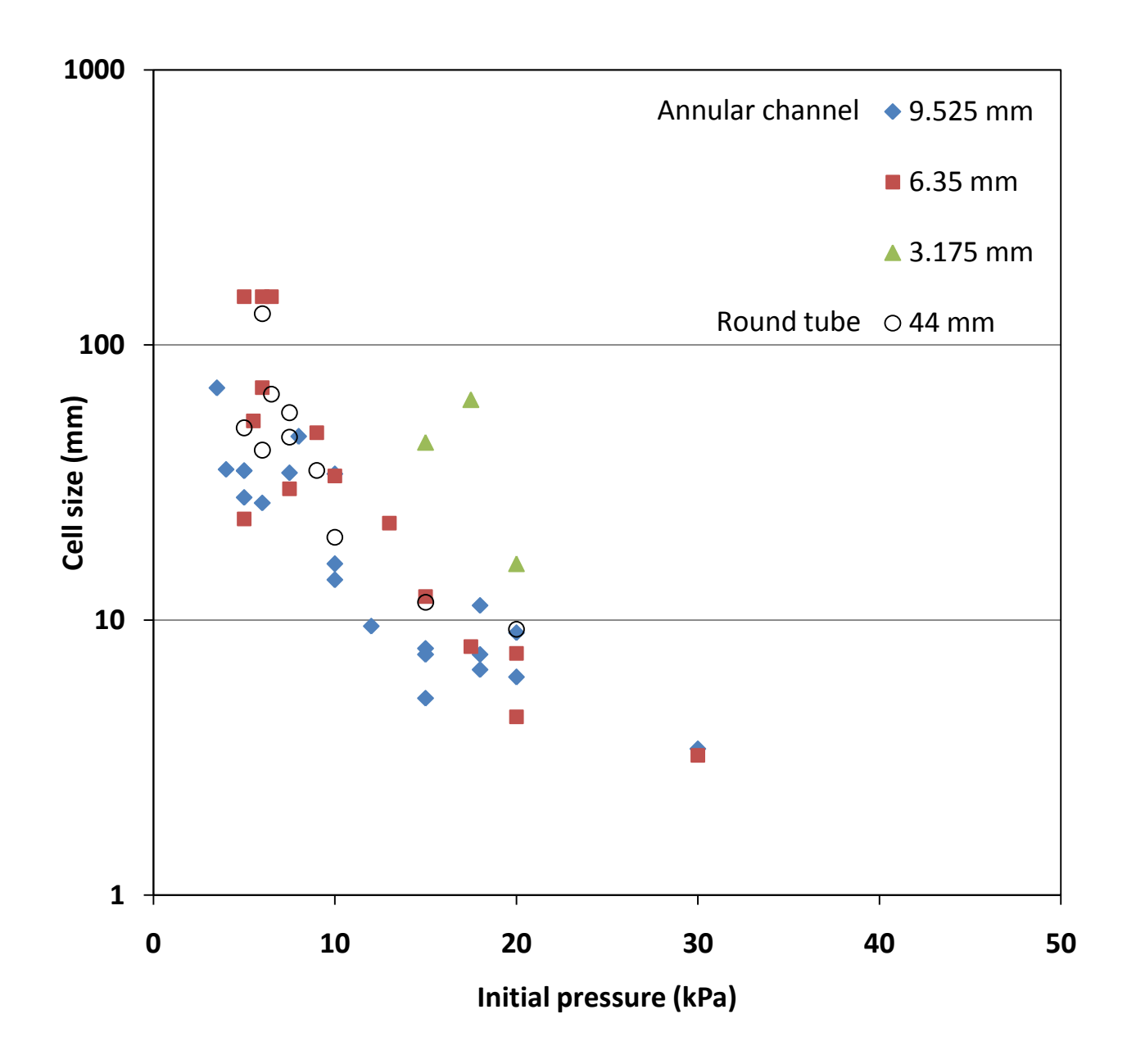


Figure 35: Variation of cell size with initial pressure in C_2H_2 +5 N_2O +50%Ar in annular channels.

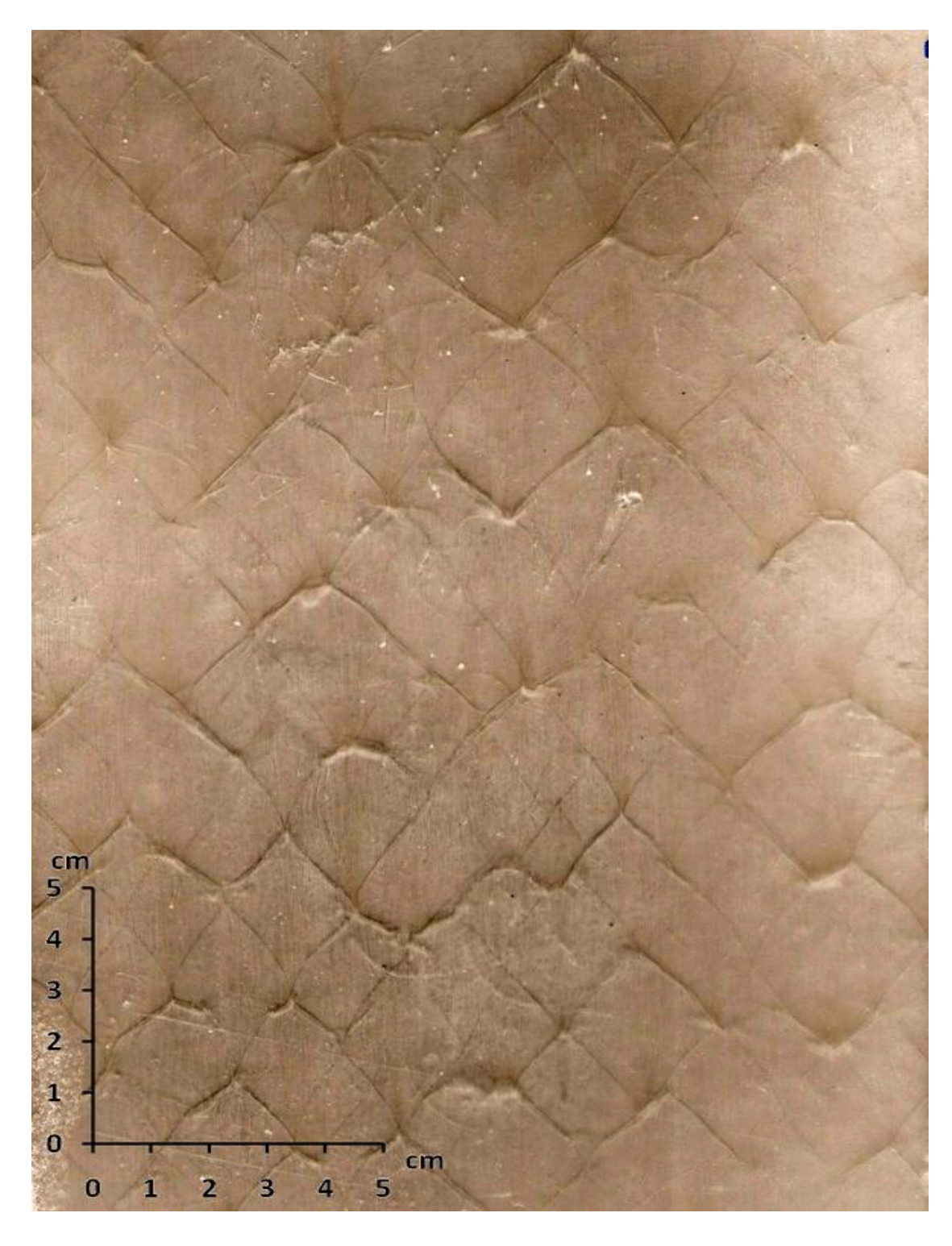


Figure 36: Smoked foil record of a detonation ($C_2H_2 + 2.5O_2 + 70\%$ Ar, p_0 = 6 kPa, 51 mm diameter round tube).

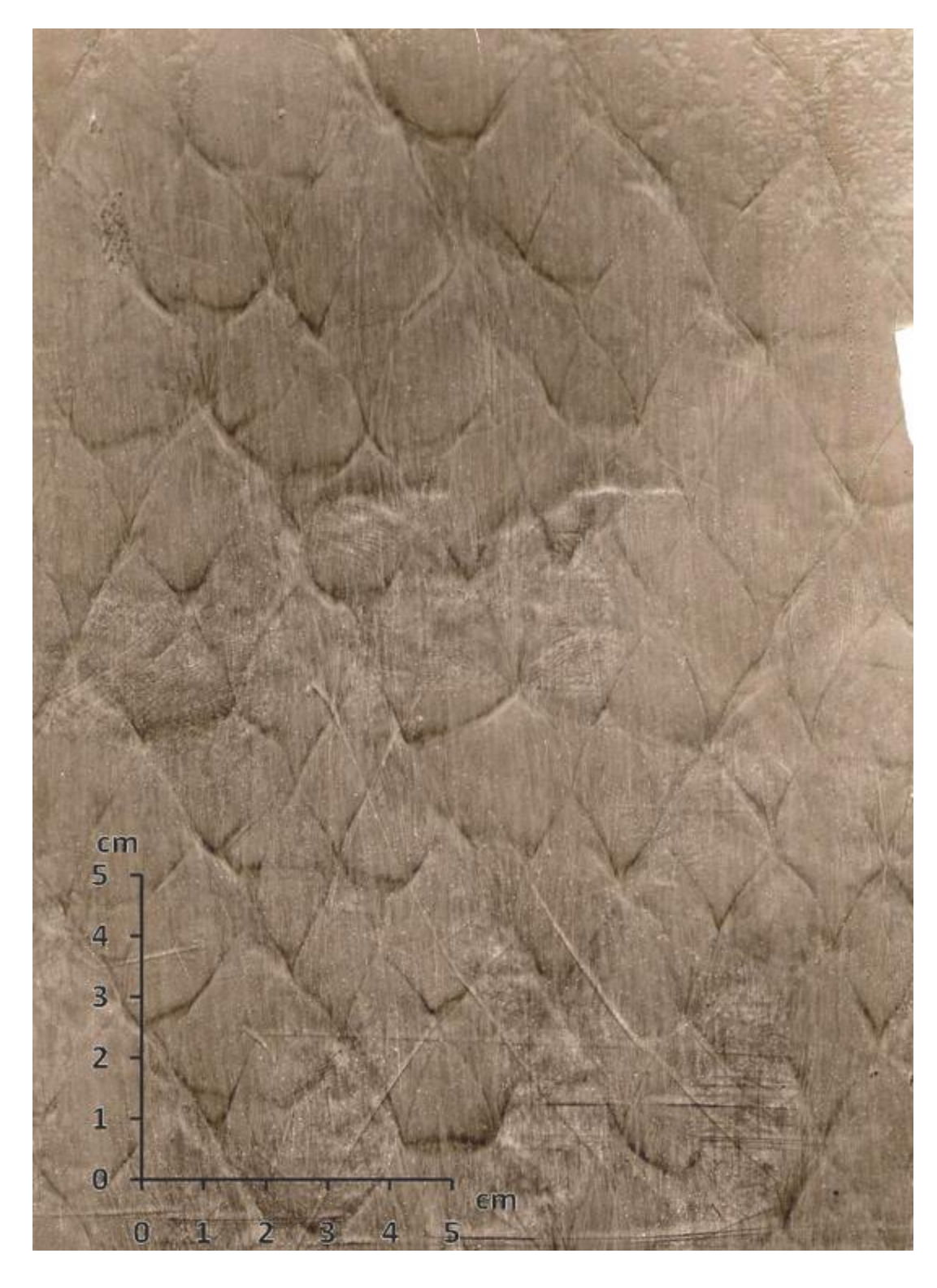


Figure 37: Smoked foil record of a detonation (C_2H_2 +2.5 O_2 +70%Ar, p_0 = 8 kPa, 6.35 mm channel gap).

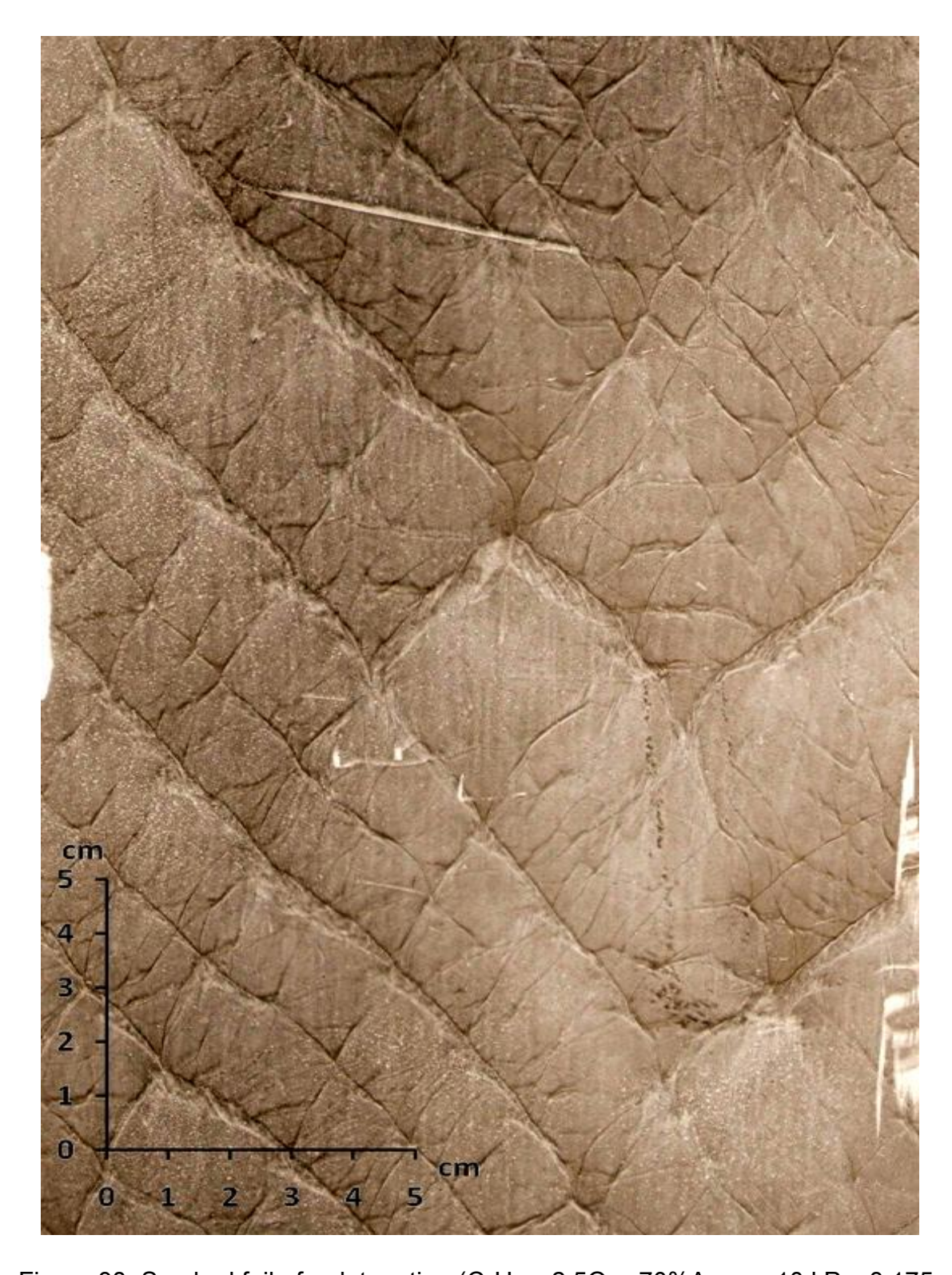


Figure 38: Smoked foil of a detonation ($C_2H_2 + 2.5O_2 + 70\%$ Ar, p_0 = 10 kPa, 3.175 mm channel gap).

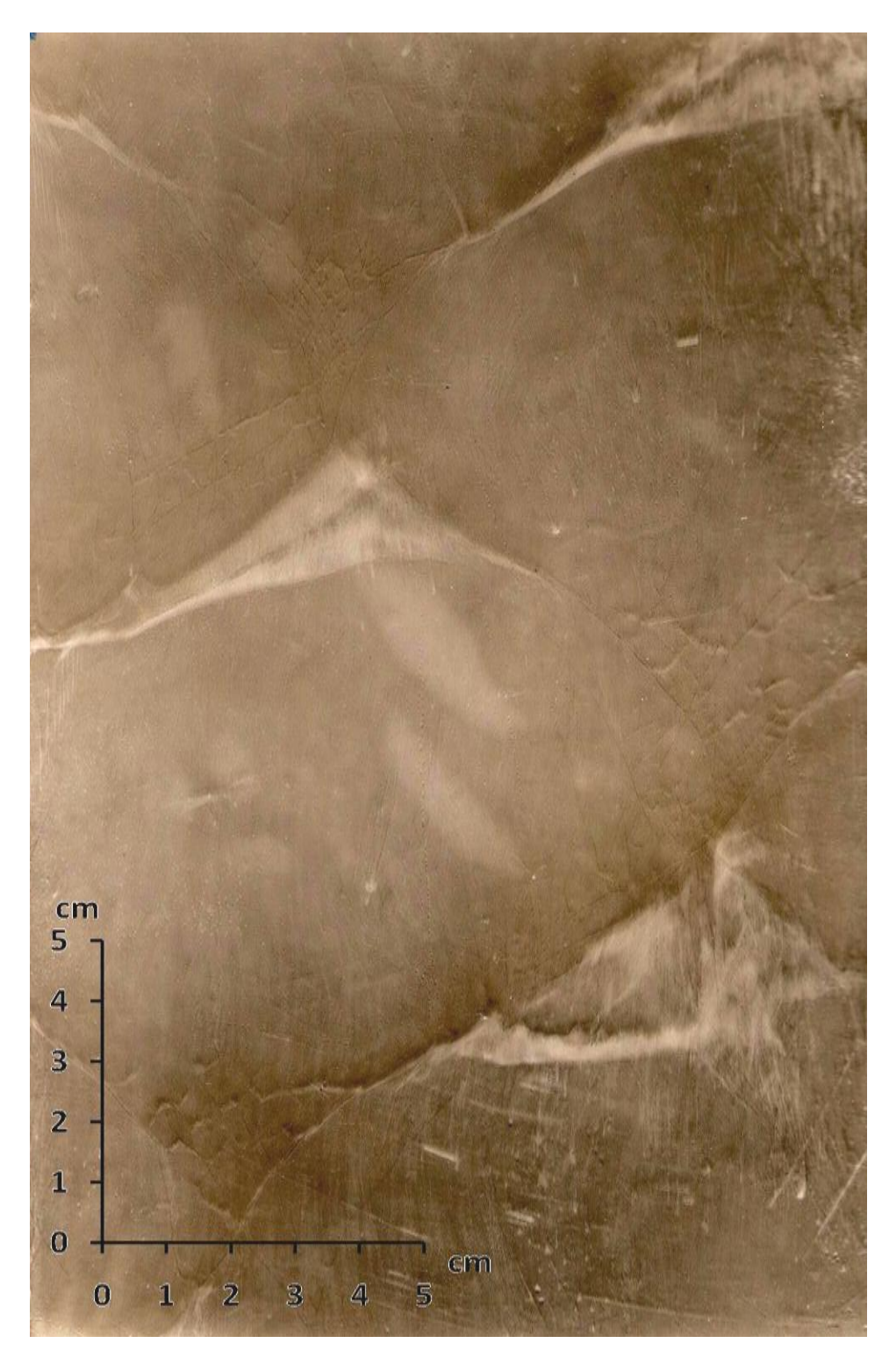


Figure 39: Smoked foil record of a detonation (CH $_4$ +2O $_2$, p $_0$ = 7.5 kPa, 44 mm diameter round tube).

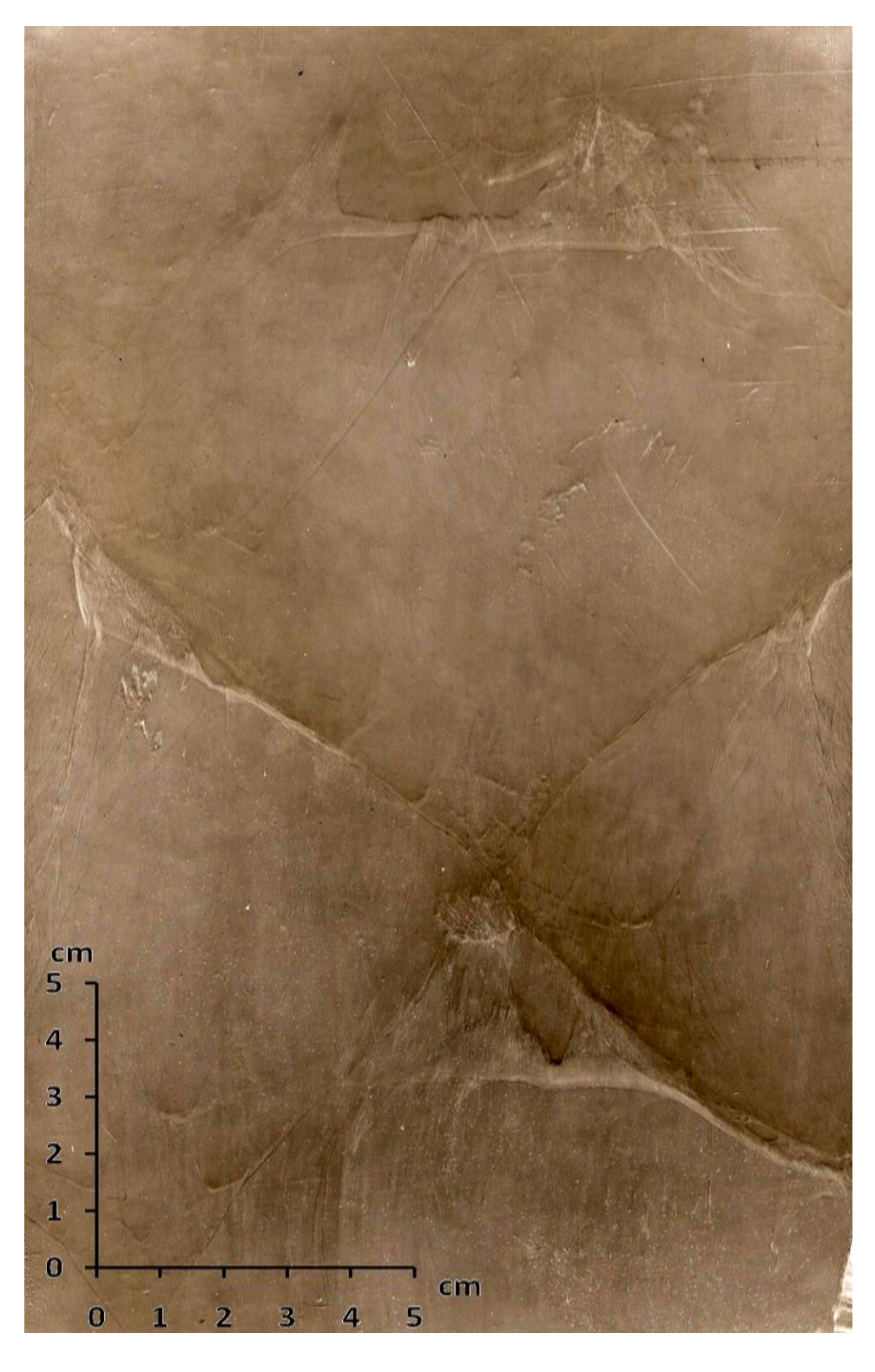


Figure 40: Smoked foil record of a detonation (CH $_4$ +2O $_2$, p $_0$ = 4 kPa, 44 mm diameter round tube).

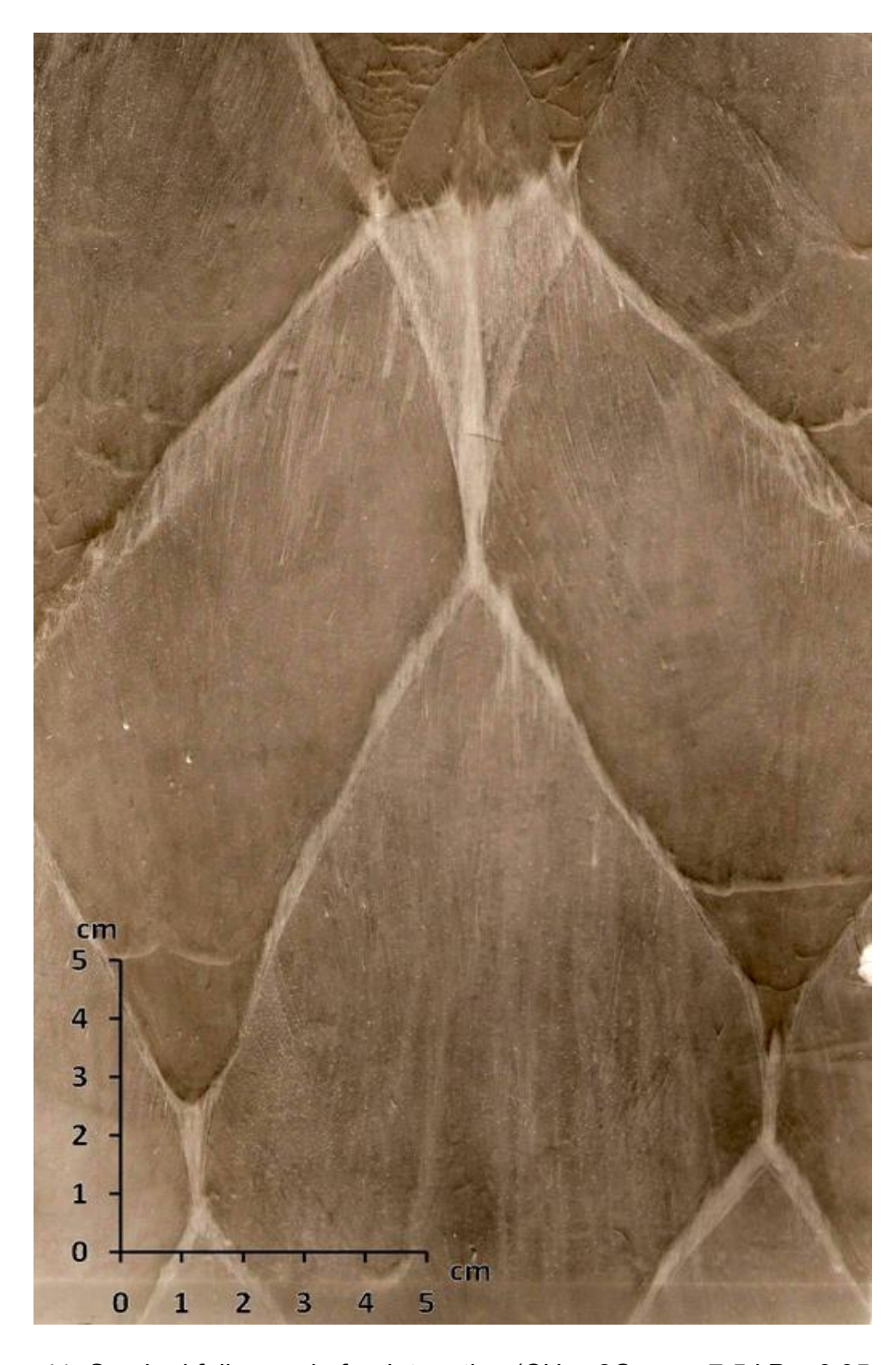


Figure 41: Smoked foil record of a detonation (CH $_4$ +2O $_2$, p $_0$ = 7.5 kPa, 6.35 mm channel).



Figure 42: Smoked foil record of a detonation (CH $_4$ +2O $_2$, p $_0$ = 8 kPa, 3.175 mm channel).

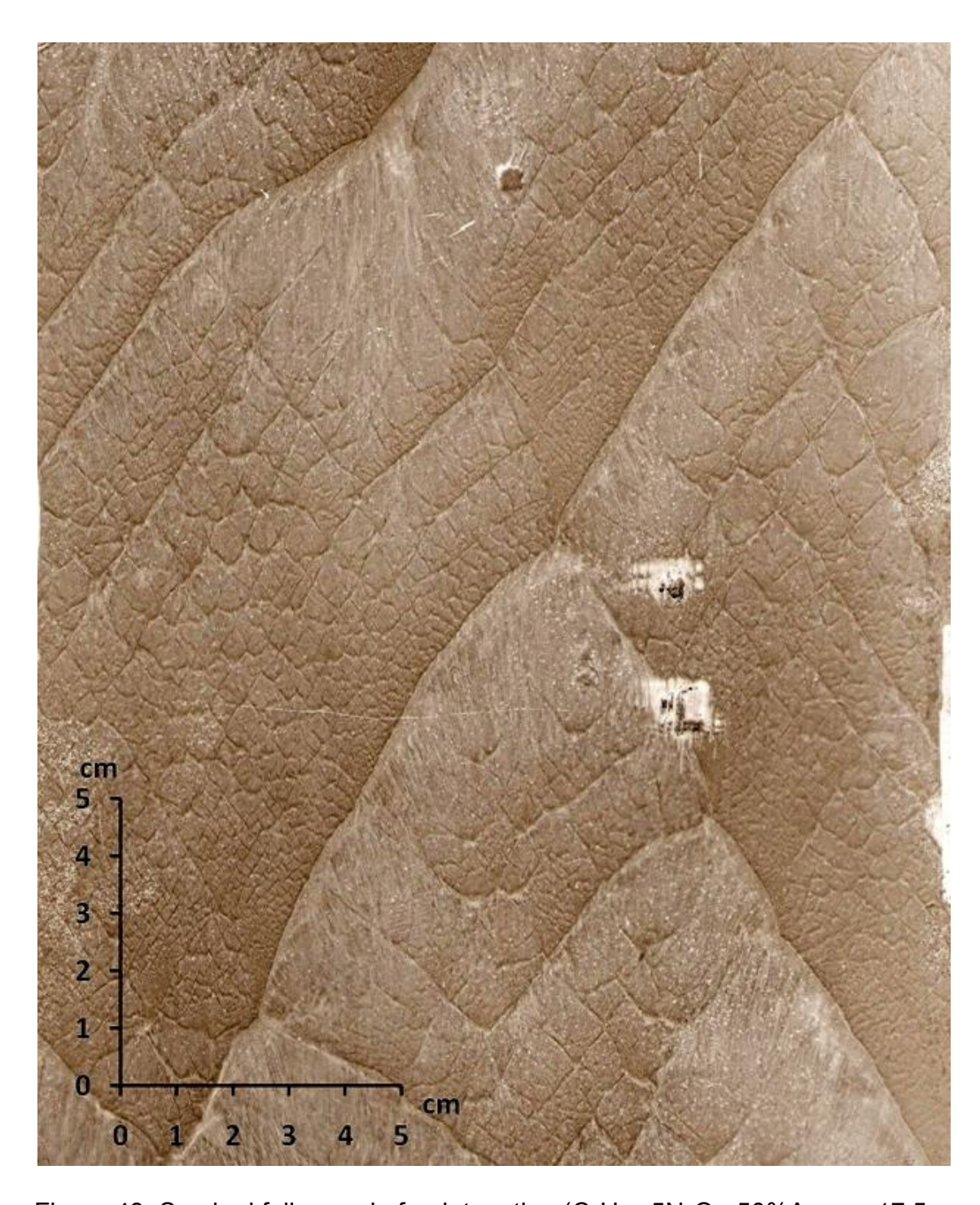


Figure 43: Smoked foil record of a detonation (C_2H_2 +5 N_2O +50%Ar, p_0 = 17.5 kPa, 3.175 mm channel).

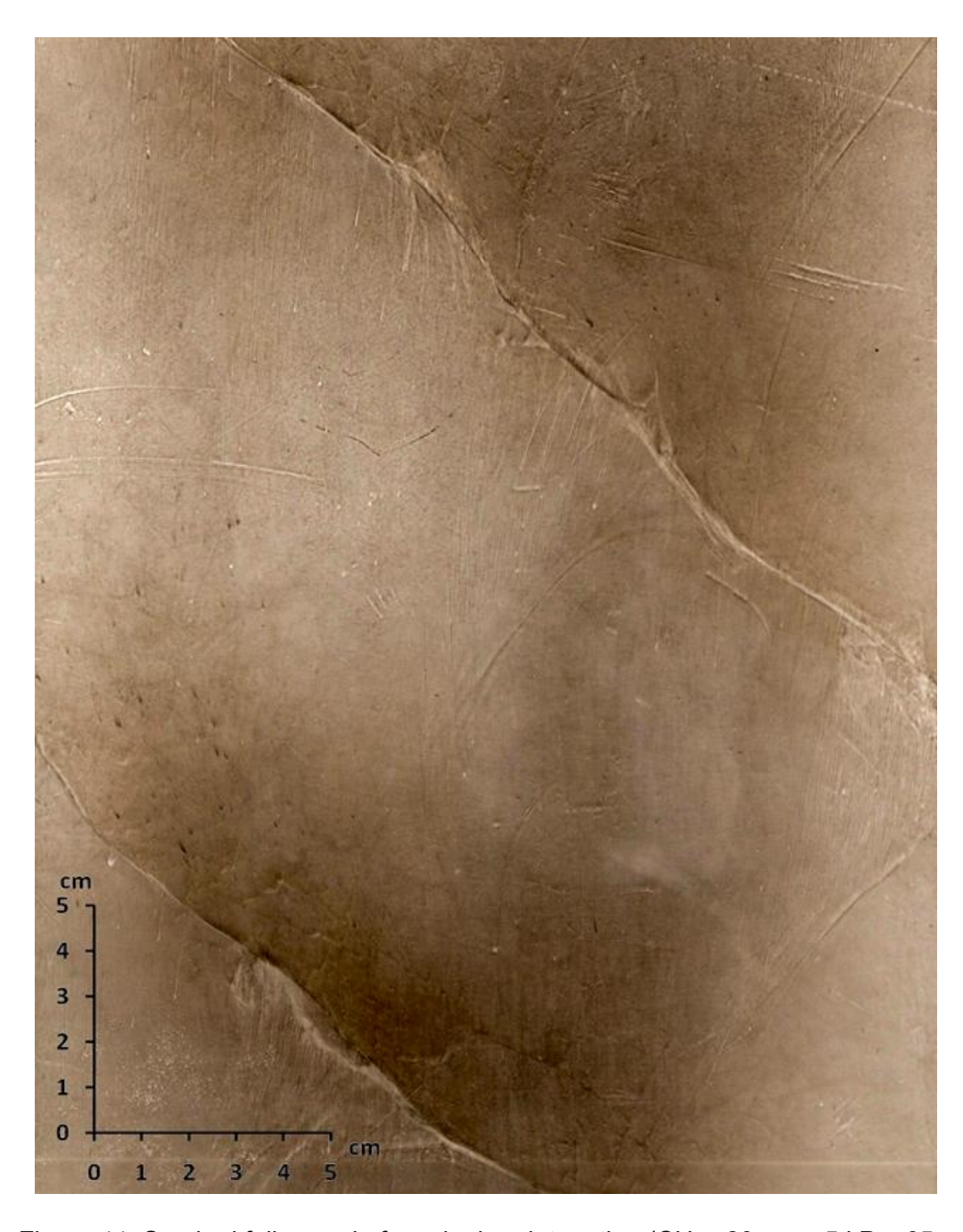


Figure 44: Smoked foil record of a spinning detonation (CH $_4$ +20 $_2$, p $_0$ = 5 kPa, 65 mm diameter round tube).



Figure 45: Smoked foil of a spinning detonation (CH $_4$ +20 $_2$, p $_0$ = 3.25 kPa, 44 mm diameter round tube).

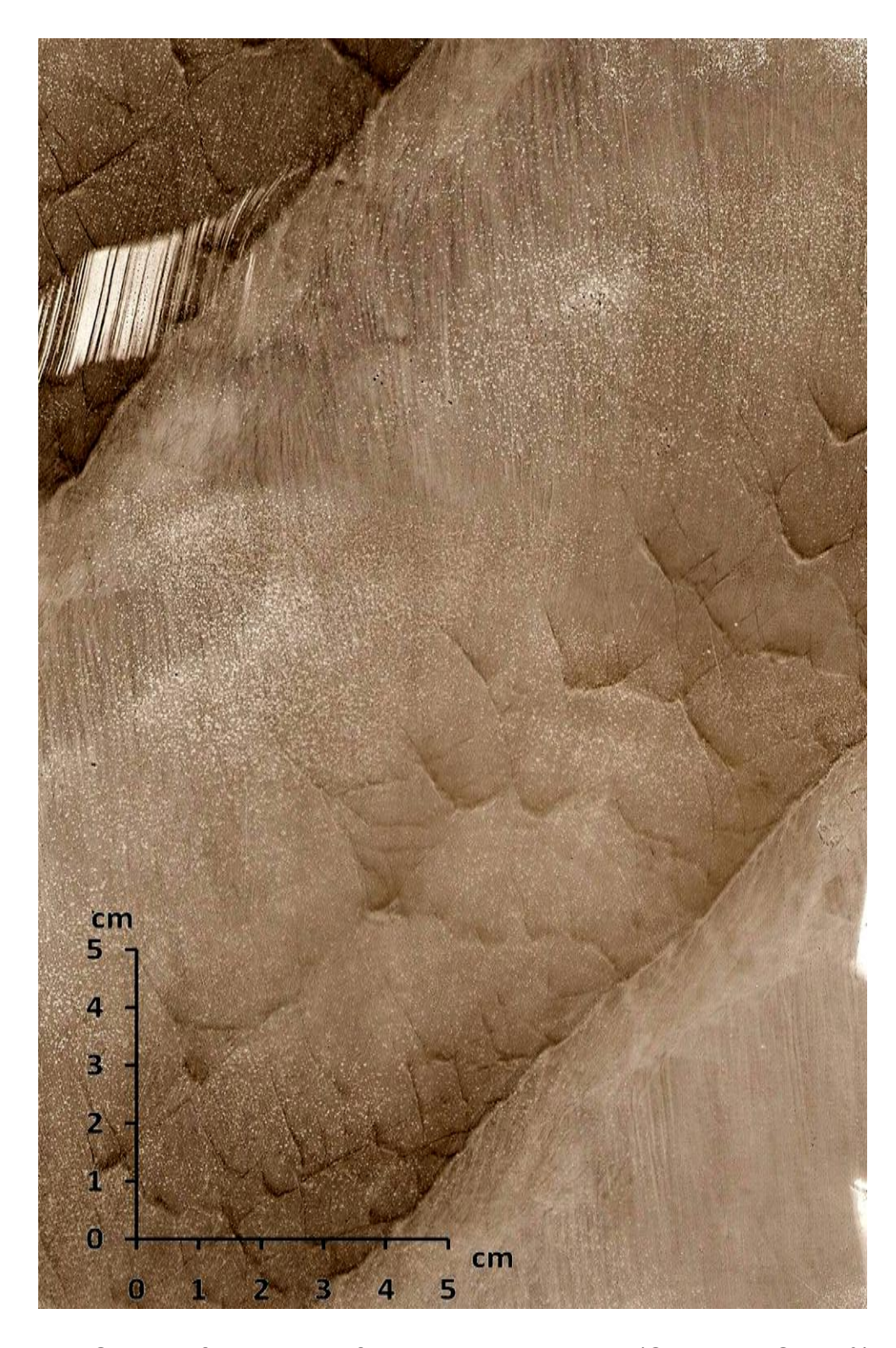


Figure 46: Smoked foil records of a spinning detonation ($C_2H_2 + 5N_2O + 50\%Ar$, p_0 = 3.5 kPa, 6.35 mm channel).

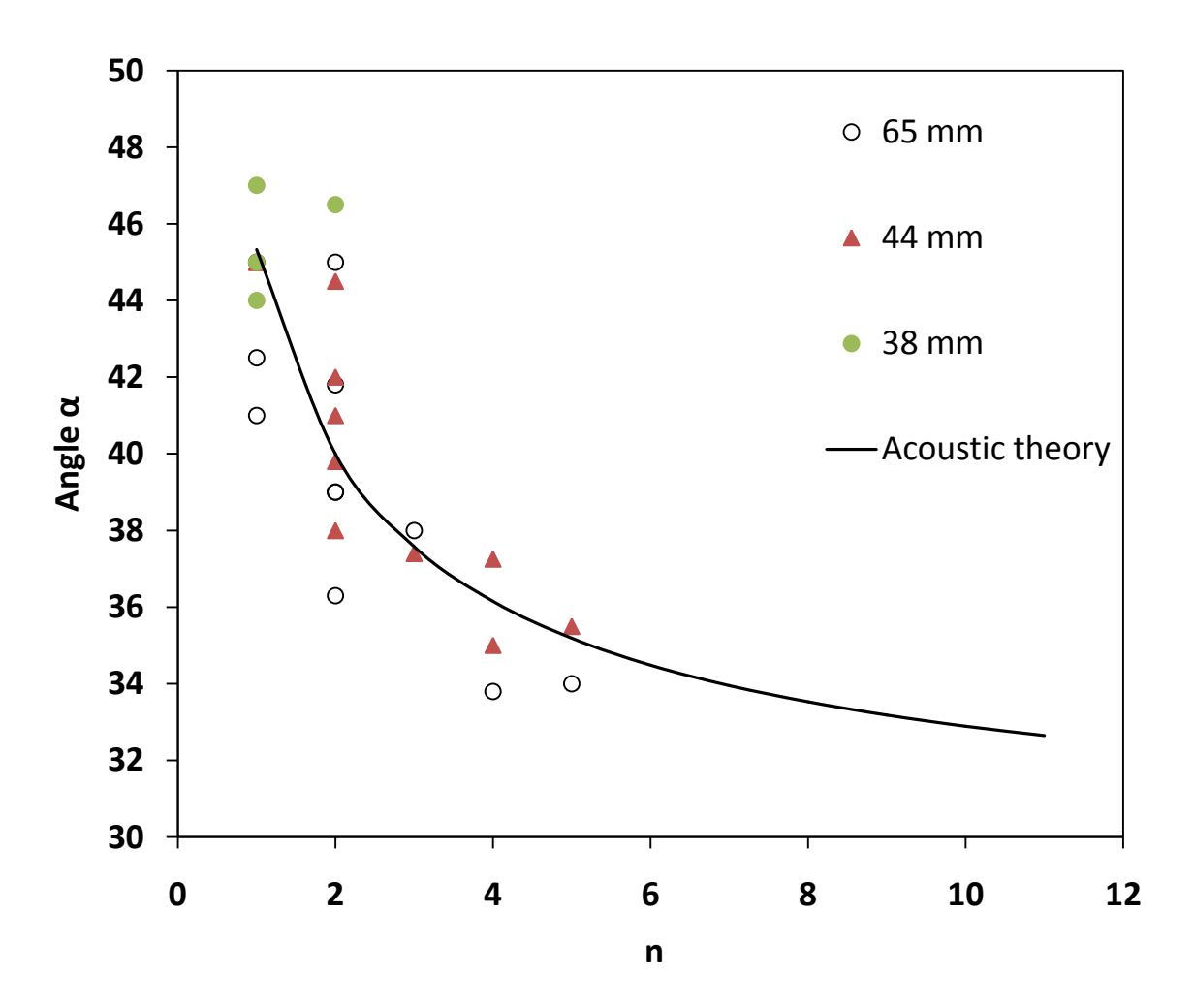


Figure 47: Comparison between measured and computed values of α from acoustic theory in C_2H_2 + 2.5 O_2 +70%Ar for round tubes.

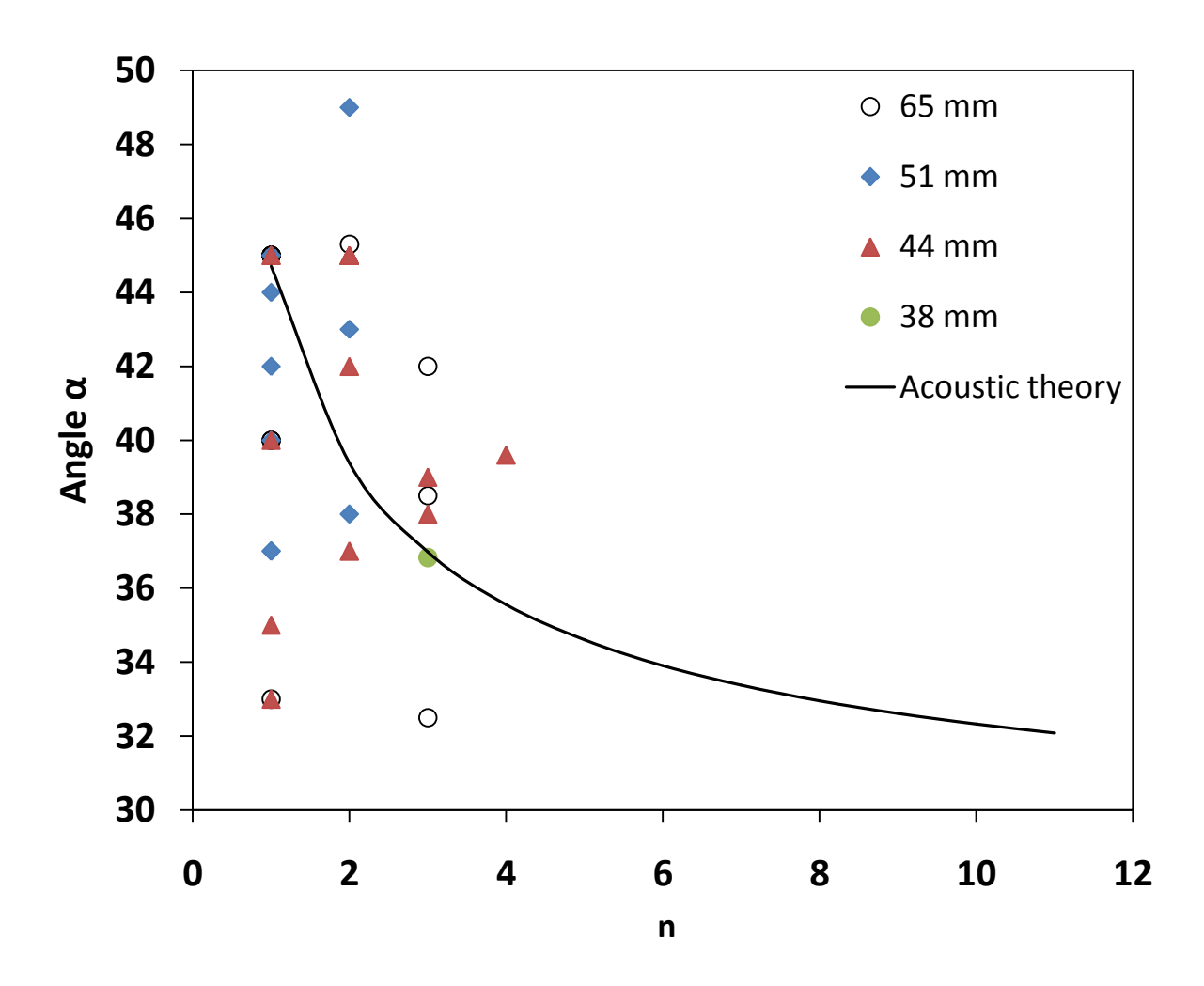


Figure 48: Comparison between measured and computed values of α from acoustic theory in CH₄ + 2O₂ for round tubes.

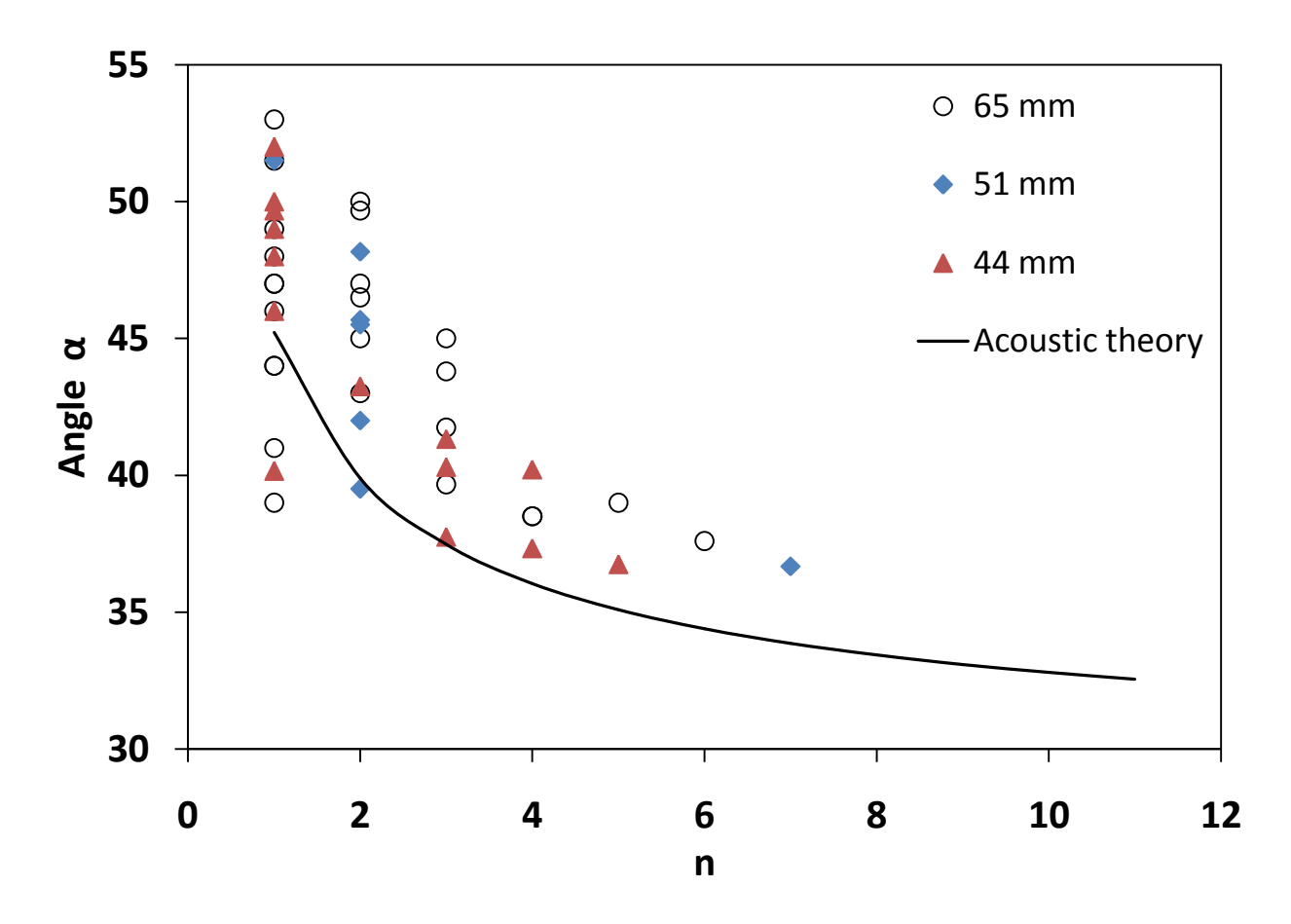


Figure 49: Comparison between measured and computed values of α from acoustic theory in C_2H_2 + $5N_2O$ +50%Ar for round tubes.

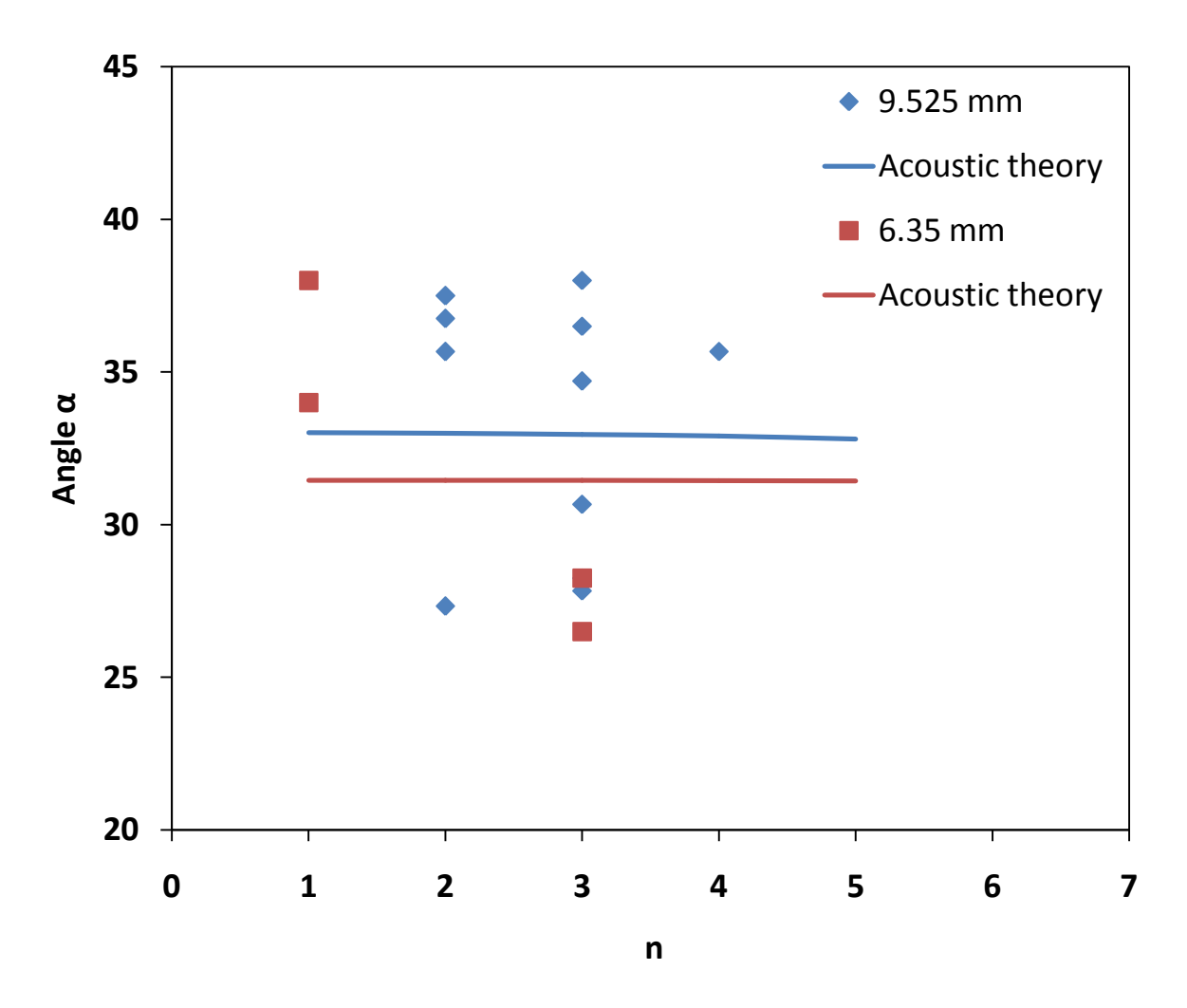


Figure 50: Variation of angle with mode n in C_2H_2 + 2.5 O_2 +70%Ar mixture in annular channels.

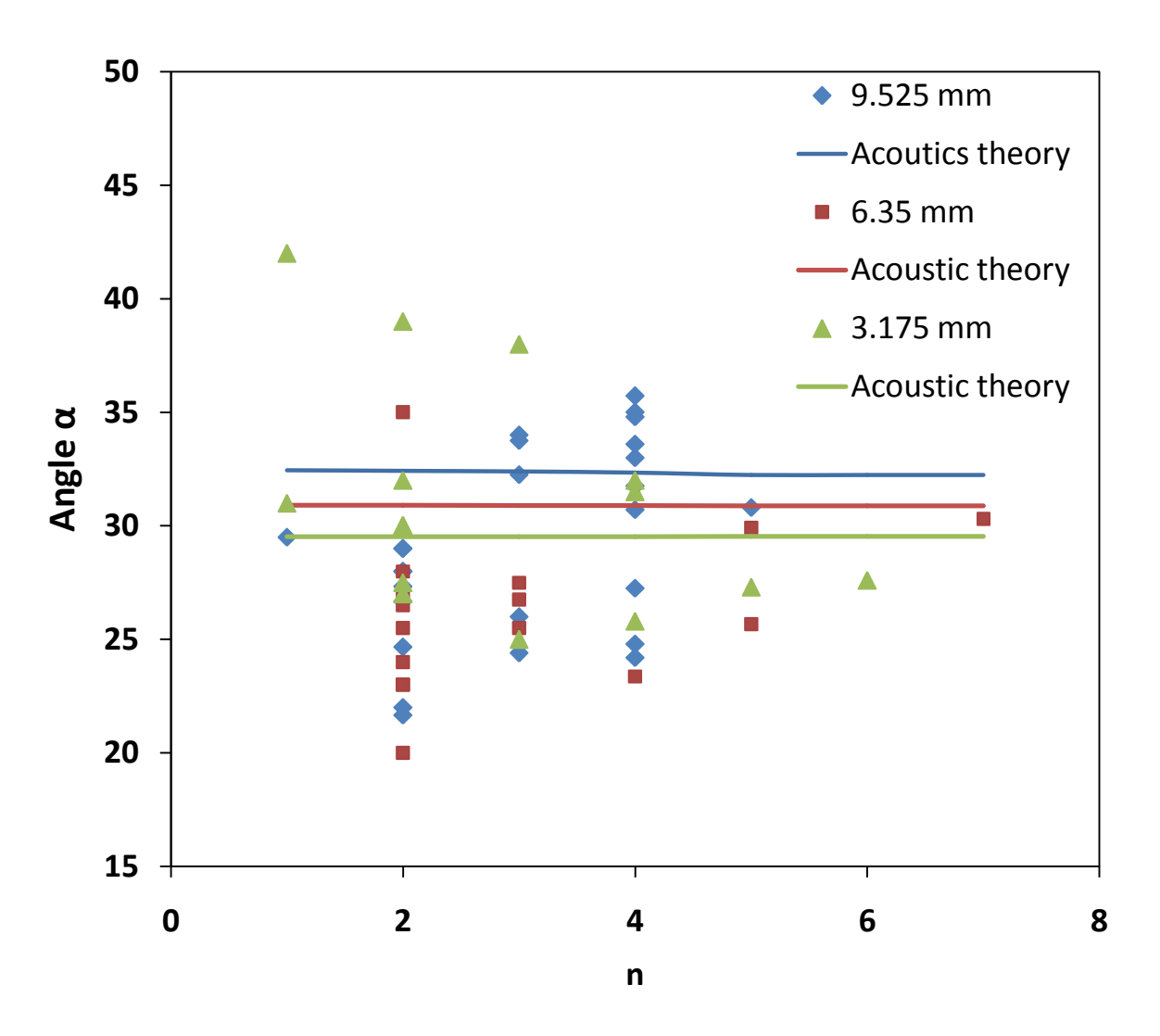


Figure 51: Variation of angle α with mode n in CH_4 + $2O_2$ mixtures in annular channels

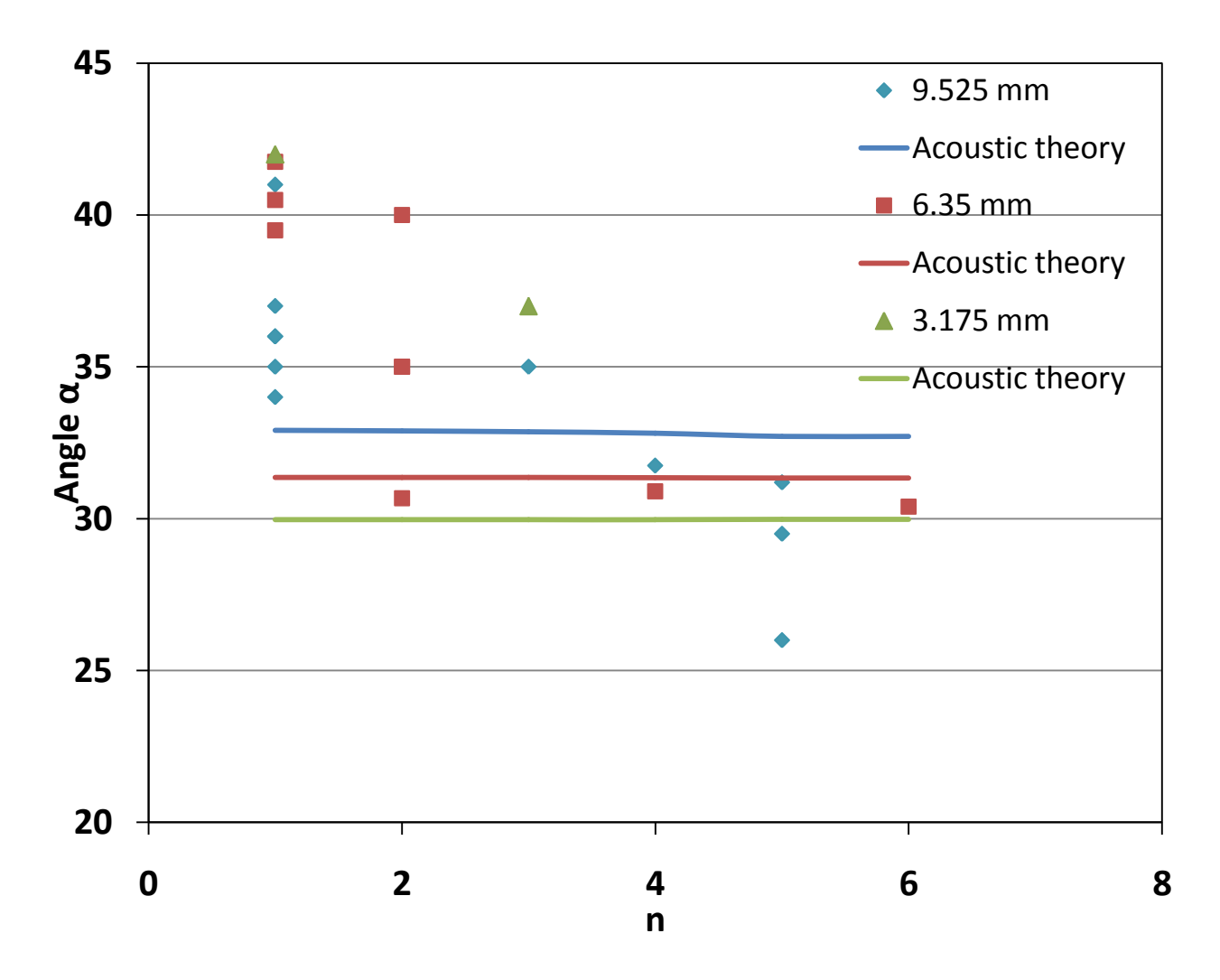


Figure 52: Variation of track angle α with mode n in C_2H_2 + $5N_2O$ +50%Ar mixtures in annular channels.

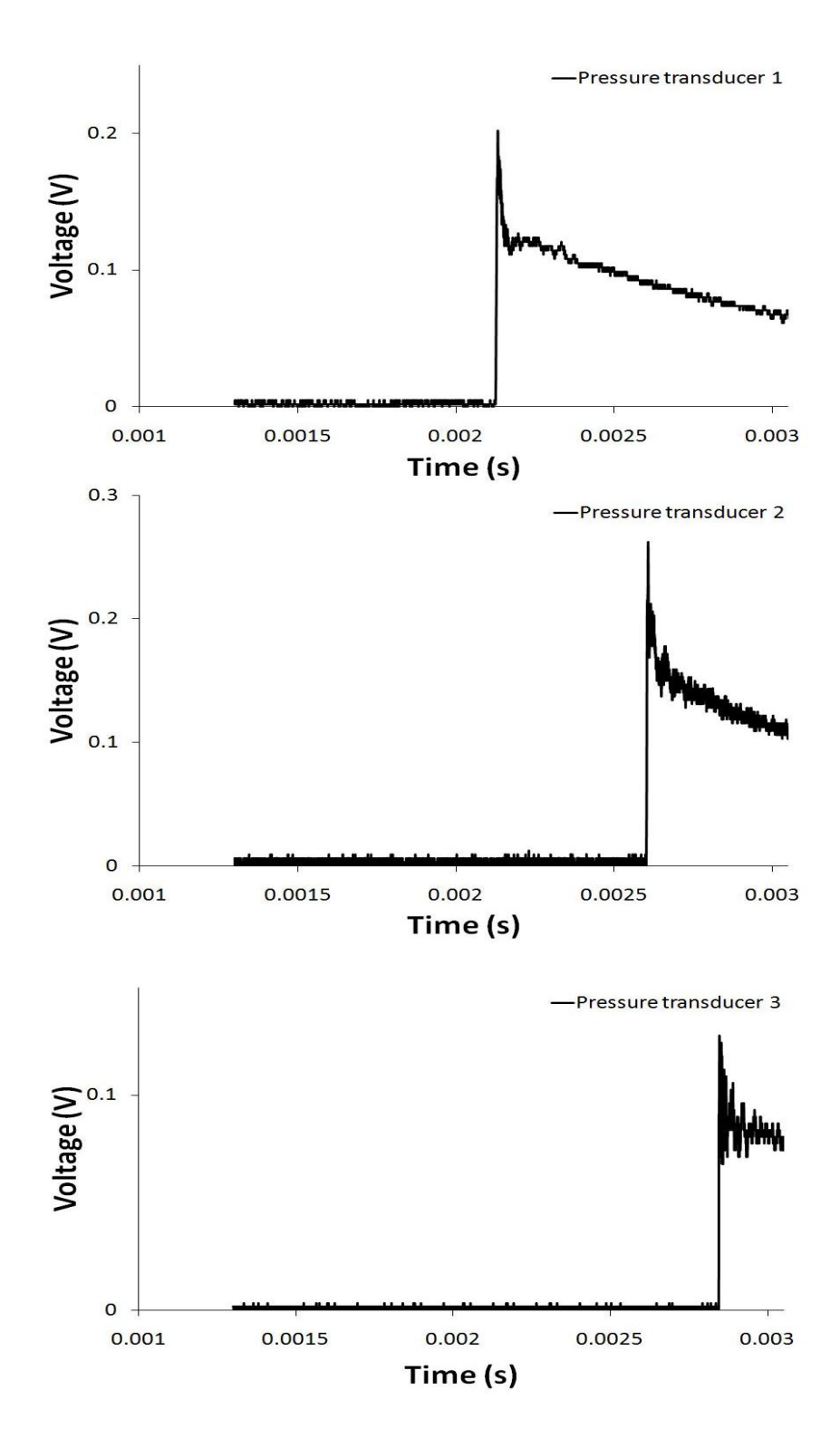


Figure 53: Typical pressure trace well within the limit ($C_2H_2 + 2.5O_2 + 70\%$ Ar, 9.525 mm channel).

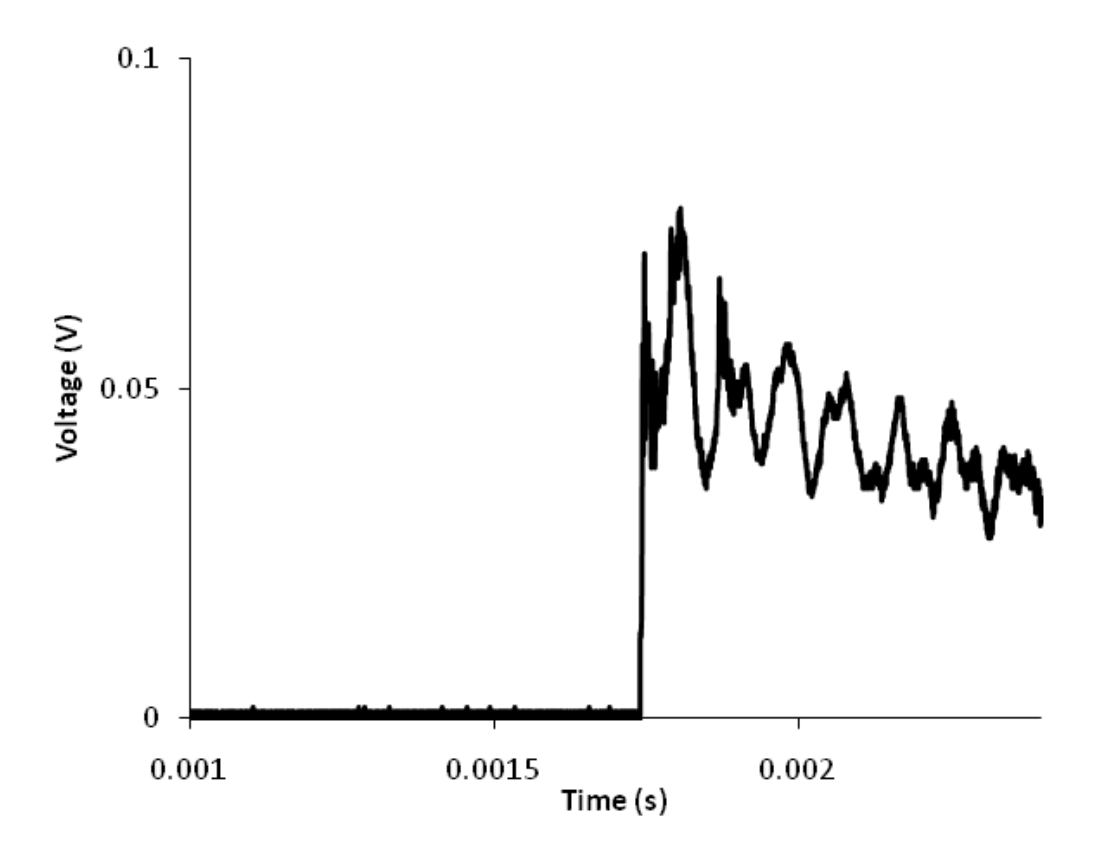


Figure 54: Pressure trace of a spinning detonation (CH $_4$ +2O $_2$, p $_0$ = 4 kPa, 65 mm diameter tube).

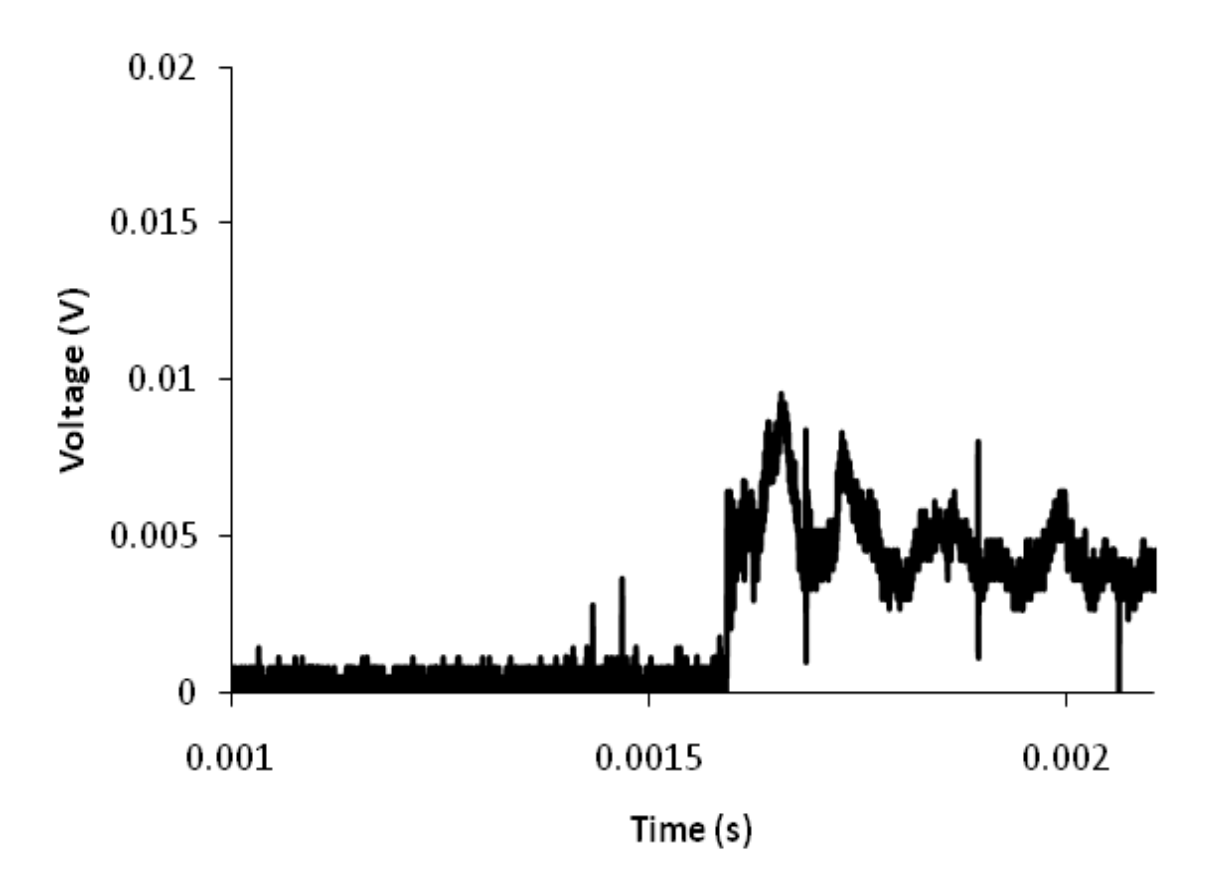


Figure 55: Pressure trace outside the limits of detonation ($C_2H_2+5N_20+50\%Ar$, 65 mm diameter tube, p_0 = 1.25 kPa).

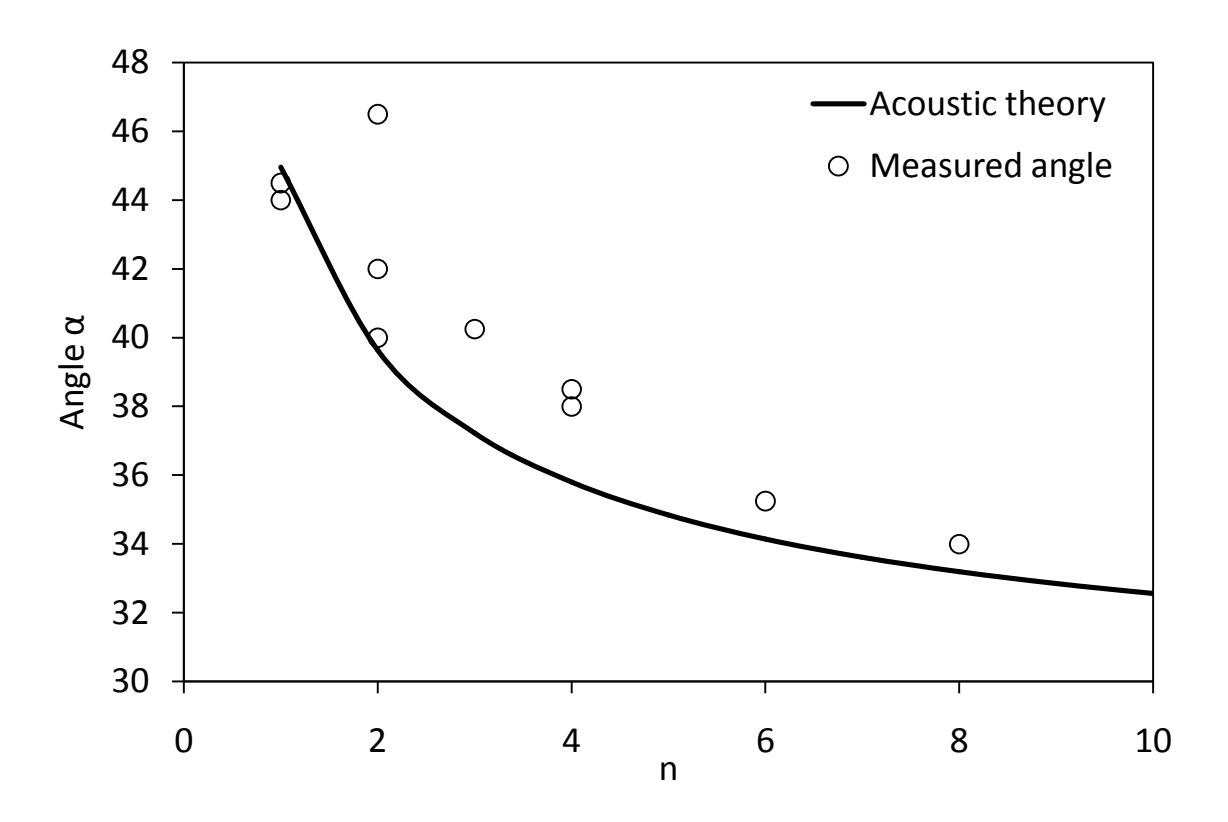


Figure 56: Theoretical and experimental values of track angle α in hydrogenoxygen mixtures in round tube.